Transmission Design of

The Zero Inertia Powertrain

Transmission Design of

The Zero Inertia Powertrain

Dit proefschrift is goedgekeurd door de promotoren:

prof.dr.ir. M. J. W. Schouten
en
Prof.Dr.-Ing. B.-R. Höhn

Co-promotor:

dr.ir. P. C. J. N. Rosielle

Contents

Summary

Modern passenger cars represent a technologically advanced form of flexible mobility, and its popularity has grown ever since its creation. The internal combustion engine, the prime mover of road vehicles, has been strongly improved in the recent past, although its efficiency still varies strongly with fluctuating power requests. Using any transmission type, *e.g.,* a stepped-gear or Continuously Variable Transmission (CVT), fuel efficient engine operation is hardly to combine with *driveability*, *i.e.,* an instant availability of power when pressing the accelerator pedal. This problem, caused by the inertia of the engine, can be solved by adding a secondary power source to the powertrain. Limiting the costs, weight and volume of the additional component is crucial for reaching the mass production stage and widely spread use. Still no cost-effective solutions are found yet.

Since the costs of a system or product are greatly determined by its first principles, a study on the fuel saving principles using an additional power source and on the concepts that embody the power source is made. This study has lead to an innovative powertrain concept *the Zero Inertia (ZI) powertrain* in which kinetic energy is exchanged between an additional flywheel and the engine's inertia. Alternatively, kinetic energy exchange between a flywheel and the vehicle inertia is studied, although is not found feasible at this time. The new ZI transmission concept, using well established low cost components such as a plain, low speed, steel flywheel and a planetary gear set, is analyzed thoroughly and its functionality is optimized for a mid size passenger car with 1.6 *l* petrol engine. A design tool, representing the combination of powertrain kinematics and dynamics and the kinematics of a planetary gear set in general, showed to be helpful to distinguish the functional and constructive design parameters and to find a start for the parameter optimization. Only two mutually independent parameters appeared to influence the functionality, being the maximum energy content of the flywheel and the geared-neutral transmission ratio. These parameters which determine the amount of assisting power when shifting to a higher engine power level are optimized for vehicle speeds between 30 and 120 [km/h]. To enable fuel saving at stand still of the vehicle, two clutches were added to the ZI powertrain configuration to enable engine restart and direct launch of the vehicle. This powertrain configuration is named the *ZI Stop-Go powertrain*. Consequently a prototype transmission, based on a conventional CVT, is constructed and two transmissions are built whereof one with the ZI functionality and one with the ZI Stop-Go functionality. Various innovative construction aspects have enabled the realization of the two transmissions to be compact and efficient.

The work of this thesis, [Vroemen, 2001] and [Serrarens, 2001] is carried out within the *EcoDrive* project. The general project goal of this project is saving 25% of fuel on a specific driving cycle, with respect to the same vehicle with a 4-speed automatic transmission (4-AT), and without loss of driveability. With the help of simulations, validated with measurements in a test vehicle, a fuel consumption reduction of 18% is reached. Next to this result, a con-

siderable driveability improvement is demonstrated, especially at higher vehicle speeds (> 50 [km/h]). The contributions of the research covered in this thesis helped to largely achieve the project target, *i.e.,* a significant fuel saving with improved driveability.

x

Part I

General Introduction

Chapter 1

Introduction and Project Goals

This thesis concerns the mechanical design of an innovative automotive transmission concept, termed the 'Zero Inertia (ZI) powertrain'. This powertrain combines a Van Doorne Continuously Variable Transmission (CVT), a low-speed flywheel and a planetary gear stage, targeting for 25% fuel saving without compromizing the vehicle's acceleration response. An extension of the ZI powertrain, termed Stop-Go, using two additional clutches to enable shutdown of the engine during vehicle halts, should yield about half the projected fuel saving. The underlying research of this thesis resulted in the realization of two transmissions, able to demonstrate the practical applicability of the ZI and ZI-Stop-Go powertrain concepts in a mid-size passenger car. This work is one out of three theses that describe different topics of the ZI powertrains. In [Serrarens, 2001] the modeling, control and testing of the ZI powertrain is focused on. In [Vroemen, 2001] modeling, control and testing of the CVT and the ZI Stop-Go powertrain are the main topics.

The ZI and ZI Stop-Go transmissions are materializations of the goals set in the 'EcoDrive' project. EcoDrive is a cooperation between Van Doorne's Transmissie (VDT) in Tilburg, the Technische Universiteit Eindhoven (TU/e) and TNO Automotive in Delft. The project was initiated by VDT and subsidized by the Dutch governmental program EET (Economy, Ecology and Technology). The ZI powertrain is the result of the EcoDrive assignment to achieve considerable fuel saving with a CVT and an additional power source in a powertrain for passenger cars. The properties of the additional power source can be exploited to save fuel by having the engine run in operating points with better fuel economy. This should occur without deteriorating the vehicle's longitudinal dynamic response, in other words, without compromising *driveability*.

The formulation of this assignment has a historical background at the Technische Universiteit Eindhoven. In the late 1970s a project was initiated to integrate a high speed flywheel in a powertrain enabling the engine to operate intermittently as a constant speed aggregate in its most efficient operating point. This lead to the materialization of an optimized Flywheel Hybrid[1] Driveline (FHD-III) and its fuel economy was demonstrated in [Kok, 1999]. The driveability was never assessed, nevertheless interest in this area began to increase.

---

[1]The definition of *hybrid vehicles* will be presented in Section 3.1.

EcoDrive

The main project goal of EcoDrive is twofold. One part of the project concentrated merely on improving the efficiencies of the engine and the CVT, aiming at an increased total driveline efficiency (System Integrated driveline, SI). The second part (HYbrid driveline, HY) was to design the hard- and software of a new powertrain with CVT and additional power source that saves 25% fuel on the New European Drive Cycle (NEDC) compared to a 5-speed manual transmission (5-MT) vehicle and that has a driveability level comparable to commercially available mid-sized passenger cars. The EcoDrive SI project was primarily a cooperation of VDT and TNO Automotive, whereas in the EcoDrive HY part VDT and TU/e worked together. The EcoDrive project started back in 1997 and will be finalized at the end of 2001.

A year after kicking-off the EcoDrive HY project, it was reformulated into the 'EcoDrive ZI' project, for reasons that will be explained further on. Figure 1.1 elucidates the organization and the resulting concepts of the EcoDrive project.
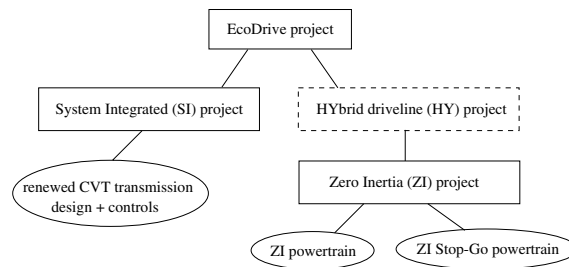
Figure 1.1: EcoDrive project organization

In this thesis and in [Vroemen, 2001] and [Serrarens, 2001], the findings of the EcoDrive ZI project are described. Results of the renewed CVT transmission design and control achieved in EcoDrive SI can be found in [Veenhuizen and van Spijk, 2000].

Zero Inertia powertrain

Choosing for the materialization of a certain powertrain concept starting from a problem description depends for the larger part on the conclusions of a preliminary investigation. In the case of EcoDrive HY, such a preliminary investigation lead to a simple configuration and operation principle of a hybrid powertrain with internal combustion engine, CVT, flywheel and a few clutches based on the findings of the FHD-III, [Serrarens and Veldpaus, 1998].

Along with the search for the 'ideal' flywheel hybrid powertrain, interest was put in the functional problems of basic CVT powertrains. A basic CVT powertrain is afflicted with the paradox that it can realize a high fuel economy and driveability, but hardly at the same time. Triggered by this phenomenon, the idea came up to try and find a way to break up this paradox with a flywheel inertia. This lead to the aforementioned Zero Inertia powertrain. The ZI concept is based on the notion that some unwanted inertial effects of the powertrain can in principle be nullified by exchanging kinetic energy between an additional flywheel and the engine sided inertias. As such, high fuel economy obtained by optimizing the engine operating points is no longer penalized by reduced driveability. It was decided to elaborate further

quarter	1997	1998	1999	2000	2001
①		specification and layout first order concept flywheel hybrid ready — Zero Inertia invented	parameter freeze ZI & ZI Stop-Go modeling and drafting of ZI and ZI Stop-Go — start of component manufacturing	testing and identification of CVT and hydraulics — implementation of CVT control software — 3 years	roller bench experiments with test vehicle — engine identification and optimizing powertrain control — ZI Stop-Go on testrig
②	Kick-off EcoDrive orientation on flywheel hybrids and CVT control	ZI Stop-Go invented generating knowledge on ZI and ZI Stop-Go	purchase of VW Bora, 1.6l fuel economy assessm. & test driving with 4AT — further modifying vehicle for ZI	installing the flywheel first testrig measurements of ZI transmission	First test driving without flywheel on test track — fuel economy without flywheel — First test driving with ZI on test track — trouble shooting Stop-Go
③	start with setup of layout, operation and component specification of a flywheel hybrid powertrain	compiling detailed project scenario — ZI design started	ZI transmission prototype implemented in vehicle & exposed at CVT'99 — start testrig modifications interfacing, signal cond'ng driver stages	start Stop-Go modeling — start implementation of ZI in test vehicle	finishing concept PhD theses — testrig experiments ZI Stop-Go fuel economy of ZI
④	sustained research on specs	EcoDrive HY reformulated kick-off EcoDrive ZI project — 1 year	transmission prototype without flywheel operational on testrig	finishing of implementing ZI — assembling Stop-Go transmission — troubleshooting test vehicle	

Figure 1.2: EcoDrive ZI project chronology

on the ZI powertrain leading to a reformulation of the EcoDrive HY into the EcoDrive ZI project.

outline of this chapter

The remainder of this chapter is organized as follows. In Section 1.1, the course of the project is chronologically described. In Sections 1.2 and 1.3 the problem description underlying this thesis is described. The main contributions of the present research and the outline of this thesis are presented in Section 1.4.

1.1 Project chronology

In Figure 1.2, the chronology of the EcoDrive ZI project is displayed. The decision to concentrate on the ZI and the ZI Stop-Go powertrains, required some organizational and financial reformulations of the goals first set in EcoDrive HY. It was decided to design and built a prototype ZI transmission, develop control software and conduct fuel consumption and driveability tests. The ultimate project goal, *i.e.,* demonstrating 25% fuel consumption reduction on the NEDC, could not be reached by ZI alone. Therefore the Stop-Go extension upon the ZI powertrain was introduced. The feasibility of the original project goal was questioned and a new goal was set, being 25% reduction of fuel consumption of a 1.6 ℓ petrol engine with ZI Stop-Go compared to the same engine in conjunction with a 4-speed automatic transmission (4-AT), or a CVT in 'performance mode'. Due to the limited time schedule and the desire to investigate systems step-by-step it was decided to implement ZI in a test vehicle and to test the feasibility of ZI Stop-Go on a test rig only. The fuel economy of ZI Stop-Go is estimated by measuring the fuel consumption of the ZI powertrain in the test vehicle and predict the additional fuel saving by Stop-Go through computation.

5

Regarding Figure 1.2, the main observation is that the time span between the invention of the ZI powertrain and first successful road testing covers just over three years. Conceiving and designing the ZI concept for a vehicle implementation took just over half a year. The materialization and mounting on the test rig of the first ZI transmission required around one year, whereas the testing of the transmission and its controls on a test rig and in a vehicle required an additional one and a half year. Reasons for the relatively short development time appear to be:

- the fact that the ZI idea itself hardly necessitates research on components, enabling the use of of proven technology;

- the control system hardware requires no major adaptations compared to a standard CVT powertrain, instead new developments in software are achieved;

- prompt freezing of the mechanical layout through reasoning according to first principles;

- the use of simple kinematic, dynamic and energy models to gain quick insight in the mechanisms and to optimize the system parameters of the prototype ZI transmission;

- the use of an available CVT and other available transmission components to make the extension towards a ZI transmission;

- step-by-step testing of the ZI powertrain, by consecutively testing the available CVT transmission on a test rig, followed by the ZI transmission on the test rig and finally in the vehicle. This way, inevitable setbacks could be handled reasonably quickly;

- the use of flexible and state-of-the-art test rig facilities, which were developed within the EcoDrive project;

- the modest modifications required within the engine compartment in order to make the ZI powertrain fit into the test vehicle;

- coordinated teamwork, frequent team meetings and ticking off achieved milestones.

1.2 Problem description

As explained, the main project goal for EcoDrive ZI is 25% fuel economy improvement on the NEDC cycle compared to 4-AT, under the constraint of uncompromized driveability. In general there are different ways to achieve this, when altering the powertrain only. Four of them are mentioned:

a) matching fuel-optimal engine operating points that fulfill the momentary power demand, to the actual vehicle speed;

b) shutting down the engine at full vehicle stops to save the fuel normally consumed during idling;

c) matching the engine operating point with the highest efficiency to the average power request, requiring an additional power source, and

d) effective reuse of the vehicle's kinetic energy.

In the initial assignment of EcoDrive HY all off the above principles were combined into one concept. In the EcoDrive ZI project only the principles a) and b) are chosen, materialized as the ZI and ZI Stop-Go powertrains, respectively. From Figure 1.3, three problem descriptions

6
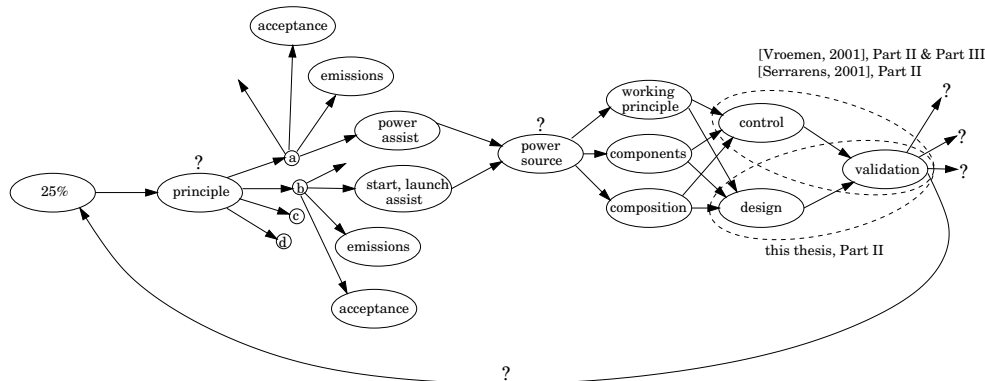
Figure 1.3: Research trajectory for EcoDrive ZI

are identified. The first is how to motivate the choice for fuel saving principles a) and b). Both principles need a power assist system in order to meet the driveability objective. This will be explained in more detail in Chapters 3 and 4. The second problem then is how to motivate the choice for the power source, being a flywheel for both ZI and ZI Stop-Go. The third question is up to what extent the main project target of 25% is met, and the reasons for that. Naturally, a number of research questions evolve when developing, examining and validating the new concepts. This may be regarded as scientific or engineering spin-off from the project.

In this thesis, the first and second research questions are answered in Chapter 3. Answers to the third research question, and directions for future research are presented in Chapter 12, Part III.

1.3 Research objectives

The ZI an ZI-SG powertrain concepts use kinetic energy exchange to enable the engine to run more fuel efficiently and to assist the engine in power transients. To enable kinetic energy exchange between a flywheel and a load, being either the engine inertia or the vehicle mass, a variator is needed. The combination of flywheel system and variator is further indicated with flywheel energy exchange system or kinetic energy exchange system. The first research objective is to determine the maximum performance of alternative flywheel energy exchange systems which can potentially be used in a passenger car. Since weight, packaging, power loss, safety and costs are the mayor constraints, and maximum energy and power level are the mayor benefits the relation between them has to be identified and optimized to the application. The second objective is to define the required specification of the flywheel energy exchange system according to its functionality in the powertrain. The third objective is to find a correlation between the performance and specification and to design a powertrain that is able to match the project goal of saving 25% of fuel without compromising the driveability. The fourth objective is to optimize the design for a specific vehicle, being a mid-size passenger car. The final objective is to construct two prototype transmissions, able to prove the concepts of fuel saving and uncompromized driveability.

Besides, in cooperation with the authors of [Serrarens, 2001] and [Vroemen, 2001] the

additional objective was defined, to give a thorough overview of fuel saving principles, and the associated (development, cost, packaging, etc.) efforts.

1.4   Main contributions and outline of this thesis

In this thesis the principles and arguments behind the design and the construction of the ZI and ZI-SG powertrain are discussed. The powertrains are innovative in three ways. First, it is decided to assist the engine in power transients with the use of a mechanical power source, *i.e.,* a flywheel, while known power assist systems for passenger cars use an electrical power source. Mechanical energy exchange systems are mostly found to exchange energy with the vehicle mass. A prototype system for busses is realized and shown in [Thoolen, 1993]. Second, the variator between the flywheel and the engine in the ZI-powertrain is integrated with the already present mechanical variator between the engine and the wheels of the vehicle using an epicyclic gear. It is not new to use an epicyclic gear in parallel with a mechanical variator. However the connection described in [van Druten *et al.*, 1998], enabling the flywheel to decelerate when the engine accelerates while shifting the CVT, is not seen before in automotive applications. Finally, various innovative construction aspects enable a compact and efficient upgrade from a conventional CVT to a ZI-transmission. Because of the rather unconventional design, insights have to be gained in the parameters that influence the characteristics of the powertrain. First, a design tool using a simple representation of the powertrain kinematics and dynamics in a single mechanism is developed. Extending this tool with a general representation of epicyclic gears, insight is gained in the characteristics of the ZI-powertrain and in the parameters that influence its functionality. A distinction between functional and constructive design parameters is made. After optimizing both the functional and constructive parameters, taking into account their specific constraints, two prototype transmissions are designed, and built to prove the suitability of the concepts of ZI and ZI-SG.

The main contributions of this thesis and the underlying research are listed below, at the same time indicating the outline of this thesis:

- a thorough overview of fuel saving principles for a passenger car (Chapter 2);

- an initiative to quantitatively weigh the improvement of fuel economy of alternative powertrain operation against the drawbacks of additional costs, weight, volume, complexity, driveability, *etc* (Chapter 3);

- two novel transmission concepts, referred to as the Zero Inertia powertrain and the Zero Inertia Stop-Go powertrain, introduced in Chapter 4;

- overview of design aspects of sub- and super-critical flywheel systems (Chapter 5);

- development of an optimization procedure for the design of flywheel systems, directed to minimal power loss, followed by the design of two alternative flywheel systems for passenger car application (Chapter 6);

- short overview of the usage of a flywheel in a passenger car (Chapter 7), followed by the specification for a kinetic energy exchange system to exchange energy with the vehicle mass or with the engine inertia (Chapter 8);

- development of drive train design tools, including a general representation of epicyclic gears, giving insight in the interaction between kinematics and dynamics in the ZI-powertrain which uses an epicyclic geared inertia (Chapter 9);

8

- distinction and optimization of functional and constructive design parameters for the ZI-powertrain (Chapter 10 and 11);

- creation of a modular transmission design able to demonstrate the suitability of the concept of ZI and ZI-Stop-Go (Chapter 11).

Finally, Chapter 12 summarizes the outcome of this thesis and gives directions for future research.

Chapter 2

Fuel Saving Principles

2.1 Introduction

Modern passenger cars represent a technologically advanced form of flexible personal mobility. They are comfortable, high performing and relatively safe. Imagining global society without passenger cars is simply impossible. Despite all efforts, the passenger car is still a fairly inefficient means of individual transportation. Figure 2.1(a), from [Delsey, 1991], shows the distribution of fuel energy to the various heat producing processes involved with driving a passenger car. A more realistic graph might be the pie-chart of Figure 2.1(b), from [DOE and

(a) based on the "Euromix" average   (b) based on city driving, no cycle given
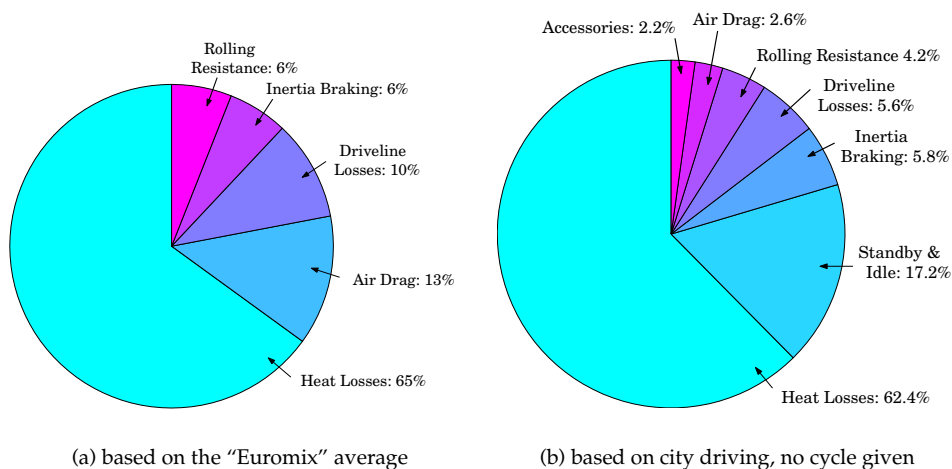
Figure 2.1: Typical energy distributions for a passenger car

EPA, 2001] (measured drive cycle is not given). From both figures it follows that only between 15% and 25% of the energy in the gasoline is actually used to propel the vehicle—that is to

overcome vehicle inertia, aerodynamic drag and rolling resistance—and to power accessory systems like air conditioning. The rest of the energy is lost in the form of heat transfer to coolant and ambient air, friction within the engine and transmission, and pumping of air into and out of the cylinders (*e.g.,* during idling).

Regarding these figures, insight can be gained into how fuel economy might be improved. In general, methods for reducing the fuel consumption can be divided into four categories:

1. improving the efficiency of the individual powertrain components, *i.e.,* engine, transmission and power take-off;

2. reducing the external load of the powertrain, *i.e.,* vehicle mass, rolling resistance and air drag;

3. alternative powertrain operation, *i.e.,* E-line[1] tracking, Stop-Go[1], Start-Stop[1] and brake energy recovery (BER)[1];

4. non-vehicle technology, *i.e.,* driving behaviour, infrastructure and traffic management, law, policy and legislation.

In this chapter, all four categories are briefly discussed. The following chapter concentrates on alternative powertrain operation in more detail. Engine emissions are only briefly treated.

2.2 Improving component efficiency

A conventional passenger car driveline basically comprises an internal combustion engine, a launching device (friction plate clutch, torque converter, magnetic powder coupling, *etc.*), a torque amplifying transmission (any kind), differential and drive shafts, see Figure 2.2. The fuel tank, cooling system, battery, electric starter motor and various Power Take-Off (PTO) components, such as the alternator, fuel pump, water pump, power steering pump, and ignition, draw up the indispensable but fuel consuming periphery of the driveline. Part of the mechanical power generated by the engine is lost in the transmission and to the PTO. The net torque in the drive shafts propels the wheels. Ways for decreasing the driving resistance are discussed further on. First, various methods and potentials for fuel economy improvement by enhancing the efficiency of individual driveline components are discussed.

2.2.1 Engine efficiency

The engine efficiency has been strongly improved in the recent past, although it is still the least efficient component in the powertrain. Despite its disappointing efficiency, the modern combustion engine, the prime mover of road-going vehicles, is a more or less optimal combination of low manufacturing cost and -energy, power density, volume, efficiency, durability, maintainability, recycleability and controllability. A point of concern about this machinery is the load-dependent efficiency characteristic. Without employing more advanced powertrain concepts this dependency hampers the most fuel-optimal utilization of the combustion engine.

The fluctuating power requests needed for the vehicle's motion, demand the operating conditions of the engine to be changed accordingly. In this respect, there are two main reasons why fuel consumption may be larger than theoretically achievable, namely:

---

[1] To be defined in Section 3.2
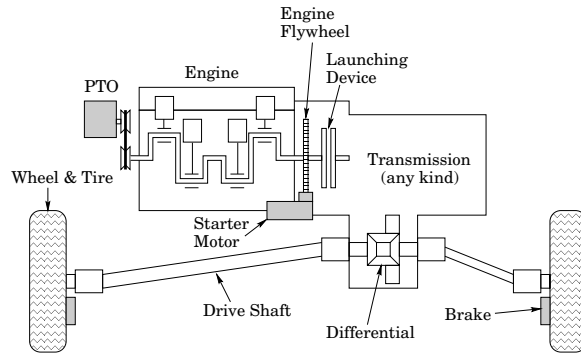
Figure 2.2: Basic (front wheel) driveline

- the energy-specific fuel consumption [g/kWh], also known as "Brake Specific Fuel Consumption" BSFC, depends on the operating point, defined by the engine torque and speed, that fulfill the requested power;

- the BSFC varies with the power demand itself.

The BSFC is best viewed in a so called engine map. In this map various quantities may be visualized by iso-curves being a function of static engine speed and engine output torque. In the map of Figure 2.3 the BSFC curves of a 1.6 ℓ, multi-point injection petrol engine are sketched. Also hyperbolas graphing constant engine power are drawn. The BSFC varies
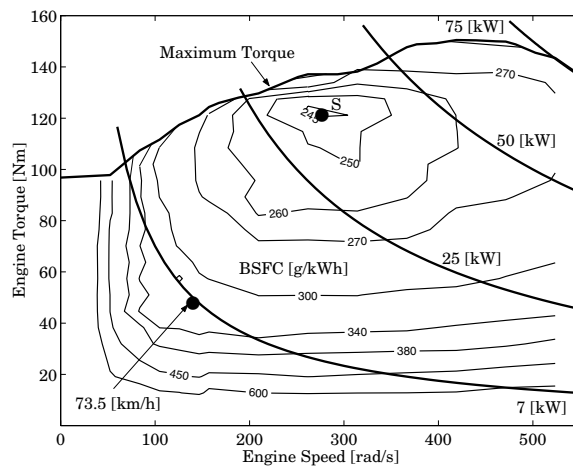
Figure 2.3: Brake specific fuel consumption (BSFC) in engine map

substantially along and between the power hyperbolas. The operating point with the lowest BSFC, indicated in Figure 2.3 by 'S', is termed the *sweet spot*.

The influence of the chosen operating point on the fuel economy is substantial. In an illustrative example a mid-sized passenger car runs at 73.5 [km/h], indicated by the dots in Figures 2.3, 2.4(a) and 2.4(b). Figure 2.4(a) displays the fuel consumption per traveled kilometer (DSFC) as a function of constant vehicle and engine speed. The fuel consumption per second (TSFC) as a function of engine output power is plotted in Figure 2.4(b).

(a) Distance specific fuel consumption (DSFC)

(b) Time specific fuel consumption (TSFC)
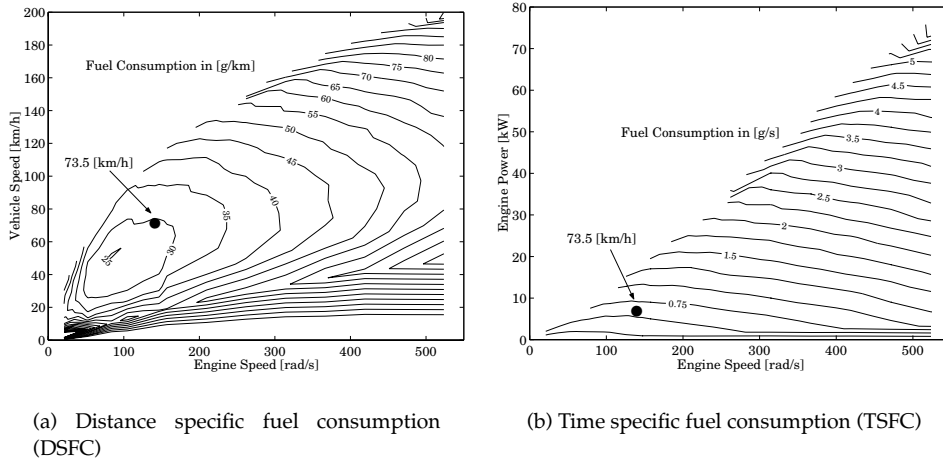
Figure 2.4: Alternative representations of the fuel consumption

Maintaining the constant vehicle speed at higher engine speeds substantially raises the fuel consumption per traveled kilometer, *cf.* Figure 2.4(a). For instance, up to twice as much fuel is consumed if the vehicle speed is kept at 73.5 [km/h] with an engine speed of 500 [rad/s]. Regarding Figure 2.4(b), a full acceleration (exploiting maximum engine power) from 73.5 [km/h] would consume about ten times more fuel!

engine improvements

Since decades many successful efforts to improve driveline component efficiency have been undertaken. The internal combustion engine has been given the most attention, leading to a multitude of solutions which improve the combustion efficiency, along with the emissions. Treating them all would go far beyond the scope of this thesis. However, the most important solutions for the petrol engine, being the engine type considered in the EcoDrive project, should receive some attention.

Variable valve timing has improved the efficiency, performance and emission quality. Advancing the intake valve timing for higher engine speeds improves the homogeneity of the air/fuel mixture and in general improves the combustion performance. This increases the engine torque or alternatively provides the same torque using less fuel. Furthermore, retarding the closing of the exhaust valve for higher engine speeds leaves part of the exhaust gases in the cylinder while the new air/fuel mixture is already entering the cylinder (overlapping of intake and exhaust period). Consequently, the mixture can be leaner resulting in further com-

bustion of unburned constituents and hence lower emissions. *Exhaust Gas Recirculation (EGR)* further exploits this technique by actively recirculating the exhaust gases through a by-pass channel controlled by a valve. Through the combination of *variable spark timing* and metered *fuel-injection*, complete combustion (stoichiometric operation) is possible for varying engine speed, load and temperature, further reducing fuel consumption and emissions.

The fuel consumption, the emissions and the engine performance are often conflicting targets. Especially emission standards hinder the further improvement of the engine efficiency [Oppenheim *et al.*, 1994]. This is caused by the fact that engine operating conditions are often shifted to regions with less NO_x, HC and/or CO emissions, but increased specific fuel consumption (also leading to higher CO_2).

Techniques related to engine technology as described may result in a lower fuel consumption for *equal engine power* demands. On the other hand improving the efficiency of other driveline components such as the transmission and PTO will reduce the energy demand for *equal covered vehicle distance*.

2.2.2 Transmission efficiency

Only recently, improving the efficiency of stepped transmissions (MT and AT) has been given more attention, whereas that of the CVT has been a concern since *mature* versions of the push belt CVT started to be commercially produced (early nineties). From [Kluger and Long, 1999] it is concluded manual transmissions have overall efficiency values of 96.2% and leave little room for improvement (up to 96.7% at most). Kluger and Long furthermore evaluate the overall efficiency of ATs at 85.3%, whereas the efficiency of the best current AT could be improved up to 86.3%. Finally, the overall efficiency of belt type CVTs is estimated at 84.6%, and may be improved towards 88.4% by reducing the pump losses. These hydraulic pump losses for the larger part determine the efficiency of CVTs and of ATs, and are relatively high at low transmission loads. Improved pump and hydraulic circuit design can substantially increase the efficiency of CVT and AT. The design of the pump, friction fluids and mechanical part of the CVT is subject of ongoing research. Alternatively, the actuation of the clutches and of the CVT may be (partly) electrical, thus replacing the hydraulic losses by potentially lower electrical losses. For instance, in [van Tilborg, 2001], it is shown that the pump losses in the CVT can be reduced by applying part of the pulley clamping force electro-mechanically.

Finally, the overall efficiency of toroidal or traction drive CVTs (*e.g.*, see [Machida, 1999]) is estimated by [Kluger and Long, 1999] at around 91%, and may be improved by 1.8% with the implementation of more advanced traction fluids. This type of transmission is well suited for high power applications, though production numbers are still limited.

2.2.3 Power take-off

The fuel consumption could be further reduced if also the power demand by the PTO is somehow lowered. For example, methods to improve the efficiency of the alternator are discussed in [Bürger *et al.*, 1994]. They projected a potential fuel saving of 1% when the alternator efficiency is improved by 5%. Enhancing the efficiency of all auxiliary systems is possible by increasing the on-board voltage level, giving rise to the recent development of a 42 Volt on-board grid. The alternator and starter can then be re-engineered into an integrated unit referred to as *starter-alternator (SA)*. A higher voltage leads to lower currents and reduced electric transmission losses. This is necessary for operating the increasing number of on-board electric systems, which in turn does not guarantee a lower fuel consumption altogether.

15

2.3 Reducing the external load

2.3.1 Vehicle mass

The increase of vehicle mass is mainly caused by higher safety and comfort standards. A better crash protection usually results in higher vehicle weight and thus fuel consumption. Vehicle weight is also increased due to the expanding amount of on-board auxiliary systems such as air conditioning, power-assisted steering, electrically operated windows, sun roofs, mirrors, seats, door-locking, in-car entertainment, *etc.* Furthermore, these systems claim supplementary power to operate. Besides the growing demands for more safety and comfort, drivers also claim an unspoilt driving pleasure. For that reason, the enhanced engine efficiency may well be overshadowed by an increased power demand. This can also be seen in
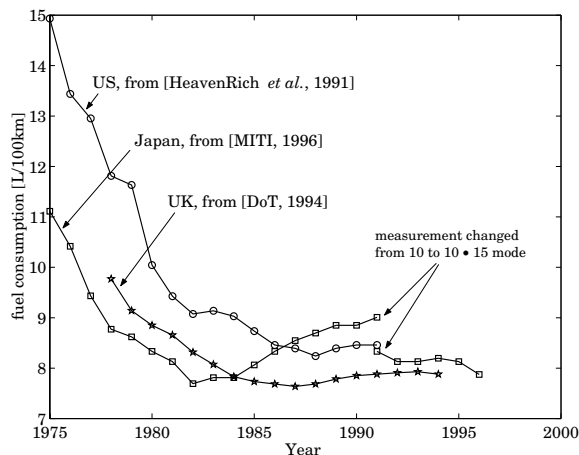
Figure 2.5: Average fuel consumption of new-sold passenger car fleet in UK, US and Japan from 1975 to 1996

Figure 2.5 (sources from [Heavenrich *et al.*, 1991], [MITI, 1996], and [DoT, 1994, 1994]) where the fuel consumption of the average *new-sold passenger car* is shown between 1975 and 1996 for US, UK (assumed to be representative of Europe) and Japan. The absolute fuel consumption indicated by the curves can not be directly compared as such because they use different test driving cycles. The increase of fuel consumption after 1980 for Japan, which is not seen for the US and the UK, is explained by the increased use of rather inefficient vehicle electronics (for in-car convenience) and weight of the average Japanese car. The improvements in engine efficiency on the one hand, and especially the increase of auxiliary power demand on the other, start to even out in the US and the UK during the late 1980s, flattening the average fuel consumption.

2.3.2 Rolling resistance

The rolling resistance of a vehicle is predominantly due to the tires, apart from negligibly small wheel bearing losses. The actual tire rolling resistance consists for a very small part of tire-road friction and for the larger part of tire deformation losses. The magnitude of these losses is

determined by what might be termed 'internal' and 'external' factors. The internal factors such as the tire material, the tire shape, and the tire size (width especially), substantially influence the rolling resistance. For example, two tire designs of the same overall size, but with different shapes and materials may differ in rolling resistance by a factor of two [Junio et al., 1999]. External conditions influencing the tire rolling resistance are the tire pressure, tire load, road surface conditions, (internal and ambient) temperature, speed, dynamic conditions (wheel torque, cornering) and the wheel alignment (toe-in and camber). For instance, an additional 0.3 [bar] of tire pressure lowers the tire rolling resistance by about 7% [Junio et al., 1999].

Reductions of tire rolling resistance may be accomplished by using better materials especially, and to a lesser extent by applying 'smart' tires (e.g., monitoring and controlling the tire pressure) as well as active suspension (decreased dynamic tire load). The application of these technologies is limited by requirements for wet skid conditions, high speed driving, tire damping (noise and comfort) and cost. Nevertheless, a reduction of rolling resistance of 50% for 2006 (compared to 1999) is projected by Good Year [Junio et al., 1999].

2.3.3 Air drag

The shape and size of the passenger vehicle body have changed during one hundred years of automotive technology. Frontal area and shape directly influence fuel consumption through friction with the ambient air. The car designers' utmost challenge is to mediate between interior space and exterior aerodynamical shape and size. The air resistance is made up of the pressure drag including pressure induced turbulence drag, surface resistance and through-flow resistance. The longitudinal aerodynamical drag force on the vehicle is approximately proportional to the frontal area, the square of vehicle speed and a characteristic value c_d—better known as the air drag coefficient—depending on the body shape. Increasing comfort demands and occupants' stature do not allow a significant further decrease of the average vehicle frontal area. For instance, the growing popularity of the Multi Purpose Vehicle (MPV), has even increased the average frontal area.

Nonetheless, continuous re-fashioning of the vehicle shape has reduced the c_d-coefficient tremendously, see Figure 2.6. The theoretical minimum of c_d lies somewhere around 0.15. The General Motors' Precept concept vehicle, reaching $c_d = 0.163$, comes close to this minimum. For normal passenger cars, a number of important measures influence the aerodynamics. The most important measures are the decrease of the rear window angle with the horizontal axis, the smoothness and rounding of the rear window stile (C-stile) and a high but short trunk with a sharp transition down at the end. Taking such measures may lead to a higher vehicle mass because of the unfavourable ratio between surface and volume. This might be compensated by lighter materials or by improved constructional design.

The lower air resistance due to a smaller air drag coefficient leads to a higher maximum speed of the vehicle, hence requiring an increased speed ratio coverage of engine and/or transmission. The latter demands for a higher overdrive bringing the engine operating point towards lower engine speeds at virtually equal engine torque. Fuel economy can be improved by about 1 % for 3 % air drag reduction, [Seiffert and Walzer, 1989]. Naturally, this number depends on the combination of the specific vehicle and engine and should therefore be interpreted with care.

17
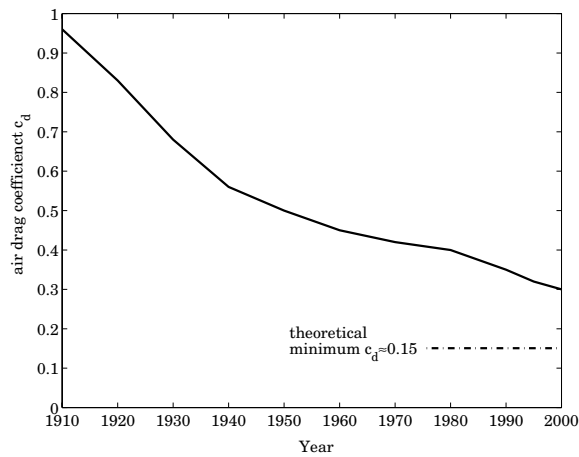
Figure 2.6: Historical trend for the average air drag coefficient

2.4   Alternative powertrain operation

Fuel economy can be improved by more optimal operation of the existing powertrain components or by extending the powertrain with more components to enhance its functionality. By such means operating regions with poor engine efficiency can be avoided. In this section, four principles which aim at more efficient engine operation, or at avoiding excessive fuel consumption otherwise, are briefly discussed. In Chapter 3, these fuel saving principles will be given more attention.

- *E-line tracking* amounts to controlling the engine in such a way that for each requested engine power the fuel consumption is minimal. For modest driving this comes down to restraining the engine speed to extremely low values;

- *Stop-Go (SG)* systems halt the engine during full vehicle stops and facilitate a new vehicle launch either by first restarting the engine and then launching the vehicle, first launching the vehicle and then restarting the engine, or launching and restarting at the same time. Clearly, the fuel otherwise consumed during engine idling can be saved;

- *Start-Stop (SS)* refers to delivering the required energy by intermittently operating the engine in the sweet spot (defined in Section 2.2.1). Because the engine power delivered in the sweet spot will generally be different (usually higher) than the demanded wheel power, some sort of energy buffer is needed, as well as a generator and motor to compensate for the momentary power surplus (while the engine is on) and power deficit (while the engine is off), respectively;

- *Brake Energy Recovery (BER)*. The mechanical energy stemming from the engine is partly accumulated in the vehicle's inertia. This energy can be recuperated whenever decelerations of the vehicle are requested by the driver. Reusing this energy for vehicle propulsion or to power auxiliary functions, in principle decreases the net fuel consumption.

18

In designing an alternative powertrain for the sake of a higher fuel economy, the drawbacks of such a redesign should have minor influence on the final vehicle concept, at least in proportion to the gained reduction of fuel consumption. A method for rating the fuel reduction against additional efforts and penalties is discussed in the next chapter. The following section lists some developments potentially leading to a better fuel economy, but not directly linked to vehicle technology.

2.5 Non-vehicle technology

There are a number of measures that are not directly related to powertrain or vehicle technology but are rather driven by external factors such as driving behaviour, legislation, policies, traffic management, infrastructure, *etc.* These factors are briefly illustrated in this section.

2.5.1 Driving behaviour

The behaviour of the driver and the traffic conditions strongly influence the fuel consumption. In [An and Ross, 1993] the fuel consumption as a function of *average* trip speed is measured, showing that minimal fuel consumption is reached between 65 and 80 [km/h]. On the other hand, if the fuel consumption is measured for *constant* vehicle speed this optimum lies around 50 [km/h], as will be shown in [Serrarens, 2001].

Average vehicle speed but also the number and intensity of accelerations and decelerations are highly related to the traffic conditions and the drivers' state-of-mind during a trip. Without increasing the travel time, a significant decrease of fuel consumption can be reached if the driver alters his or her driving behaviour. Theoretical studies by [Evans, 1979] and [Waters and Laker, 1980] showed that around 15 % fuel reduction is possible. The evaluation of a driver-friendly fuel efficiency support tool as in [van der Voort *et al.*, 2001] showed that with a 5-speed manual transmission even 20% fuel can be saved in rural areas. Essentially, the support tool gives advice to the driver when to shift gears according to measurements of the vehicle conditions and of the actual accelerator pedal deflection.

2.5.2 Infrastructure and traffic management

Fuel consumption is closely related to the vehicle speed, which in turn is strongly influenced by the road infrastructure. In city driving the traffic flow is often hampered by frequent stop-and-go actions due to crossings, different speed of the traffic participants, *etc.*

Active control of traffic flow, also termed *traffic management* can decrease the congestion through leveling the traffic speed. Reducing the average speed by such means can also reduce the fuel consumption. Personal mobility is still the most favourable way of human transportation. On the other hand, when active control of traffic implies that traffic flow is homogenized, the distinction with public transportation becomes somewhat smaller. Traffic management therefore also requires a change in attitude of the traffic participants.

Recent investigations in intelligent vehicle guidance, platooning and automated highways look ahead in this direction. Through tight intercommunication between vehicles or indirectly through in-road sensors, active distance control between vehicles can minimize congestion and homogenize traffic density. Moreover, the safety can be increased but at the cost of individual vehicle control. Developments in this area are ongoing, mostly still encountering problems with robustness and safety.

Along with adapting traffic systems, vehicle technology itself should continuously re-iterate to find a new optimum between fuel economy and the changing vehicle utilization. Governments can be effective in helping these actors to bring their influence in tune.

2.5.3 Law, policy and legislation

Speed limits set by law can manipulate the average speed in urban, rural and highway driving. On the other hand, a substantial decrease of speed limits is hardly accepted by society. Governmental legislation in the area of emissions and fuel consumption stimulate car manufacturers and research institutes in their search for new vehicle propulsion and fuel technologies. One can think of fuel taxes, emission standards and categorization of vehicles with respect to fuel consumption (using labels). Also subsidizing research initiatives in this area helps to find new ways for improving fuel economy and reducing emissions. Through educational programs, governments can make new generations more aware of the limited fossil fuel resources and the environmental impact of transportation. In this way the social basis for spending money and capacity of society into the improvement of fuel economy and reduction of emissions will get broader.

Chapter 3

Normalized Innovation Values

In practice, the most promising fuel saving principle is the one that achieves the highest ratio between fuel economy on the one hand and additional costs, size, weight, *etc.* on the other. The fuel economy obtained by exploiting an innovative idea may be termed *innovation value* whereas the mentioned penalties besides those related to development risks, complexity and driveability are termed *innovation efforts*. Hence, the most promising innovation is the one with the highest innovation values demanding the least innovation efforts. In this chapter, an attempt is made to judge the values over the efforts for the powertrain-related fuel saving principles mentioned in Section 2.4 or combinations thereof. This is defined as the *normalization* of the innovation values. Based on the normalization, the ZI powertrain proves to be the second best solution for saving fuel. The eventual decision to develop the ZI powertrain is supported by additional constraints overruling the outcome of the normalization. These constraints are set by the project target aiming at a fuel saving of 25% (the optimal solution can potentially save more) in combination with the limited project resources.

The remainder of this chapter is organized as follows. In Section 3.1 the theoretical fuel saving potentials are calculated and the results are analyzed. Next, in Section 3.2 the corresponding efforts, such as component efficiency, weight, driveability penalties and production costs, are discussed. In Section 3.3 the actual normalization of the innovation values is performed. Finally, in Section 3.4 conclusions are drawn with respect to the value of the ZI powertrain as a purely mechanical solution for saving fuel.

Throughout this chapter, examples of so-called *hybrid* vehicles are presented. For completeness, first a number of definitions related to hybrid vehicles are given in the next section.

3.1   Hybrid powertrains

A *hybrid* powertrain uses different types of power sources to propel the vehicle. The power source which primarily determines the range of the vehicle, is called the *primary* source. Additional power sources are referred to as *secondary* sources.

Hybrid vehicles can be operated in four different *modes*. The *conventional* mode applies when the primary source is *mechanically* connected to the wheels and moreover is the only active power source. If besides the primary source, a secondary source is mechanically connected to the wheels and active, the *parallel* mode applies. The *series* mode refers to the situation where the primary source is *not* mechanically connected to the wheels, hence all wheel

power is delivered by a secondary power source that acquires its energy non-mechanically from the primary source. Finally, the parallel mode and the series mode can occur at the same time. That case is referred to as the *combined* mode.

It is chosen to indicate the different types of operation as *modes*, instead of reverting to the commonly used terms *series, parallel and combined hybrids*, since a hybrid vehicle can generally be operated in either of the four mentioned modes. In practice, the combined mode is mostly encountered in so-called 'power-split' configurations, involving a planetary gear set.

Figure 3.1 schematically depicts a generic hybrid vehicle, capable of operating in all discussed modes. The component E represents the primary power source, whereas the wheel W on the right side of the figure represents the vehicle load. In between are a transmission T, a generator G, an accumulator A, and a motor M. The transmission T strictly has a variable transmission ratio, and possibly incorporates a planetary gear set. Fixed reductions are omitted for clarity, but may be present in any of the connections. All components may be separated by connecting interfaces, *e.g.,* mechanical (clutches) or electrical (actuation, wiring). The generator and motor can be separate devices but may also be combined into one component. In case of a flywheel as the secondary source, the motor, the generator and the accumulator are in fact all combined into a single device.
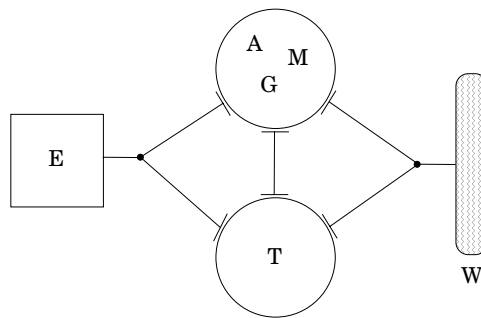
Figure 3.1: Generic hybrid powertrain configuration

As an example, the Toyota Prius powertrain is shown in Figure 3.2. Here the transmission T is a planetary gear set. The primary source E, a gasoline engine, is connected to the carrier of the planetary gear. The annulus gear is connected to the load W as well as to a secondary power source M1/G1, while the sun gear is connected to yet another secondary power source M2/G2. Both M1/G1 and M2/G2 can be operated as motor or as generator and are connected to the accumulator A. Because M1/G1 is directly connected to the wheels, it can be used as sole mover, hence the Prius is operated in series mode then. In all other cases, either the parallel or the combined mode applies. Charging the accumulator is possible using either parallel or combined mode. If the engine is delivering power, the secondary power source M2/G2 *must* always be active (motor or generator mode) to maintain a torque balance over the planetary gear set. Furthermore, the secondary source M1/G1 should always operate as a motor (either in series or combined mode) if the accumulator is fully charged.

22
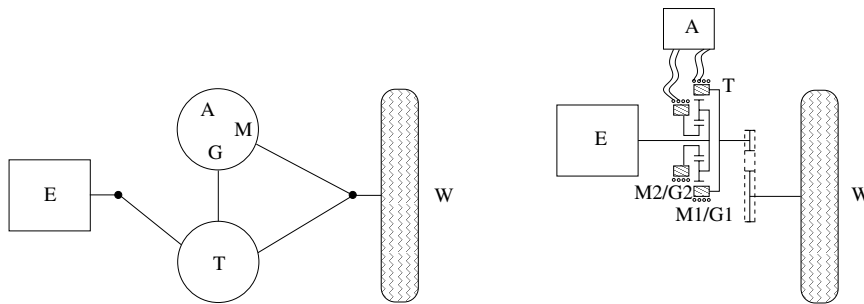
Figure 3.2: Toyota Prius powertrain (right) and its generic form (left)

3.2   Innovation values: fuel economy

First insights in fuel saving potentials are gained when mapping certain driving cycles directly onto the specific fuel consumption characteristics of the internal combustion engine. The innovation value (fuel economy) of each fuel saving principle is analyzed for the rural, city and highway driving cycle within the HYZEM (HYbrid technology approaching efficient Zero Emission Mobility) envelope and the NEDC. A driving cycle is a time representation of a requested vehicle speed trajectory, used for generating fuel consumption figures on a roller-bench with controllable brake facility (chassis dynamo meter). In practice, a human driver has to follow the speed trajectory within a certain margin. Measuring the fuel consumption as such appears to be somewhat deceptive, depending on the type of powertrain. For powertrains with manual transmissions the gear changes are prescribed during the drive cycle. This is not true for (all kinds of) automatic transmissions, for which in principle the gear shift strategies—or equivalently the engine operating points—may be chosen freely.

In the calculations underlying this chapter, for simplicity the vehicle is assumed to track the reference speed exactly. Furthermore, the freedom of choosing the engine operating points is adopted here in order to fully exploit the fuel saving principles. These assumptions provide a clear understanding in the mechanisms of the four fuel saving principles.

The influence of the transmission and conversion efficiencies on the fuel saving principles is regarded separately. The efficiency is unknown a priori and maximizing it is seen as one of the developing efforts to be undertaken. The underlying computations of this section hence assume a transmission efficiency of 100%. This assumption implies that the computed fuel consumption over a particular drive cycle and according to a certain fuel saving principle will be a theoretical minimum. It is therefore interesting to investigate how close this minimum can be reached in practice.

Using the outcome of this section, the innovation values will be corrected for efficiency and for increased weight and subsequently normalized in Section 3.3 using the efforts of various materializations presented in Section 3.2.

The fuel saving of the four principles, mentioned earlier in Section 2.4, is determined as follows:

- E-line tracking. The fuel saving of E-line tracking is determined with respect to operating lines roughly resembling operating lines seen in practice, see Section 3.2.1. Such lines are always a compromise between driveability and fuel economy;

- Stop-Go. The fuel saving due to Stop-Go operation is determined by subtracting the total amount of fuel otherwise consumed during engine idling at vehicle halt;

- Start-Stop. The fuel economy potential can be computed by assuming that the required energy is generated intermittently in the sweet spot if the momentary drive power is below or equal to the sweet spot power P_{ss}. Above P_{ss}, E-line tracking is performed;

- Brake Energy Recovery. The recovered energy can be used in a number of ways making it hard to determine the fuel saving potential unambiguously. In this section, the accumulated fuel required to deliver the energy needed for vehicle acceleration is assumed to be delivered in the sweet spot and is in Section 3.2 assumed to be fully recovered.

3.2.1   Reference vehicle

The vehicle that will be used as a reference in all the comparisons throughout this chapter is a mid-size passenger car, that weighs 1360 [kg], has a rolling resistance of 55 [Nm] and a c_d value of 0.31. It is termed the *reference vehicle*. The engine is a 1.6 ℓ 4-cylinder petrol engine with a maximum power rating of 75 [kW] at 540 [rad/s], and is assumed to be operated on the *reference operating line*, that is defined further on. The E-line collects the engine operating points which are fuel-optimal for a given power level, and can be uniquely determined for any engine. Figure 3.3 depicts the E-line and operating lines $OL_{x\%}$ comprising operating points with $x\%$ higher fuel consumption compared to the E-line. Also depicted is the *Wide Open Throttle (WOT) line*, which represents the maximum engine torque as a function of the engine speed. The E-line is jagged because of the limited number of measurements combined with the small
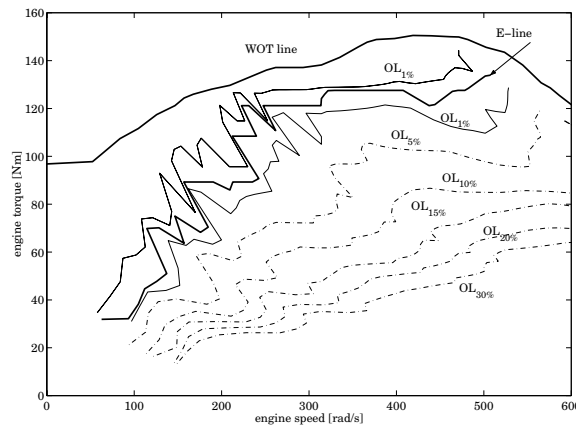
Figure 3.3: E-line and operating lines with $x\%$ more fuel consumption

differences in fuel consumption around the E-line, as is shown by the two lines indicating a margin of 1% extra fuel consumption with respect to the E-line. In practical implementations, a smoothened version of the E-line is used.

In today's passenger cars, if equipped with either a CVT or AT, an operating line roughly between the $OL_{15\%}$ and $OL_{20\%}$ lines is applied for stationary situations. Using such an operating line results in an acceptable driveability but clearly penalizes the fuel economy, as

compared to the E-line. Here, the $OL_{15\%}$ is chosen as the reference operating line for computing the fuel saving potentials. This operating line is highly similar to those used in 4-AT and CVT in 'performance mode'.

3.2.2 Influence of driving cycles

There exists a wide variety of certified driving cycles, showing large differences in power requests, dynamics, average speed, *etc.* From these cycles, the HYZEM and NEDC are chosen to determine the innovation values. The HYZEM cycle consists of three sub cycles, namely the urban (city), rural and highway cycle. Since the HYZEM was obtained by averaging typical vehicle usage in Europe it is thought to be a good representation of everyday driving. The potentials of the four fuel saving principles depend highly on the considered cycle.

In Figure 3.4 power histograms of the HYZEM (urban, rural, highway) and NEDC cycles are shown. The required power is calculated using a model of the reference vehicle. The power histograms are obtained using steps of 1 [kW]. Especially for the NEDC and the urban drive cycle, the time fraction spent at zero power (vehicle halts) is remarkably large. Furthermore, power demands larger than half the maximum engine power are rare on the depicted driving cycles.
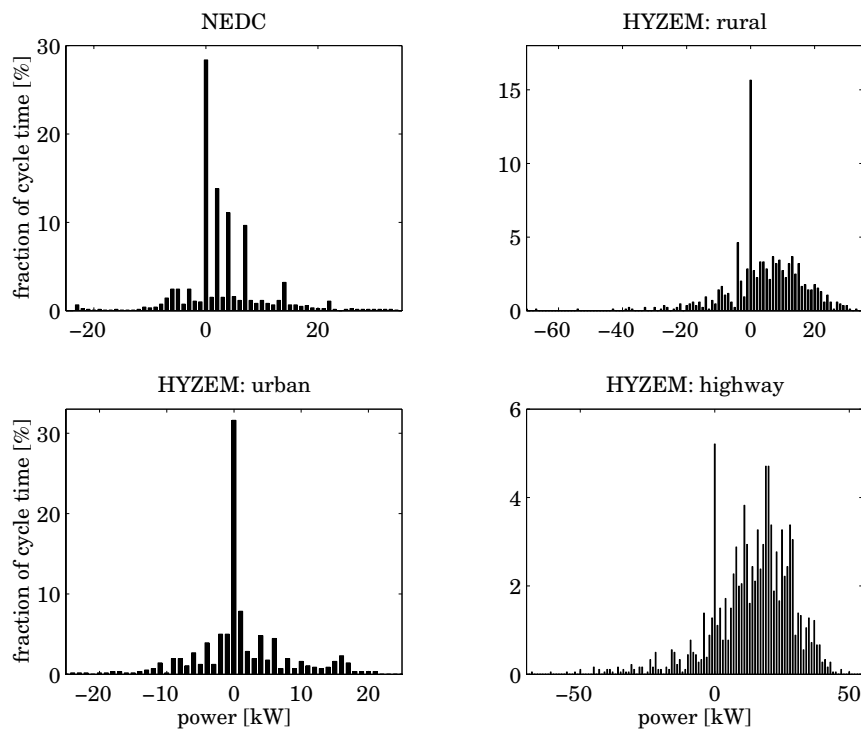
Figure 3.4: Time histograms of power distribution over the drive cycles

3.2.3 Fuel economy

In this section, the fuel savings with respect to the reference operating line $OL_{15\%}$ are evaluated, using the mentioned drive cycles, for each of the four fuel saving principles.

E-line tracking

The accumulated fuel consumption in [g] and the percentage of fuel consumption reduction for the four driving cycles are shown in Table 3.1. From this table it is apparent that the

CYCLE	$OL_{15\%}$ [g]	E-LINE [g]	E-LINE FUEL SAVING [%]	IDLE [g]	STOP-GO FUEL SAVING [%]
NEDC	556.7	493.5	11.4	64.4	11.6
rural	568.4	498.0	12.4	19.0	3.3
urban	205.1	183.5	10.5	30.5	14.9
highway	2460.3	2142.1	12.9	13.0	0.5

Table 3.1: Fuel savings using E-line tracking and Stop-Go

fuel consumption reduction for E-line tracking is between 10 and 13.0%, approximating the maximally achievable fuel saving $((1 - 1/1.15) \times 100 = 13\%)$ of E-line tracking with respect to the $OL_{15\%}$. The 13% fuel saving is reached when the contribution of engine idling converges to zero, which is almost the case on the highway sub cycle, where a relatively short standstill time applies (5.5% of the total cycle time). Furthermore, the average power level on this cycle is high compared to the other cycles.

Stop-Go

The fuel savings when using Stop-Go (also see Table 3.1) can amount up to 15% on the urban sub cycle, assuming that the restarts of the engine require no additional energy. Also, incomplete combustions during starting, leading to a slight increase in fuel consumption and emissions are not treated here. Hence it is assumed that the fuel saving exactly equals the accumulated idle fuel consumption (where the time-specific idle fuel consumption is taken to be 0.23 [g/s]). The impact of Stop-Go on the highway sub cycle is obviously limited, again due to the limited contribution of engine idling.

Start-Stop

The Start-Stop principle can be best explained looking at the specific fuel consumption (BSFC) of the engine as a function of the output engine power. For the E-line and the $OL_{15\%}$ this BSFC characteristic is plotted in Figure 3.5. From this figure it can be concluded that around P_{ss}=32 [kW] there is a minimum, previously called the sweet spot. Consequently, fuel can be saved when for all requested powers below P_{ss}, the drive energy is delivered in the sweet spot operating point. Operating the engine in the sweet spot requires intermittent (duty-cycled) operation of the engine to match the generated energy to the required drive energy. Furthermore, an accumulator is required to store the generated energy. Apart from that, Start-Stop necessitates an extra motor and generator to compensate for the momentary power deficit and surplus, respectively. For power requests beyond P_{ss} the engine must be operated on a regular operating line. In this case, the E-line is chosen.
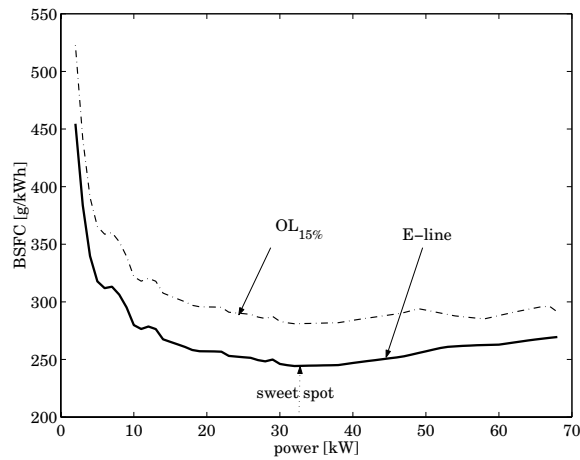
Figure 3.5: Brake specific fuel consumption for the $OL_{15\%}$ line and the E-line

The maximum fuel saving potential for the Start-Stop principle with respect to $OL_{15\%}$ and with respect to E-line+Stop-Go, is shown in Table 3.2. The latter fuel savings (last column) are included to show the merit of Start-Stop for requested power levels larger than zero and smaller than P_{ss}. Note that Stop-Go and E-line tracking for power levels beyond P_{ss} were chosen to be an integral part of the Start-Stop principle.

CYCLE	$OL_{15\%}$ [g]	START-STOP [g]	FUEL SAVING [%]	FUEL SAVING W.R.T. E-LINE + STOP-GO [%]
NEDC	556.7	347.5	37.6	14.6
rural	568.4	419.4	26.2	10.5
urban	205.1	119.8	41.6	16.2
highway	2460.3	2018.4	18.0	4.6

Table 3.2: Fuel savings using Start-Stop

A number of observations are made. First, the saving potential is especially high for city driving (urban and NEDC). This can be explained by the poor engine efficiency at low output power levels even in case of E-line tracking, in combination with the large share of required power levels beneath P_{ss} for such cycles. Second, the improvement of fuel economy over E-line+Stop-Go is rather limited for the highway cycle. For such a cycle, the power histogram is largely concentrated around P_{ss} and beyond. Moreover, around the sweet spot the specific fuel consumption is already quite low and rather insensitive for the power level, *cf.* Figure 3.5. The resemblance between the fuel savings for urban and NEDC with respect to E-line+Stop-Go may become clear when observing the similarity between the power histograms of the two (see Figure 3.4).

brake energy recovery

In principle, the kinetic energy of the vehicle that is normally dissipated at the wheel brakes can be recovered. In this section, a number of rigorous assumptions underlie the calculated fuel saving potentials of brake energy recovery:

- all vehicle braking is performed by a generator. This assumption implies radical demands on the maximum power of the generator and control periphery as well as its reliability and safety;

- the kinetic energy is completely re-used for propulsion of the vehicle;

- all transmission and conversions involved occur with 100% efficiency.

In Section 3.3, these assumptions are partly released. Table 3.3 lists the computed savings using these assumptions. The first (numerical) column repeats the fuel consumption figures for $OL_{15\%}$. The above assumptions imply that the required drive energy exactly equals the energy which is dissipated by the road load. The fuel needed for delivering this energy is calculated operating the engine in the sweet spot, and hence is the minimal fuel consumption theoretically possible with the reference vehicle and the adopted engine. Delivering the road load energy using other strategies than sweet spot poses problems of ambiguity. The recovered brake energy can be reused for assisting the engine in a number of ways. The strict relationship between the requested drive power and specific fuel consumption may then disappear. This ambiguity does not occur when persistently delivering the cycle energy in the sweet spot. This implies that the computations assume that the Start-Stop principle is integrated in brake energy recovery.

Note that such operation is impossible during prolonged driving at power levels higher than P_{ss}. However, in the highway cycle, the power levels above P_{ss} (32 [kW]) are linked to short term vehicle accelerations, while the average power level on this cycle still is below P_{ss}. Also, in the computations it was implicitly assumed that the surplus of requested power beyond P_{ss} is delivered by the additional accumulator, in order to keep the engine in the sweet spot.

CYCLE	$OL_{15\%}$ [g]	ROAD LOAD IN SWEET SPOT [g]	FUEL SAVING [%]
NEDC	556.7	269.8	51.5
rural	568.4	284.8	49.9
urban	205.1	65.6	68.0
highway	2460.3	1823.2	25.9

Table 3.3: Fuel savings using brake energy recovery and Start-Stop

3.3   Innovation efforts

In this section a number of innovation efforts is defined and evaluated for the fuel saving principles. Somehow quantifying these efforts—often just using relative ranks such as 'high', 'low', 'average'—provides ways to compare the saving principles. Efforts, when applicable, treated for each principle are:

- additional fuel economy penalties depending on the specific technology and configuration (transmission and conversion efficiencies, supplementary weight, *etc.*);

- driveability aspects such as instant power reserve, engine restarts, noise-vibration-harshness (NVH), comfort, predictability;

- impact on total vehicle design, for example packaging, vehicle dynamics, safety;

- additional costs of development, manufacturing, materials;

- complexity leading to penalties for robustness, durability, maintenance, control development;

- environmental aspects such as recycleability, emissions.

3.3.1   E-line tracking

transmission efficiency

The fuel economy for E-line tracking is influenced by the limited transmission efficiency η_t. Especially in the case of cycles showing insignificant idling phases, the influence of the transmission efficiency on the fuel economy is near to linear. For instance, increasing η_t from 80 to 100%, reduces the fuel consumption of the reference vehicle (at the $OL_{15\%}$) on the urban cycle by 13.6%. For the highway cycle this fuel economy improvement is 18.6%, that is almost the transmission efficiency difference, 20%. Lowering the efficiencies of two identical vehicles, one controlled at the $OL_{15\%}$ and the other at the E-line, hardly influences the *relative* fuel saving (less than 0.5% when altering the η_t from 80 to 100%).

driveability

Driveability is for the larger part determined by the instant availability of power when pressing the accelerator pedal. The so-called *power reserve* is the product of the actual engine speed and the *torque reserve*, where the torque reserve is defined as the difference between the actual and maximum (WOT) engine torque. As can be seen in the engine map (Figure 3.3), when for a given power level the engine is operated at a higher engine speed and a larger torque reserve, a much larger power reserve results at the expense of fuel economy. This observation is more exemplified in Figure 3.6, where the *power reserve* is plotted against the actually delivered engine power. The driveability is improved tremendously when leaving the E-line for an operating line below it. For instance, choosing $OL_{15\%}$ degrades fuel efficiency by 15% but increases the power reserve by a factor 4 to 7. The dashed line indicates the maximum power reserve possible, truncated by the engine speed that corresponds to maximum engine power. All operating lines coincide at this line, tending to zero power reserve when approaching the maximum engine power (75 [kW]).

In the previous reasoning it was assumed that the engine torque can be changed instantaneously and without penalty. Changing the engine speed could (eventually) increase the output power as well, though the dynamic response of the vehicle—and thus its driveability—is penalized greatly when the engine acceleration is too large.

The physical background for this can be found in the primary-sided or, for short, *primary inertia*, *i.e.,* the total inertia of the components directly connected to and including the engine. Although the primary inertia is relatively small compared to the vehicle inertia, for good driveability it is of great relevance that the engine can be swiftly accelerated by *shifting down*

29
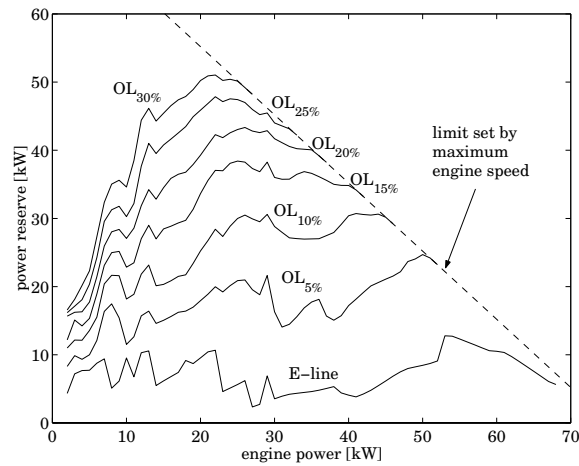
Figure 3.6: Power reserve as a function of stationary power for various operating lines

the transmission, *i.e.,* lowering the transmission ratio (defined as output speed divided by input speed). The engine power reaches its maximum at a fairly high engine speed. If the transient to this maximum power is required to be fast, the acceleration of the primary inertia (shortly) requires a power level similar to the power needed for the actual propulsion of the vehicle. When in such a case the engine was operating at low speed and high torque, *i.e.,* with a small power reserve, fulfilling an acceptable power transient is deemed impossible. Instead, to facilitate the acceleration of the primary inertia power flows from the vehicle to the engine, consequently shortly decelerating the vehicle instead of accelerating it.

When shifting down the transmission more slowly, the increase of wheel power might show a latency as the available power reserve is just enough to accelerate the primary inertia and cannot be used for a prompt increase of wheel power. This degrades the sensitivity of the accelerator pedal as the requested higher power is delivered after the primary inertia has accelerated. This phenomenon is referred to as 'jet start' (also known as shift-shock, rubber belt effect, torque hole, worn clutch effect). Jet start behaviour is known from aircraft propulsion, where initially all combustion power must be used to accelerate the turbines before the increased engine power can be used to propel the aircraft. For pedal back-out the phenomenon also occurs but then reversely, because the instant decrease of power is counteracted as the engine speed decreases.

Jet start can be minimized by persistently operating the engine at high speeds at the expense of fuel economy, for example using the line $OL_{15\%}$. Even then, the transmission ratio shift speed cannot be arbitrarily high, so an advanced control strategy is required to yield an acceptable compromise between fuel economy and driveability. The advantage of using controls (software) to counteract the driveability problem is that such a solution can be flexible and cheap, as opposed to rigid and generally more expensive hardware solutions. On the other hand, pure hardware solutions will be more robust and often inherently stable, whereas software solutions cannot extend physical system limitations. The additional costs for modified hardware (and to a lesser extent, software) largely depend on production numbers.

An example of a pure hardware solution is lowering the primary (engine) inertia while

30

simultaneously increasing the number of cylinders in order to compensate for the lack in torsional damping, as suggested, *e.g.,* in [Guo *et al.,* 1988]. Such a solution is quite expensive and moreover rather ineffective, since the remaining inertia can still adversely influence driveability. If the primary inertia were zero, the engine output torque would be independent of the engine acceleration. The 'Zero Inertia' solution, to be elucidated in Chapter 4, will be shown to partly realize this.

If the compromise between fuel economy and driveability is considered unacceptable, E-line tracking demands an additional power source. The additional power source has to fill up the power gap between the actual power level and a (higher) requested power level. This should be done as long as the engine itself has not reached the requested power level yet, *i.e.,* during acceleration of the engine by altering the transmission gear ratio.

Figure 3.7 shows an illustrative example of this mechanism. In the example, it is assumed that the driveability level reached with the $OL_{15\%}$ is acceptable in practice. In other words, the additional power source should at least raise the power reserve of E-line tracking up to the power reserve reached when tracking the $OL_{15\%}$, see Figure 3.6. The left plot in Figure 3.7 depicts the engine combustion power $P_{combustion}$, the power from the primary inertia $P_{inertia}$, and their combined total $P_{e.total} = P_{combustion} + P_{inertia}$. The right plot shows the wheel power $P_{desired}$ as it is assumed to be desired. To arrive at the desired power, an additional power, depicted in the middle as P_{assist}, is needed. In this example, a stepwise power transient from 20 [kW] (roughly corresponding to a stationary vehicle speed of 110 [km/h]) to 50 [kW] is desired. Operating on the $OL_{15\%}$, this step can be performed without increasing the engine speed, see Figure 3.6. When starting from the E-line, the engine power reserve is only 10 [kW], hence a power assist source of at least 20 [kW] is needed. However, for a prolonged increase of wheel power, the engine must be accelerated to arrive at a speed where it can maintain the desired power level of 50 [kW]. In this example the engine speeds up from 230 [rad/s] to 330 [rad/s] (corresponding to 20 and 50 [kW] on the E-line, respectively) in a time interval $\Delta t = 0.8$ [s]. Hence, an additional power $P_{inertia}$ between 7 and 10 [kW] is required to perform the acceleration of the engine inertia. As a result, the necessary power level P_{assist} of the assist source amounts up to 27 [kW], such that $P_{e.total} + P_{assist} = P_{desired}$.
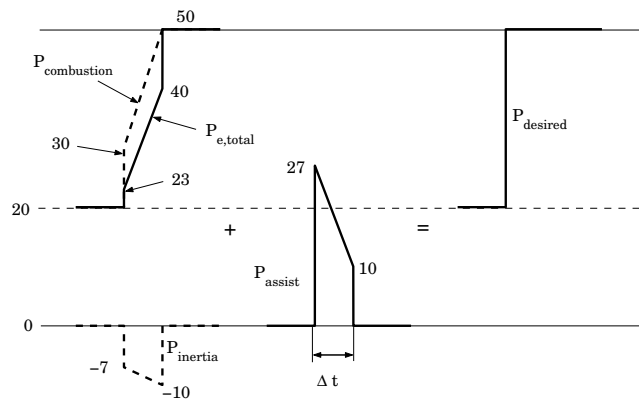
Figure 3.7: Realization of a power transient; power levels in [kW]

power assist sources

Examples of power assist solutions are:

- electric motor + battery;

- electric motor + battery + ultra-capacitor;

- flywheel + transmission;

- flywheel + electric motor.

Table 3.4 lists some relevant weight-specific ([·/kg]) quantities for a number of power source technologies and related components. In this table, PM refers to permanent magnet, EM means electric motor (synchronous and asynchronous), NiMH is Nickel Metal Hydride, Li-ion means Lithium-ion, FESS refers to Flywheel Energy Storage Systems and embodies high speed flywheels (carbon-glass fiber composites) in vacuum casing combined with a directly connected electric motor. The ZI flywheel refers to the low speed, steel flywheel that is used

	P [kW/kg]	V [l/kg]	E [Wh/kg]	C [€/kg]	η [%]	L [cyc.]
PM synch. EM	1	0.3	–	?	87–92	
asynch. EM	0.4	0.7	–	15–80	85	
NiMH battery	0.18–0.9	0.6–1.3	17–100	10–50	65–85	1–$2 \cdot 10^3$
Li-ion battery	0.15–1.4	0.6–0.7	30–120	15–100	90	$> 10^3$
ultra-capacitor	1–5.5	0.8	1–50	> 10	85–98	$> 5 \cdot 10^5$
flywheels (FESS)	0.75–1.5	0.4–1.0	2–50	30	83–90	$> 10^7$
ZI flywheel	1.5–3.5	0.14	0.2–2	10	98–99	$> 10^8$
(planetary) gearing	1–3	0.3–0.8	–	10	96–99	$> 10^7$
clutch (slipping)	1.5–2	0.3	–	10	50	$< 10^5$

Table 3.4: Specific values: P=specific (peak) power, V=specific volume, E=specific (peak) energy, C=specific cost, η=conversion efficiency into mechanical or electrical power, L=lifespan

in the ZI powertrain, and is discussed in this thesis. Gearing and clutches are included to show the possibly needed efforts for extracting power mechanically. The specific values for clutches are valid for a slipping clutch, since those situations are limiting the power density, especially. Values are taken from [Dietrich, 2000, Lehna, 1998, Paefgen and Lehna, 1997, Thoolen, 1993, Office of Technology Assessment, 1995, Kok, 1999] and include the corresponding power-electronics and cooling in case the energy domain is electrical. Some exceptions are not included in this table. For instance, [Dietrich, 2000] reports on *alu-elco* capacitors that reach specific power values of 10 [kW/kg] though always in combination with specific energies no higher than 0.01–0.1 [Wh/kg]. Furthermore, American Flywheel Systems, in conjunction with Honeywell claims energy densities which seem very high (over 130 [Wh/kg]) relative to other flywheels that have been built, though no official performance publications exist [Office of Technology Assessment, 1995]. The lifespan of the ZI flywheel is deemed higher than FESS because the material stress is far below the maximum allowable value, and moreover, the bearing speeds are lower. Considering this table the following observations are made:

- the ultra-capacitor and the ZI flywheel have the highest specific power. The latter shows low energy density;

- batteries excel in energy density but are costly and lower in efficiency and lifespan;

- FESS possesses mediocre figures in every category; lifespan, however, is exceptional.

Some of the technologies are also graphically presented in a spider diagram, see Figure 3.8. Webs lying further outward indicate higher ranking, and thus lower efforts. For that purpose, specific cost and volume are inverted, whereas for the lifespan L, logarithmic values are used.
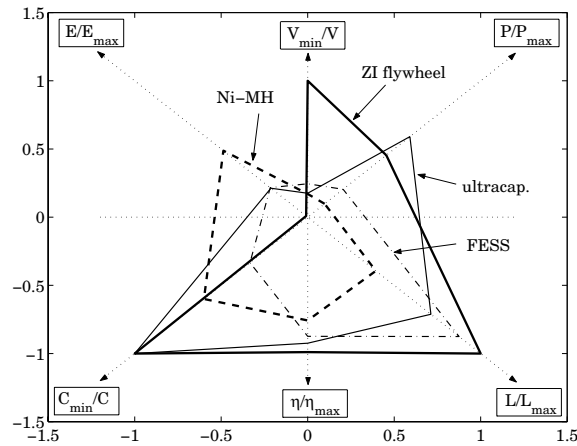
Figure 3.8: Spider diagram for comparison of innovation efforts related to various power sources, 'min' and 'max', corresponding to the specific values in Table 3.4

An example power assist system is elaborated, for a power level of 27 [kW] and energy contents of 18 [Wh]. The power specification is based on the discussion in the above section, where a power assist level of 27 [kW] was concluded to be necessary for an acceleration from 110 [km/h], when operating the engine on the E-line. For lower vehicle speeds, the power requirements are smaller, mainly because the difference in engine power reserve between the E-line and the $OL_{15\%}$ decreases. On the other hand, the mentioned difference in engine power reserve increases with higher vehicle speed, in principle yielding higher power assist demands. However, the acceleration performance from vehicle speeds far beyond 110 [km/h] is considered to be less relevant in practice. The energy contents specification is obtained as the sum of the kinetic energy increase for the maximum speed transient (approximately from 100 [rad/s] to 550 [rad/s]) and the combustion energy that is lacked during the transient time interval Δt (Figure 3.7).

For these specifications, a mechanical system with ZI flywheel is compared with two electrical power assist systems, one with a NiMH battery and one with an ultra-capacitor, see Table 3.5. The ZI flywheel system clearly outperforms the other two. The NiMH system is least attractive, especially with respect to weight and total efficiency. Furthermore, both electrical systems are more expensive by an order of magnitude. On the other hand, the electrical systems can potentially be used for other functions in a more flexible way. As a commercially available example, the Honda Insight uses a 10 [kW] (peak) neodymium PM brushless DC motor weighing approximately 50 [kg], a 0.94 [kWh] NiMH battery-pack weighing 20 [kg],

	mass [kg]	volume [l]	cost [€]	efficiency [%]
asynch. EM + NiMH	126	103	4970	41
asynch. EM + ultra-cap.	78	55	3330	60
ZI flywheel + gearing	34	16	340	91

Table 3.5: Comparison between three power assist systems for 27 [kW], 18 [Wh]

and an ultra-capacitor of circa 6 [kg]. Besides, a high-density inverter is present which operates as a DC-DC converter as well as a motor cooler. In total, the additional weight of the secondary power source of the Honda Insight, which is designed for power assist and Stop-Go operation, is around 75 [kg]. The additional weight adversely affects fuel economy. The combined effects of efficiency and weight are evaluated in Section 3.3.

An interesting example of a hybrid system for application in the upper-size vehicle class is the so-called *E-Automat* developed at the University of Chemnitz [Tenberge, 2001], which combines an existing 6-AT with a circa 10 [kW] electric motor.

miscellaneous efforts

Apart from the fact that an additional power source is needed to solve the driveability problem associated with E-line tracking, a CVT is required to exactly track the E-line. In case a stepped transmission is used, some penalty on the fuel consumption reduction is to be expected. On the other hand, the fact that the transmission efficiency of a CVT is generally lower than that of a stepped transmission (especially MT) will partly cancel out the obtained fuel reduction [Yamamoto and Aoki, 2000]. Moreover, for E-line tracking the transmission must be automatic (AT or CVT) or automated (Automated Manual Transmission, AMT). Furthermore, the ratio coverage of the transmission must generally be much larger than that of commercially available stepped transmissions and even CVTs. However, the penalty on fuel consumption reduction when using a 6-AT, 6-AMT or CVT (ratio coverage between 5 and 6) is comparatively small [Hofmann *et al.*, 1998]. Additionally, requiring the ratio coverage to be much higher necessitates significant modifications (*e.g.*, larger transmission size, 'i^2-transmissions' [Höhn, 1994; 2001]). Finally, an electronic throttle (drive-by-wire) is necessary, but is getting more common in modern passenger cars anyway and the additional cost is relatively small.

The remaining efforts are related to software development especially. Drive-by-wire poses additional safety and reliability issues. Furthermore, E-line tracking tends to decrease CO_2 emissions but increase NO_x, thus new engine management strategies dedicated to E-line tracking are mandatory. For a CVT or a wide-spread 6-AT, manufacturing costs and complexity are relatively high. The production numbers for AT are much higher than for CVT and the latter is still maturing with regard to durability, robustness and maintenance infrastructure. Operating the engine at very low speeds and high torques may introduce additional problems with respect to NVH. On the other hand, cruising at low engine speeds is generally associated with high comfort.

The additional power source may be used for other functions as well, *e.g.*, as a starter-alternator. Such a machine is well equipped to meet the increasing electric power demands (such as air conditioning, power steering and brake assist), which are debit to the increased research into a 42 Volt on-board electrical net. Furthermore, a starter-alternator but also a low speed flywheel may be used to implement a Stop-Go system, *i.e.*, engine shutdown at vehicle standstill. This is the topic of the following section.

34

3.3.2 Stop-Go operation

Stop-Go, like E-line tracking, requires an additional power source. Different technologies can be thought of to facilitate the frequent engine restarts, that is an electric motor, a flywheel, *etc.*

system requirements

The engine speed where combustion is resumed is a trade-off between starting-time and power demand on the one hand and emissions and noise on the other. Also, when the launching clutch is engaged after engine restart, the engine torque must be sufficient to propel the vehicle. When assuming the engine must be accelerated towards idle speed (around 800 [rpm]) within 0.15 [s], the power and energy requirements for Stop-Go are 12.6 [kW] and 0.26 [Wh], respectively. In case of an *impulse-start* (*i.e.,* using inertia force to start the engine, see [Vroemen, 2001]), the power requirements can be lower, but the starting-time may be longer if the inertia has to be accelerated first.

efficiency

The efficiency of the additional power source is important for the absolute amount of energy needed for an engine restart. The additional losses (*e.g.,* due to an increased mass) when not using the extra power source deteriorate fuel economy. Depending on the way the energy required for Stop-Go is subtracted from the powertrain, the fuel saving potentials may vary. For instance, when combining Stop-Go with brake energy recuperation, the fuel savings due to Stop-Go are as large as indicated in Table 3.1. On the other hand, when the energy is generated by the engine running in arbitrary operating points, the absolute fuel saving is as large as the fuel required for idling minus the fuel required for generating the accumulated restart energy. If the restart energy is generated in the sweet spot an unambiguous upper limit for the fuel saving can be obtained. Incorporating this as well as 50% efficiency (average) for the Stop-Go system itself (see Table 3.6), the *deterioration of the fuel saving* amounts up to just 0.3% for the urban and the NEDC cycle, whereas for the other two cycles the difference is even less significant.

In Stop-Go, the efficiency of the transmission between engine and wheels does not influence the *absolute* fuel-savings, but the *relative* savings instead. A decrease in fuel-consumption due to an improved transmission raises the relative fuel-savings for Stop-Go. For example, the fuel consumed on the urban cycle decreases by 13.6 [%] when improving the transmission efficiency from 80 to 100%, while the potential relative fuel-savings from Stop-Go increase from 12.8 to 14.9%.

Table 3.6 compares the three systems from Table 3.5, but now for Stop-Go application. The two electrical systems are assumed to use *direct-start* (starter-alternator directly connected to the crank shaft), the flywheel system naturally uses impulse-start. An impulse-start system, whether purely mechanical or 'semi-electrical' (*i.e.,* the rotor of the starter-alternator is used as inertia) always requires an additional clutch. Again the mechanical solution offers advantages

	mass [kg]	volume [l]	cost [€]	efficiency [%]
asynch. EM + NiMH	56	46	2205	41
asynch. EM + ultra-cap.	35	25	1470	60
flywheel + gearing + clutch	20	9	200	49

Table 3.6: Comparison between three Stop-Go systems for 12 [kW], 0.26 [Wh]

over the two electrical systems, although the total efficiency is better for the ultra-capacitor variant.

driveability

In commercially available Stop-Go systems, the vehicle response to accelerator pedal motions is delayed, because none of them simultaneously start the engine *and* launch the vehicle. The combined time needed for engine restart followed by possible clutch-actuation delays, should not exceed approximately 0.2 [s]. Longer delays are known to cause annoyance and lack of confidence by the driver. The ZI Stop-Go solution, as treated in Part III, is able to immediately launch the vehicle and meanwhile restart the engine. The potential for acceptance is expected to be higher this way. For Stop-Go systems in general, the frequent engine restarts should be more refined and silent, for reasons of comfort.

miscellaneous efforts

The reliability of the engine start should be increased by an order of magnitude with respect to conventional starter systems, because of the more frequent engine restarts. Also, some dedicated type of (battery or flywheel) State-Of-Charge (SOC) management must anticipate for a possible energy deficit, and consequently decide not to shut down the engine.

The engine emissions can be lower than in a conventional engine start. They largely depend on the engine speed where combustion is resumed and on the engine temperature. More importantly, the temperature of the catalytic converter should not drop dramatically during engine shutdown. Straightforward solutions include heating and encapsulation of the catalyst. The power take-off supply must be taken over by the secondary power source while the engine is shutdown.

A possible additional function of starter-alternators is active oscillation attenuation, for the driveline and for the engine especially, see [Zeyen and Pels, 1997]. Other than actively, the rotor of an electric machine will also attenuate oscillations in a passive way, mechanically and electrically. Because the additional power source can replace the conventional engine-flywheel, the impact on overall vehicle design may be relatively small, though larger than for E-line tracking due to the significant changes in vehicle operation.

3.3.3   Start-Stop operation

The efforts linked to duty cycled engine operation are related to the following three types of operation and the transitions between them:

- engine on: sweet spot operation;

- engine off: driving on secondary power source;

- conventional driving beyond sweet spot.

Start-Stop at least requires the series mode. In terms of the definitions from Figure 3.1, the primary power source E then charges the accumulator A by the generator G while the motor M propels the wheels W. Depending on the accumulator's SOC, the primary source E is shut down intermittently. Start-Stop can also be realized using parallel mode, but then the series mode has to be incorporated as well. When E directly propels the wheels W, G diverts the surplus of power (delivered in the sweet spot) into A. When A is fully charged either M or E

should propel the vehicle. The former then equals the series mode, whereas the latter in fact is conventional driving.

component efforts

For sweet spot operation the surplus of power varying from zero to P_{ss} has to be stored in the accumulator. The transmission between the primary and secondary energy source has to be able to split P_{ss} into a varying power P_w to the wheels and a power $P_{ss} - P_w$ to the accumulator. Hence the generator, accumulator and motor have to be dimensioned such that powers maximally up to P_{ss} can be dealt with. The primary source must be shut down when either the SOC of the accumulator has reached its upper limit, or when the power request is below P_{ss} and the SOC has not reached its lower limit yet. The primary source must be restarted whenever the SOC drops below the lower limit or when the power request is higher than P_{ss}. This manner of engine operation requires sophisticated controls in order not to impair driveability under the constraint that fuel economy should be optimized. This is not always as straightforward as it seems. For instance, consider a stationary situation where the primary power source is shutdown and the secondary source is delivering a power slightly below P_{ss}. If the driver suddenly asks for a large increase in power, the primary power source must be restarted quickly. Clearly, the power reserve to restart the primary source is close to zero, and hence insufficient. In order not to withdraw this power from the vehicle, yet another secondary source is needed. The Nissan Tino [Matsuo *et al.*, 1999] operates as such. The situation is even worse in the Toyota Prius (recall Figure 3.2), where electric motor M2/G2 is responsible for restarting the engine E, and in doing so actually exerts a negative torque at the wheels through the planetary gear. Moreover, to enable the switching between the sources, clutches or some kind of infinitely variable transmissions are needed.

efficiency

The efficiencies of the conversion and transmission of energy greatly influence the fuel saving potential. Let E_{cyc}^+ be the energy needed at the wheels for driving a certain cycle, and E_{cyc}^- the potentially recoverable energy which is normally (*i.e.*, in a conventional vehicle) dissipated at the brakes or in the engine. The actually recovered energy E_{BER} will generally be smaller than E_{cyc}^- if the generator power is limited. The net energy that is minimally needed for all but the vehicle's kinetic energy is $E_{cyc} = E_{cyc}^+ - E_{cyc}^-$. If part of this energy is drained from the accumulator and not *replenished* before the end of the driving cycle, the type of operation is called *charge depleting* [Müller and Köhle, 2000]. If on the other hand no charging from outside the vehicle takes place during the driving cycle, the vehicle is said to be *charge sustaining*. If the vehicle is charge sustaining and, moreover, the accumulator's SOC at the start and at the end of the driving cycle are equal, all the required energy must be supplied by the primary power source. This situation is depicted in Figure 3.9, where η_T and η_{II} are the efficiencies of the transmission and of the 'secondary path', respectively. The latter efficiency at least comprises the efficiencies η_G, η_A and η_M of the generator, accumulator and motor, respectively, and also the mutual conversion efficiencies $\eta_{G \to A}$, $\eta_{A \to M}$, $\eta_{M \to W}$, and either $\eta_{E \to G}$ or $\eta_{W \to G}$, depending on the direction of the energy flow. If the secondary sources are directly connected to the primary source and the wheels, $\eta_{E \to G}$ and $\eta_{M \to W}$ are both equal to 1. The accumulator efficiency η_A is included to somehow reflect the effect of (time-dependent) self-discharge. For flywheels, η_A accounts for air drag induced self-discharge, while η_G and η_M are 1, since no energy conversion is required. For a hybrid vehicle like the Nissan Tino [Matsuo *et al.*, 1999], the power of both secondary power sources must pass through the transmission, hence the
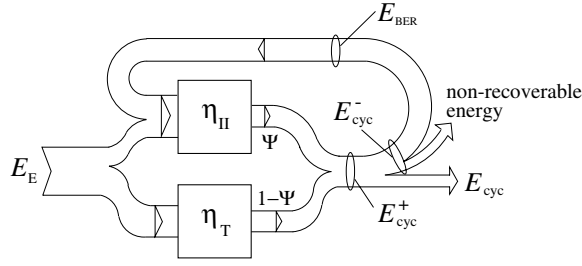
Figure 3.9: Energy flows

transmission efficiency η_T would appear twice in η_{II}. On the other hand, part of the secondary power may not always have to pass through the accumulator, thus increasing η_{II}. The total energy E_E that is to be delivered by the primary source, is given by

$$E_E = E_{cyc}^+ \left(\frac{1 - \Psi}{\eta_T} + \frac{\Psi}{\eta_{II}} \right) - E_{BER} \tag{3.1}$$

where the term E_{BER} is only present if brake energy can be recovered. Else, all energy E_{cyc}^- is non-recoverable.

The factors Ψ and $1 - \Psi$ represent the relative parts of E_{cyc}^+ that pass through η_{II} and η_T, respectively. Ψ depends on the duty-cycle strategy of the engine, as well as on the driving cycle, and is not known a priori for a given hybrid powertrain or arbitrary journey, except for a pure series hybrid, where $\Psi = 1$. If the engine is intermittently operated only in the sweet spot, Ψ must be larger than 0, in order to meet power demands below P_{ss}. In fact, Ψ can be viewed as a '*hybridization factor*', although other definitions are encountered in literature. For instance, [Baumann *et al.*, 1998] defines the Degree Of Hybridization *DOH* for a hybrid vehicle operating in two different Energy Domains (ED), as

$$DOH = 1 - \frac{|P_{max,ED1} - P_{max,ED2}|}{P_{max,ED1} + P_{max,ED2}} \tag{3.2}$$

For $DOH = 1$ the hybridization is maximal, whereas $DOH = 0$ for a conventional vehicle and also for a purely electric vehicle. In [Müller and Köhle, 2000], hybrid vehicles are classified depending on the relative share of the battery in the total energy storage on the one hand, and of the electric motor in the total output power on the other.

In Figure 3.10 contour lines of the *relative fuel consumption* $\mathcal{F}(\Psi) = f / f_{OL_{15\%}}$ are drawn as a function of Ψ and η_{II}. Here, f represents the actual fuel consumption of the Start-Stop system with mechanical efficiency η_T, whereas $f_{OL_{15\%}}$ is the fuel consumption, when driving along the $OL_{15\%}$ operating line, with the same mechanical efficiency η_T. Realistic values $\eta_{II} = 0.44 \ (= \eta_G \cdot \eta_{G \rightarrow A} \cdot \eta_{A \rightarrow M} \cdot \eta_M = 0.88 \times 0.75 \times 0.88 \times 0.75)$ for an *electrical* secondary power source and $\eta_T = 0.85$ for a CVT, are indicated in the figure by dashed lines. The increased weight of such a hybrid vehicle (around 120 [kg], see Section 3.4) is also taken into account. The bold line Ψ_{min} indicates the minimal hybridization factor that is required if it is assumed that the engine is running *only* for power demands *above* some threshold power level P_{th}, that is yet to be determined. Below P_{th} the secondary power source, that is the motor M, is activated for vehicle propulsion. Furthermore, for wheel power demands higher than P_{th}, but
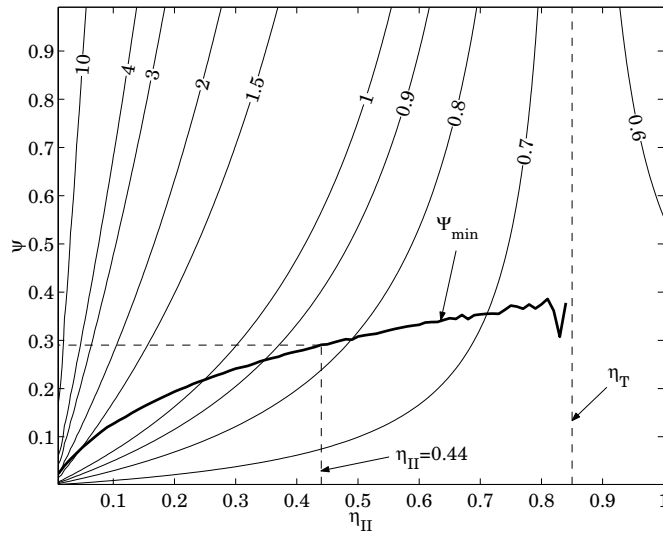
Figure 3.10: Hybridization factor and potential fuel savings as a function of total secondary source efficiency for the urban drive cycle

below $P_{ss}\eta_T$ (*i.e.,* P_{ss} corrected with transmission efficiency), the engine E is running in sweet spot and the excessive energy is stored in the accumulator A by the generator G. Finally, for wheel power demands above $P_{ss}\eta_T$, the engine is assumed to operate as the sole mover (conventional mode) along the E-line. The activity of the engine E, the motor M and the generator G as a function of the wheel power is schematically displayed in Figure 3.11. For
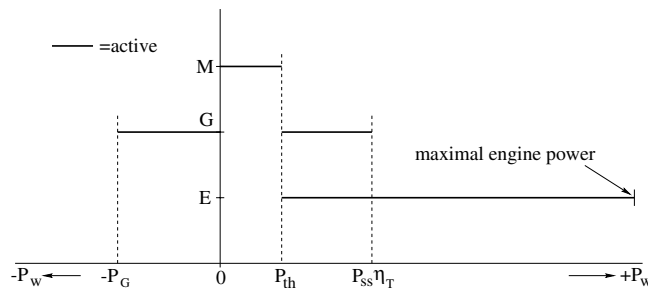
Figure 3.11: Activation of primary and secondary sources as a function of the (requested) wheel power

negative wheel power the generator G could be used for regenerative braking up to a level equal to the maximal generator power P_G. This will be elaborated further in Section 3.3.4.

The threshold P_{th} is determined assuming that the total amount of energy accumulated in the intervals where $P_{th} < P_w < P_{ss}\eta_T$ should be just enough to supply the energy necessary for

vehicle propulsion whenever $0 \leq P_w \leq P_{th}$. For an arbitrary journey, P_{th} can in principle not be known beforehand. Instead, the standardized drive cycles are taken in order to obtain some practical indication for P_{th}. Thus $P_w = P_{cyc}$ and by solving the energy balance for P_{th} given the above assumption:

$$\int_{t_0}^{t_f} (P_{th} < P_{cyc}(t) < P_{ss}\eta_T) \cdot \left(P_{ss} - \frac{P_{cyc}(t)}{\eta_T}\right) dt \quad = \quad \int_{t_0}^{t_f} (0 \leq P_{cyc}(t) \leq P_{th}) \cdot \frac{P_{cyc}(t)}{\eta_{II}} dt \quad (3.3)$$

the threshold power can be determined. In Equation (3.3) t_0 and t_f are, respectively, the start and end time of the driving cycle. The Boolean expressions inside the integrants are included to set the appropriate interval of power levels which must actually be integrated. For the four cycles used here it appeared that the threshold power levels P_{th} do not differ that much, see Table 3.7. In practice P_{th} may be chosen at 10 [kW]. With P_{th}, Equation (3.1) can be solved for

CYCLE	P_{th} [kW]
NEDC	8.6
rural	11.0
urban	8.3
highway	12.2

Table 3.7: Drive cycle power threshold beyond which the engine must be running, for $\eta_T = 0.85$ and $\eta_{II} = 0.44$

Ψ. Proceeding as such for every η_{II}, the line Ψ_{min} emerges. For $\eta_{II} = 0.44$ the fuel saving of Start-Stop is highest for $\Psi = \Psi_{min}$ and then equals 16.8%, for the urban drive cycle.

The strategy of Start-Stop operation underlying the given analysis can not be pursued in all situations given a maximum and minimum SOC of the accumulator. For instance, when the accumulator is fully charged and the cycle power demand is still above P_{th}, either the secondary source must also be running to discharge the accumulator or the engine must supply the exact cycle power in the appropriate operating point below $P_{ss} \cdot \eta_T$. Note that for power demands larger than $P_{ss}\eta_T$, the engine is always running on its own to deliver the actual cycle power. Vice versa, if the SOC is down to its minimum, the engine must be running even though the demanded cycle power may be below P_{th}. These operational constraints are not considered here but are regarded as one of the main efforts in developing the energy management. Furthermore, the powertrain component controls must ensure the driveability, comfort and reliability. Also the cooling system of the engine (engine runs at $P_{ss} = 32$ [kW] when on) has to be reconsidered for low speed driving.

The size of the motor, accumulator and the generator partly determine the potential for fuel saving. The proposed strategy is not only favourable with respect to the combined efficiency of the primary and secondary path, but also reduces the power requirements for the generator G and the motor M to an absolute minimum. Consequently, in the case where $P_{ss} = 32$ [kW], $P_{th} = 10$ [kW] and $\eta_T = 100\%$ the necessary generator power is 22 [kW], whereas the required motor power is 10 [kW]. A lower transmission efficiency η_T will lower these demands even further. For instance, if $\eta_T = 0.85$, the engine can operate in the sweet spot already when $P_w = \eta_T \cdot 32 \approx 27$ [kW]. Hence, a generator size of 27-10=17 [kW] is sufficient. If the motor and generator are combined in one machine, the size of the generator determines the actual size of the secondary power source. Downsizing the secondary power source means that the engine operating point—which should ideally be in the sweet spot—moves towards a lower power level on the E-line. According to Figure 3.5, the penalty on specific fuel consumption is

40

relatively low. For example, when shifting the intermittent engine operating point to 20 [kW], the BSFC rises by a mere 5%. On the other hand, the power requirement for the generator drops from 22 to 10 [kW]. Table 3.8 compares the efforts for two systems with generator sizes of 10 and 22 [kW], respectively. The cost saving due to a smaller generator is likely to out-

G [kW]	mass [kg]	volume [l]	cost [€]	fuel [%]
10	44	17	1740	105.2
22	96	36	3830	100

Table 3.8: Comparison of efforts for two Start-Stop generator (G) sizes

weigh the fuel saving in practice. On the other hand, if Start-Stop is combined with brake energy recovery, the fuel saving penalty associated with downsizing the generator will be more significant.

3.3.4 Brake energy recovery

Brake energy recovery must always be combined with some strategy that re-uses the recovered energy. In the following example it is chosen to combine this fuel saving principle with a Start-Stop system that operates the engine at $P_{ss} = 32$ [kW] and uses a generator of 22 [kW]. The energy balance (3.3) is augmented with the recovered energy yielding

$$\int_{t_0}^{t_f} (P_{th} < P_{cyc}(t) < P_{ss}\eta_T) \cdot \left(P_{ss} - \frac{P_{cyc}(t)}{\eta_T} \right) dt =$$

$$\int_{t_0}^{t_f} (0 \leq P_{cyc}(t) \leq P_{th}) \cdot \frac{P_{cyc}(t)}{\eta_{II}} + \int_{t_0}^{t_f} (-P_G \leq P_{cyc}(t) < 0) \cdot P_{cyc}(t) \, dt \tag{3.5}$$

where it is seen that the energy demand from the engine (left hand side) lowers due to the (last) recovery term ($P_{cyc} < 0$). For brake energy recovery, a plot similar to Figure 3.10 can be made (not shown), where for a given η_{II} and Ψ, the potential fuel savings increase, but also the locus of minimal hybridization factors Ψ_{min} tilts towards higher values. Still, again for the urban drive cycle, the fuel saving at $\Psi = \Psi_{min}$ (for $\eta_T = 0.85$) increases significantly up to 36.6% for an electrical system and to 53.3% for a mechanical system, as will be summarized in Section 3.4. If it is decided not to increase the power level of the generator, the additional efforts for brake energy recovery are relatively small, and limited to a revision of the energy management system. Because this fuel saving principle in fact constitutes brake-by-wire, safety issues must be taken into account. Moreover, the brake feel and performance should not be different from a normal vehicle. Since the generator power is limited and dependent on battery state (SOC, temperature, age), conventional disc brakes are still indispensable.

3.4 Innovation value versus effort

In this section, the innovation values are weighed against the corresponding efforts, for all four fuel saving principles. These *normalized* innovation values are evaluated for a system with a mechanical secondary power source and compared to those of a system with an electrical secondary power source. To give an indication for city and highway driving, the comparison is performed for the urban and the highway cycle.

The normalized innovation values are obtained simply as the quotient of the percentage of fuel saving and the effort (be it cost, weight or volume), always with respect to the reference vehicle. The additional weight, volume and cost are determined for the mechanical and electrical system, based on output power demands taken from the sections corresponding to the various fuel saving principles.

Additionally, the power demand for the accumulator using Start-Stop was set at 26 [kW] ($\approx 22/\eta_G$). For the electrical system, these *power* requirements are normative, but not for the mechanical system, where the *energy* demand is normative and is set at 200 [Wh], see Chapter 8. The additional weights are then obtained using Table 3.4, where the specific values for the electrical system are taken from the asynchronous EM combined with an ultra-capacitor. For the mechanical system, values between those of the ZI flywheel and FESS are taken. In practice, the electrical system may additionally require a battery.

The fuel savings presented in this section are obtained taking all the relevant efficiencies as well as the increased weights into account. Figures 3.12 and 3.13 depict the normalized innovation values for the mechanical and the electrical system, being the fuel saving relative to the additional cost [% per €], the fuel saving relative to the increased weight [% per kg] and the fuel saving relative to the additional volume [% per dm³].
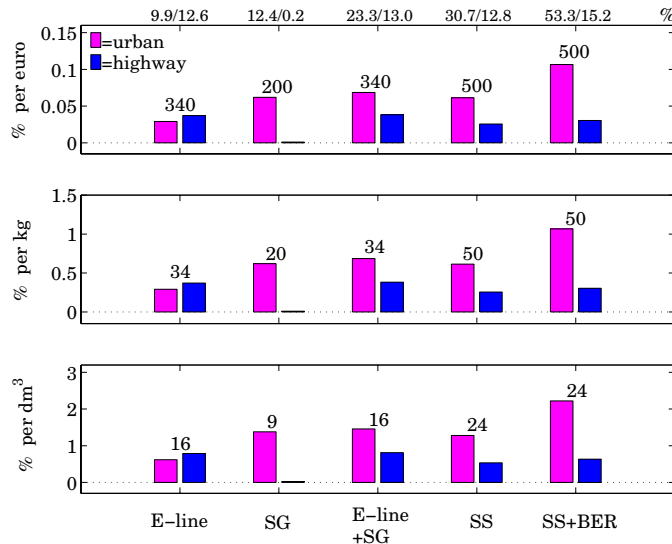
Figure 3.12: Normalized innovation values for a *mechanical* secondary source. At the abscissa are the four saving principles (SG=Stop-Go; SS=Start-Stop; BER=Brake Energy Recovery) and combinations thereof. On top of the bars is the corresponding increase of cost [€], weight [kg] and volume [dm³], respectively. Above the figure are the fuel saving percentages, corresponding to the two driving cycles and the different fuel saving principles.

At the abscissa are the four saving principles (where 'SG' means Stop-Go, 'SS' is Start-Stop and 'BER' stands for Brake Energy Recovery) and combinations thereof. For each saving principle, the left (grey) bar indicates the weighted fuel saving for the urban cycle and the right (black) bar that for the highway cycle. Written on top of the bars is the corresponding increase
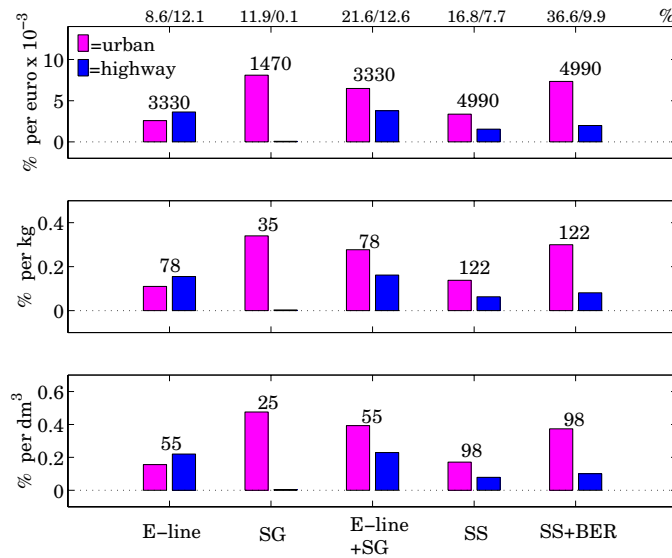
Figure 3.13: Normalized innovation values for an *electrical* secondary source. At the abscissa are the four saving principles (SG=Stop-Go; SS=Start-Stop; BER=Brake Energy Recovery) and combinations thereof. On top of the bars is the corresponding increase of cost [€], weight [kg] and volume [dm^3], respectively. Above the figure are the fuel saving percentages, corresponding to the two driving cycles and the different fuel saving principles.

of cost [€], weight [kg] and volume [dm^3], respectively. Above the figure, the fuel saving percentages are listed, corresponding to the two driving cycles and the different fuel saving principles. The bars for 'E-line+SG' and 'SS+BER' are included because these are obvious combinations. Besides that, BER cannot exist on its own.

From Figure 3.12 it is seen that the mechanical system performs well on the urban cycle for all fuel saving principles, though to a lesser extent for E-line. SS+BER scores highest, because of the large fuel saving of 53.3%.

The situation is somewhat different on the highway cycle, where the use of SG becomes close to nil. E-line (and the combination E-line+SG) achieves the best value for this cycle. The same trends are seen for the electrical system (see Figure 3.13), but in no category can such a system perform nearly as well as its mechanical counterpart (note the different orders of magnitude of the ordinate values in both figures). At least for the urban cycle, the electrical system shows a preference for SG. Because the mechanical system is much cheaper than the electrical alternative (by a factor of ten), the difference between the two with respect to the normalized values is striking. However, the electrical system can be expected to be more flexible and easier to conceive.

The fact that the achievable fuel savings are systematically higher for the mechanical system, is due to higher efficiencies of the secondary path (in case of SS and SS+BER), and a smaller increase of weight as compared to the electrical system (E-line and SG, in particular). The penalty on fuel consumption due to additional weight proved to be between 0.13 and 0.38% per % mass increase, or on average 1% fuel for every 4% additional weight. Notably,

the fuel savings obtained by SS and SS+BER on the highway cycle drop towards the values for E-line in case of the mechanical system, and even below that for the electrical system. The latter is explained by the fact that on the highway cycle, the required powers below P_{ss} are still concentrated close to the sweet spot (unlike a 'proper' city cycle) where the best strategy is to use E-line and not SS. Also, the substantially increased weight (+122 [kg]) ruins part of the fuel saving. Averaging the results of the two driving cycles reveals that both the electrical and the mechanical system score well on the combination of E-line and SG, at least on their own scale, see Table 3.9. The mechanical variant scores even somewhat higher for SS+BER than for E-line+SG. As mentioned before, the electrical systems show about ten times lower

System	E-line	SG	E-line+SG	SS	SS+BER
mechanical	33	32	53	44	69
electrical	3.1	4.1	5.1	2.5	4.7

Table 3.9: Normalized innovation value (cost-specific fuel saving [%/k€]), averaged over the urban and highway cycle, for the mechanical and electrical system

normalized innovation values than the mechanical counterpart. On the other hand (less quantitative) aspects such as driveability, safety and developing efforts level out the two principles somewhat. For instance, realizing a mechanical system for SS+BER requires a CVT with an exceptionally large ratio coverage (more than 20), and a high energy flywheel with mechanical components like clutches and gear stages, see Section 8.2. This yields additional issues of driveability and safety. The severity of these issues is much smaller for E-line+SG than for SS+BER, because of lower energy contents of the flywheel. Electrical systems, on the other hand, require few mechanical adaptations, and are flexible with regard to the controls. An electrical E-line+SG hybrid may additionally be utilized to supply electrical power for several purposes (*e.g.,* 42 Volt net). The robustness and predictability of batteries is still troublesome.

ZI powertrain: mechanical mild hybrid

The combination of E-line and SG may be termed 'mild hybrid' as opposed to 'full hybrid' in case of SS+BER, [van Druten *et al.*, 2001]. From this section, it is concluded that a mechanical hybrid is preferable above an electrical hybrid, with respect to cost especially. Furthermore, the mechanical full hybrid scores higher than the mechanical mild hybrid. Therefore, a mechanical full hybrid seems favourable for reducing fuel consumption in a passenger car. However, the development effort (engine and catalyst adaptations, control of intermittent engine operation, *etc.*) for a full hybrid, relative to its potential is large compared to that for a mild hybrid. In the EcoDrive project, after studying different concepts it was decided to develop a mechanical mild hybrid, using two new concepts, called ZI and ZI Stop-Go. Choosing for ZI and ZI Stop-Go, the project goal can largely be met using the available development time, research and engineering capacity. Furthermore, the two concepts can be designed, realized and tested separately enabling a step-by-step implementation and hence reducing development risks.

The fuel saving of E-line+SG, (here embodied as ZI Stop-Go) is estimated by computations similar to those conducted in Section 3.2.3. The estimated fuel saving of ZI Stop-Go on the NEDC with respect to $OL_{15\%}$ is around 21%.

Chapter 4

The Zero Inertia Powertrain

This chapter presents the conceptual design of the Zero Inertia powertrain in a nutshell. Section 4.1 translates the findings from the previous chapter that are related to E-line tracking into a problem description. After that, the ZI solution is derived in Section 4.2. A brief description of the ZI Stop-Go transmission is given in Section 4.3.

4.1 Zero Inertia principle

In the previous chapter it was concluded that the use of E-line tracking as a fuel saving principle necessitates an additional power assist system. Electric power assist systems are able to supply the power needed to compensate for primary inertia effects in slow transient situations, and, when physical limits are not reached, even overcompensate. However, arbitrarily fast speed changes generally cannot be compensated for, due to power and torque limitations of the electric machine. A counteracting inertia, capable of supplying the power needed to overcome inertial effects would therefore be very interesting. This mechanical power assisting device, *i.e.*, a *flywheel*, should speed down when the primary inertia speeds up and vice versa, at a rate dictated by, among others, the ratio of flywheel inertia and primary inertia. To link the speed of the flywheel to that of the primary side of the powertrain, a component with a continuously variable transmission ratio is needed. Possible components to realize this are:

1. continuously variable transmissions (CVTs);

2. couplings;

3. torque converters;

4. planetary gears.

continuously variable transmissions

Automotive CVTs can be mechanical, hydraulical, or electrical. Hydraulical CVTs are used especially in heavy vehicles (construction vehicles, trains, agricultural machinery), but have moderate efficiencies. So called electrical CVTs require an electric motor and an electric generator both of which are capable of handling the maximum power of the primary source of propulsion. Compared to an internal combustion engine with the same maximum power,

electric machines and their overhead (battery, inverter) are bulky and rather expensive, as well as rather inefficient, as was seen in the previous chapter. Modern mechanical CVTs are capable of transmitting the required power for almost every size of passenger car at efficiencies not much lower than that of conventional stepped transmissions (MT and AT). Commercially available CVTs are the Van Doorne metal V-belt CVT (*e.g.,* in the Nissan Primera), the Audi Multitronic chain belt CVT (*e.g.,* in the Audi A6), the Bando dry hybrid belt CVT (*e.g.,* in the Daihatsu Mira) and the dual cavity toroidal CVT (*e.g.,* in the Nissan Cedric).

couplings

Couplings can transmit torque between two bodies with a continuously variable speed ratio. The torque ratio is always equal to 1. A coupling that transmits the torque hydraulically is known as a *fluid coupling* (or *fluid flywheel*), otherwise the term *clutch* is more common. The torque transmitted by a fluid coupling can be influenced by varying the amount of oil. In a clutch that transmits torque mechanically, the torque can be manipulated by changing the clutch engaging pressure, either hydraulically, mechanically or electro-magnetically. 'Intermediate' solutions such as electro-magnetic and electro-rheological clutches use electro-magnetic fields to change the viscosity of the torque transmitting medium. The latter still somewhat exotic clutch is in some ways comparable to the fluid coupling because of the viscous torque transmission. Current applications of this technology are found primarily in active engine mounts. The electro-magnetic powder clutch on the other hand, has been applied successfully, *e.g.,* in the Subaru CVT.

torque converters

A torque converter basically is a fluid flywheel combined with a stator (or reactor) which is connected to the transmission casing by a one-way clutch. When the torque on the stator is such that the one-way clutch locks, this third torque transmitting member enables the amplification of input torque whenever the input speed exceeds the output speed. In effect, the torque converter acts as a hydrodynamical CVT with a quite moderate efficiency. Some torque converters have a (mechanical) lock-up clutch to enlarge the efficiency by eliminating the slip when the torque ratio approximates 1. The continuous variability is then obviously lost.

planetary gears

Planetary gears are widely used, for instance in stepped automatic transmissions. A *basic* planetary gear has three main rotating members and three submembers, see Figure 4.1. The inner member is termed the *sun*, the outer member is the *annulus* or *ring*. The intermediate member carries the three *planets* (submembers) and is therefore called *carrier*. More complex epicyclic configurations can have several sun, annulus and carrier wheels or double planets with different teeth numbers connected to the same axis, for instance see Figure 4.2. Also, planets can run on opposing planets, instead of on an opposing sun or annulus. An example of this can be found in the DNR (Drive-Neutral-Reverse) set, see Figure 4.3. Epicyclic sets as seen in practice (*e.g.,* Simpson, Ravigneaux, see, *e.g.,* [Lechner and Naunheimer, 1999]), are composed of several basic planetary gears, possibly combined with alternative planet configurations. In most automotive applications, the planetary gear is used as a concentric reduction gear, where any rotating member can be connected to ground (*i.e.,* the transmission housing). Given the speed of one member, varying the speed of a second member in turn varies the speed of a third member. This creates two speed ratios which are both continuously variable.

46
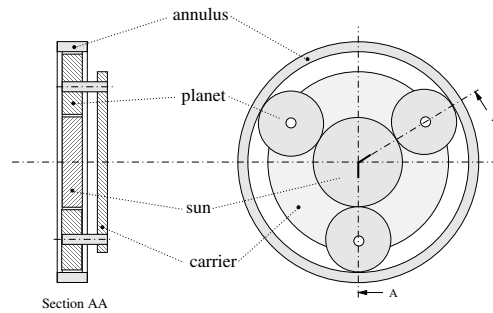
Figure 4.1: Basic planetary gear
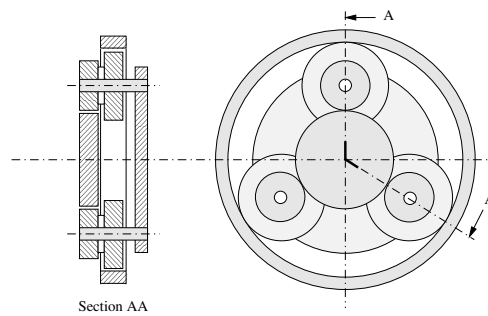
Figure 4.2: Planetary gear with stepped planet
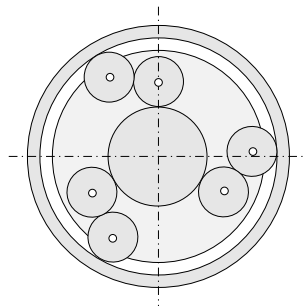
Figure 4.3: DNR (Drive Neutral Reverse) reversal stage

In this example, the speed of the second member must somehow be controllable. This is possible by active control of the torque applied to one of the members. For example, in the hybrid powertrain of the Toyota Prius [Riezenman, 1998], the speed of the members is controlled by an electric motor/generator connected to the sun. The engine is connected to the carrier and

the wheels to the annulus.

Summarizing, a number of components exist which in principle can transmit power between two rotating bodies at variable transmission ratios. In the following, further constraints will decide what solution is favourable for the intended application.

4.2 ZI Concept design

The drive train of the vehicle must be able to combine a given range of vehicle speeds with appropriate engine speeds and flywheel speeds. In general, the flywheel speeds should be high for low engine speeds and vice versa. Strictly speaking, this calls for two CVTs or similar power transmitting components. Obviously, the application of two CVTs, be it mechanical, electrical, or hydraulical, is unacceptably expensive and bulky. Furthermore, the required ratio coverage, needed to link all practical speed combinations, using a flywheel with an inertia comparable to the primary inertia, is by far larger (typically 30) than the ratio coverage of standard mechanical CVTs (typically 6). Hydraulical CVTs are not an option due to their moderate efficiencies, whereas an electrical layout would offer possibilities, although preferably not in a series hybrid configuration.

The use of a planetary gear arrangement as in the Toyota Prius is reasonably cost-effective, although the Prius uses two electric motors which renders this solution still rather expensive. An alternative solution, incorporating a planetary gear, does not control the speed of one rotational member electrically, but mechanically instead, through the use of a mechanical CVT. Such a solution would again be overexpensive, if the CVT could be used only for regulating the flywheel speed. However, if the CVT can also be used to control the engine speed, such a solution becomes increasingly interesting.

4.2.1 Resulting configuration

The easiest way to realize the suggested solution is to have a fictitious line connecting the engine and flywheel speed that rotates around a pivot in between, as illustrated in Figure 4.4. A sensible choice is to make the median speed the vehicle speed, hence the secondary speed
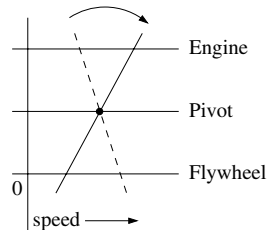
Figure 4.4: Pivot mechanism

of the CVT. By down-shifting the CVT, it is seen that while the engine increases speed with respect to the vehicle speed, the flywheel speeds down, and vice versa. This is exactly the mechanism needed to create the energy exchange between engine and flywheel. In terms of a basic planetary gear, the sketched mechanism can be realized by connecting the secondary speed to the carrier, whereas the engine and flywheel are connected to the annulus and sun,

48

respectively, or possibly, the other way around. The outlined topology (see Figure 4.5), is just
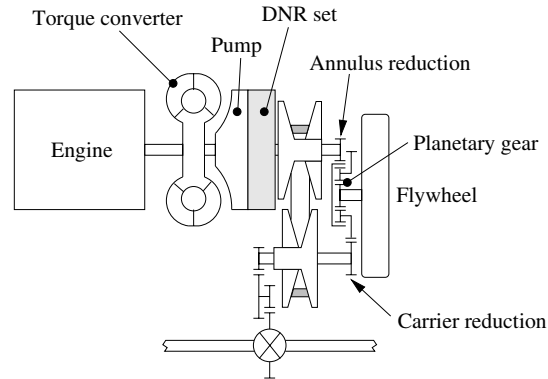
Figure 4.5: ZI powertrain concept layout

one possibility out of many, see Chapter 11.

4.3 ZI Stop-Go

The Stop-Go functionality (proposed in Section 2.4 to increase the fuel efficiency and evaluated as an interesting technology in Section 3.3) is investigated in combination with the Zero Inertia powertrain. Naturally, before vehicle launch, the energy contents of the flywheel must be sufficiently high. For this purpose, at least one additional clutch is needed in order to enable disengagement of the flywheel from the drive train at a flywheel speed high enough to facilitate a new vehicle launch. The flywheel preferably should to be able to launch the vehicle and start the engine *at the same time*. Such a specification is certainly not trivial, since most commercially available Stop-Go systems *first* start the engine, *after* which the engine can start to propel the vehicle. As was mentioned in Section 3.3.2, cranking up the engine is conceivable as a *direct-start* or an *impulse-start*, for instance see [Reik, 1999]. The first strategy has one clutch only, positioned between the starter and the primary side of the transmission, as in a conventional driveline. The impulse-start strategy uses the inertia of the starting device, which can be disengaged from the engine by an additional clutch, see [Seiffert and Walzer, 1989]. Depending on the starter-clutch(es) configuration, and on the size of the electric starter motor, the combined time needed for restarting the engine and engaging the launching clutch may be more than the driver is willing to accept. This is the case in the former Volkswagen Eco-Golf/Ecomatic [Adcock, 1998, Greve and Liesner, 1993] and supposedly also in the current Volkswagen Lupo 3L [Healey, 1999]. In the Honda Insight with Integrated Motor Assist (IMA), the electric motor power is much larger, thus enabling a pleasant vehicle launch.

To enable the flywheel system to simultaneously speed up the engine and the vehicle, one additional clutch is needed to decouple the CVT from the driveline. To see this, it is crucial to understand that, while the flywheel contributes torque to the wheels (secondary side of the CVT) it drains (some) torque from the primary side of the CVT and hence the engine. Therefore, while launching the vehicle, the flywheel tends to speed up the engine in the wrong direction. To avoid this, the CVT has to be decoupled from the secondary shaft and

the DNR set must be set in reverse. In Figure 4.6 the ZI Stop-Go layout is depicted showing the two additional clutches (C_f and C_s) as well as the existing clutches (C_l, C_d and C_r) that will be operated differently. In [Vroemen, 2001], the physical background, as well as the supervisory
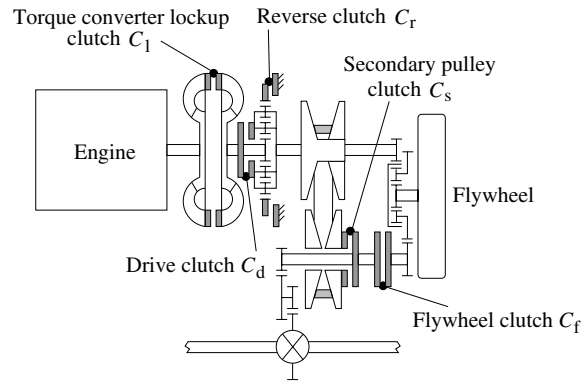
Figure 4.6: ZI Stop-Go powertrain concept layout

and clutch control strategies needed to operate the Stop-Go facility are explained.

4.4   Further reading

Given the concepts of the ZI and ZI Stop-Go powertrain, an extensive though achievable list of development (or innovation) efforts has to be tackled. These efforts are reported in this thesis, in [Vroemen, 2001] and in [Serrarens, 2001], also see Figure 1.3.

In this thesis the designs of the ZI and ZI Stop-Go concepts are illustrated as well as general ideas about flywheel usage in passenger cars. The control problem of generating appropriate setpoints for engine and CVT along with developing dynamic models for and testing of the ZI powertrain is the subject of [Serrarens, 2001]. In [Vroemen, 2001] a component controller and models for the CVT are developed. Furthermore, a second part concerns the operation, modeling and control of the ZI Stop-Go transmission.

Part II

Transmission Design

Chapter 5

Design aspects of flywheel systems

5.1 History of engineering flywheels

Kinetic energy storage in a rotating mass is generally known by engineers. Applications reach from 2000 years before Christ, when flywheels where used to make the speed of the pottery machines more regular, till the current use of a flywheel to smoothen the internal combustion engines torque. However, these examples don't show the functional use of the energy stored in the flywheel. The fluctuation in speed, and thus energy level variation, is aimed to be as small as possible. To make use of the kinetic energy stored in a flywheel, *i.e.,* for propelling a vehicle at any speed, a *variator* is needed to either alter the speed of the flywheel or alter its inertia, see equation 5.1. According to the second law of Newton the flywheel torque T equals
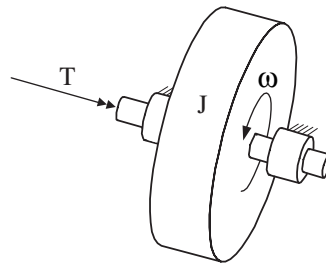
Figure 5.1: Disc shaped flywheel rotor with bearings

$$T = J\dot{\omega} + \dot{J}\omega \qquad (5.1)$$

Since, commercial development of mechanical, electrical or hydraulic speed variators (able to control $\dot{\omega}$) just started 50 years ago, and flywheels with a variable inertia (controlling $\dot{J}$) are

still not commercial available, energy exchange using a flywheel is mainly found in recent applications. In Figure 5.2 two examples of a speed variator are shown, both of which are able to induce, transmit and adapt the flywheel torque to a load attached to the secondary shaft. Because the speed of the flywheel changes continuously when exchanging energy and the load can have any speed, all flywheel speed variators have to be continuously variable or allow speed variations like a clutch. The mechanical speed variator as shown in Figure 5.2(a) con-

(a) Mechanical speed variator   (b) Electrical speed variator
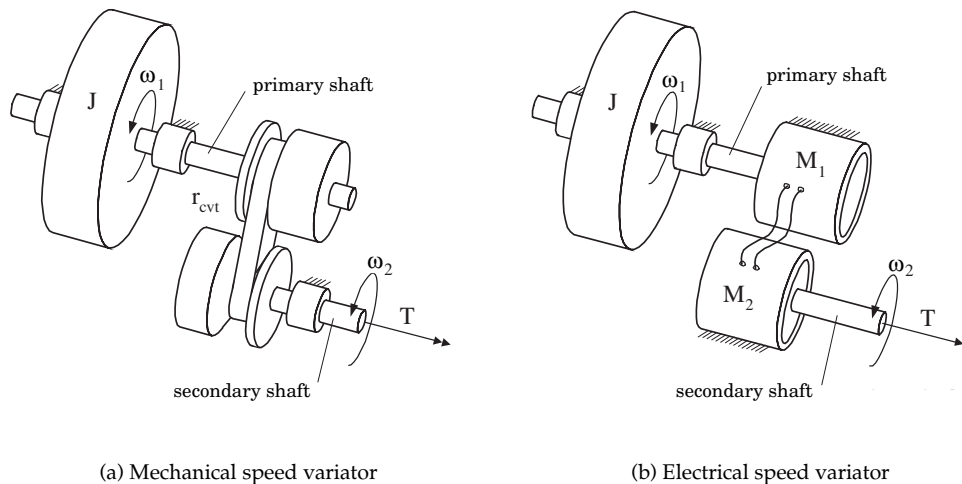
Figure 5.2: Flywheel in combination with a speed variator to enable energy exchange

sists of a V-belt clamped between two sets of conical pulleys. By forcing the opposite pulley of each set to move in axial direction the V-belt changes the speed and torque ratio between the pulley sets, see [Vroemen, 2001]. The V-belt CVT is nowadays commercially exploited by many car manufacturers, used in various machinery and is seen in every 50cc scooter.

Another, more flexible way to induce the flywheel torque and to transmit it is the electrical variator consisting of two electro motor-generators $M1$ and $M2$, shown in Figure 5.2(b). $M1$ is directly connected to the flywheel which have to speed down to generate electric power. The generated electric power is converted by $M2$ to the mechanical domain again and thus this motor can be directly connected to the load. The speed of the flywheel is controlled, independent of the speed of the load, with the use of power electronics. The integration of $M1$ with the flywheel into an advanced Flywheel Electric Storage System (FESS) is increasingly subjected to research in the last 30 years. An example of a FESS is showed in [Colotti *et al.*, 1998]. Significant technological improvements in the areas of flywheels and variators have been established. For example advanced rotor materials with high strength, magnetic bearings and vacuum systems, crucial at very high rotation speeds, make it possible to increase the specific energy of the flywheel rotor up to 140 [Wh/kg], see [Thoolen, 1993]. The mechanical variator is improved using a high strength steel-belt that is able to transmit torques up to 400 [Nm] with an efficiency up to 96%. These variators can be controlled with high precision,

54

using electro-hydraulic actuators. Likewise improvement of the power electronics using IG-BTs (Insulated Gate Bipolar Transistors), the use of rare earth magnets and advanced control strategies have improved the efficiency of the electrical variator and its specific power.

Despite all the mentioned technological improvements there is no market, other than the toys-market, that has shown a wide spread of a product or application in which a flywheel is used to exchange its energy with a load. For engineers it is now the task to find an application that takes full benefit of a flywheel energy exchange system using the available technologies, see [Genta, 1985]. The current systems using either a mechanical, electrical or hydraulic CVT enable a very high specific power, high power density, fast torque response, a large lifespan (number of cycles), time independent behaviour and have a high mechanical to mechanical efficiency. A widely spread application of these highly efficient energy conversion systems would be helpful to reduce the energy consumption growth world wide. In the following it will be explained what are the current limitations when designing a flywheel energy exchange system for automotive applications. The insights gathered can also be helpful when designing such systems for other applications.

5.2   Flywheel dynamics

The dynamic behaviour of a rigid flywheel rotor with mass m_f, rotating with speed ω in bearings on elastic supports (elastic to account for finite stiffness of bearings, shaft and structures), as shown in Figure 5.3 allows two modes of operation:

- sub-critical operation: flywheel speed ranges from zero to a speed that is safely below the first critical speed ω_{cr} (low energy storage);

- super-critical operation: flywheel speed ranges between two consecutive critical speeds (high energy storage).
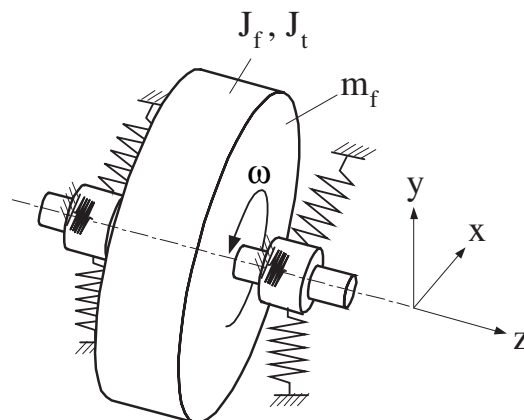
Figure 5.3: Rigid flywheel rotor on elastic supports

The undamped system of Figure 5.3 has two natural frequencies, see [Genta, 1993]. Due to the gyroscopical moments the natural frequencies depend on the angular speed of the flywheel. If the rotor is equidistantly placed with respect to the bearings, and the elastic supports have the same radial stiffness, the translational and rotational degrees of freedom are decoupled, see Figure 5.4. In the case of disc shaped flywheels, of which the inertia of the flywheel around the z-axis J_f is much greater than the inertia of the flywheel around the x- or y-axis J_t, the first critical speed ω_{cr} equals

(a) 1*st* eigenmode, rotation around the x- or y-axis

(b) 2*nd* eigenmode, translation in x- or y-direction
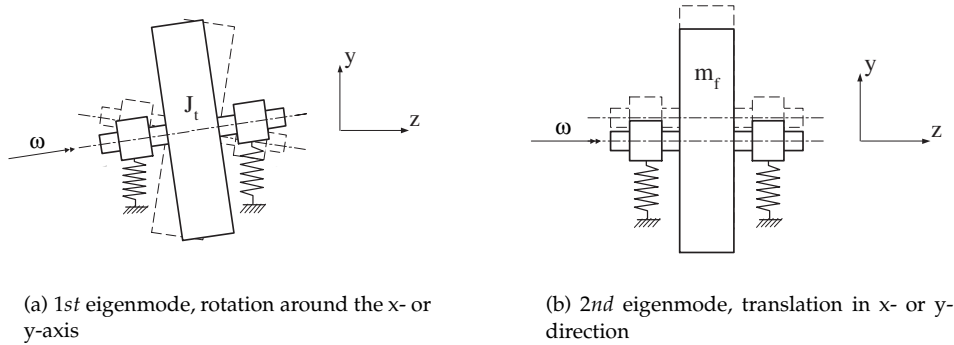
Figure 5.4: Eigenmodes of the flywheel system with decoupled translational and rotational degrees of freedom

$$\omega_{cr} = \sqrt{\frac{C_{rad}}{m_f}} \tag{5.2}$$

which appears to be equal to the translational eigenfrequency at zero flywheel speed. C_{rad} is the total stiffness felt in radial direction. The axial position of the rotor with respect to the bearings only slightly influences the first critical speed. In the case of long rotors where $J_f < J_t$ two values of the critical speed exist, see [Genta, 1993].

5.3 Design aspects of sub-critical operation

To ensure maximum energy storage for a rotor that is operated below its first critical speed, the radial stiffness has to be as high as possible. Generally the bearing stiffness will be the weakest element in the stiffness chain and thus will limit the maximum operating speed. Using ball-bearings, a total radial stiffness C_{rad} of 10^8 [N/m] is commonly reached. Due to the unbalance that is always present in a sub-critically operated flywheel a load factor n is taken into account that ensures that the dynamic load on the bearings is not more than n times larger than the static load, see [Kok, 1999]. For sub-critical operation the flywheel speed is limited according to

$$\omega \leq \omega_{cr} \sqrt{\frac{n-1}{n}} \tag{5.3}$$

The rotor has to be balanced to reduce the dynamic bearing load. Standards use the peripheral velocity of the center of mass of the rotor V_G as a measure of the eccentricity ε and define a

quality grade for balancing G, as the maximum allowable peripheral velocity of the center of mass, expressed in [mm/s]. A flywheel rotor has to be balanced in the class $G6.3$. For example when allowing 10.000 [rpm], the eccentricity has to be smaller than 6 [μm].

$$V_G = \omega_{\max} \varepsilon \tag{5.4}$$

The energy content a sub-critical flywheel system is either limited by the maximum allowable rotor speed according to equation 5.3, or by the maximum allowable stress σ_a in combination with the volume V of the rotor. The maximum energy content with respect to material stress is given by

$$E_{\max,\text{stress}} = K \sigma_a V \tag{5.5}$$

where the shape factor K for a ring-shaped flywheel equals (see [Genta, 1985])

$$K = \frac{1 + \xi^2}{3.3 + 0.7\,\xi^2} \tag{5.6}$$

with the ratio ξ of inner to outer radius, defined as

$$\xi = \frac{R_i}{R_o} \tag{5.7}$$

Table 5.1 summarizes the maximum specific energy [Wh/kg] and energy density [Wh/dm^3] for different type of materials according to the maximum allowable stress. The maximum

MATERIAL	σ_a [10^6N/m^2]	ρ_f [kg/m^3]	$E_{\max,\text{stress}}/m_f$ [Wh/kg]	$E_{\max,\text{stress}}/V$ [Wh/dm^3]
Ferro 360	120	7800	1.3	10.1
Aluminium	173	2800	5.2	14.6
Wrought steel	550	7800	5.9	46.3
Maraging steel	765	8000	8	64.4
E-glass	220	2000	9.3	18.5
Titanium	662	4500	12.4	55.7
High modulus aramid	700	1400	42	58.9
High strength carbon	1600	1550	86.9	134.7

Table 5.1: Maximum specific energy and energy density for different type of materials according to the maximum allowable stress (for 10^7 cycles), with ξ=0 [-], K=0.303 [-]

energy content of the flywheel with respect to sub-critical operation can be found by combining equation 5.2, equation 5.3 and using the expression for the kinetic energy stored in the flywheel

$$E = \tfrac{1}{2} J_f \omega^2 \tag{5.8}$$

with the inertia of the flywheel around its rotation axis J_f defined as

$$J_f = \tfrac{1}{2} m_f R_o^2 (1 + \xi^2) \tag{5.9}$$

the maximum energy stored for a sub-critical flywheel system becomes

$$E_{\max,\text{subcr}} = C_{\text{rad}} \frac{n-1}{4\,n} R_o^2 (1 + \xi^2) \tag{5.10}$$

Using equation 5.10, the energy density limited by sub-critical operation $E_{\text{max,subcr}}/V$ can be calculated for a specific rotor geometry. The volume V of the rotor is given by $V = \pi h_o R_o^2 (1 - \xi^2)$. For example, with practical values (for passenger car application) of the total radial stiffness $C_{\text{rad}} = 10^8$ [N/m], the width of the rotor h_o=0.05-0.2 [m], K=0.303 [-] and allowing a load factor n of 2, the value for $E_{\text{max,subcr}}/V$ varies between 5.5 and 22 [Wh/dm^3]. Looking at Table 5.1, for most materials the maximum energy density for a sub-critically operated flywheel is not limited by the maximum allowable material stress.

5.4 Design aspects of super-critical operation

To extend the energy storage capacity, the flywheel system can be designed such that super-critical operation is possible. First, to enable the higher rotor speeds associated with super-critical operated flywheel systems, fiber composite rotor materials, *e.g.,* high strength carbon, have to be used. Because fiber materials have a very low radial tensile strength, the design of the rotor and its manufacturing process must be aimed at preventing delamination failure. Extensive studies are carried out by [Thoolen, 1993] and by [von Burg, 1996] and practical experience with rotor manufacturing and material behaviour is gained. The combination of a cost effective and reliable manufacturing process is still under investigation ([Gabrys, 1996]). Second, the stiffness of the rotor shaft, the bearings and its support has to be adapted to the operational speed range of the flywheel to prevent and reduce structural vibrations below the maximum speed. When starting up, the first critical speed has to be passed. This often causes vibrations which have to be attenuated by proper damping characteristics of the bearing support, who also have to prevent dynamic instability. Above the critical speed defined with equation 5.2 however the rotor tends to rotate around its mass center instead of its geometrical center, minimizing vibrations by itself.

Given Figure 5.5 the "self-centering" motion of the flywheel in the super-critical speed range will be explained. The coordinate system 0xyz rotates with the flywheel at speed ω. Point 0

(a) sub-critical operation

(b) super-critical operation, "self-centering" of the rotor
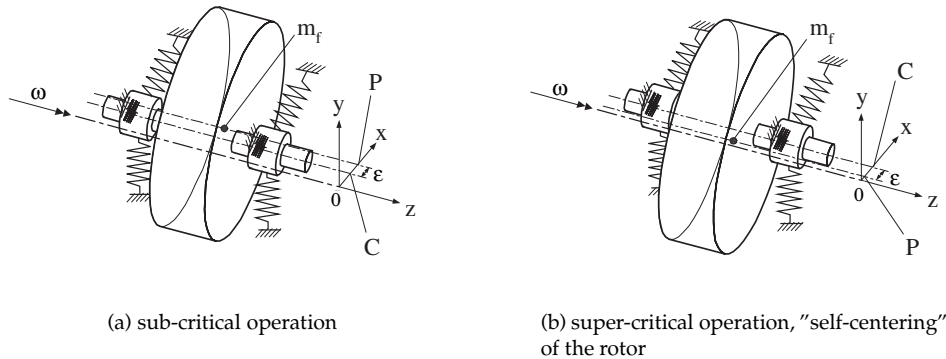
Figure 5.5: Influence of the eccentricity ε between the bearing axis and the center of mass of the rotor on the motions of the system

coincides with the position of the center of the bearings at rest. Point P lies on the line through the center of mass of the rotor and point C lies on the line through the center of the bearings. When rotating, the centrifugal force $m_f \omega^2 |\bar{0P}|$ caused by the eccentricity ε equals the elastic reaction force $C_{rad} |\bar{0C}|$. The elastic deformation $x_c = \bar{0P} - \varepsilon$ can be calculated using

$$x_c = \frac{\varepsilon}{\frac{C_{rad}}{m_f \omega^2} - 1} \tag{5.11}$$

In Figure 5.6 the deformation x_c as function of ω is plotted. The "self-centering" effect in
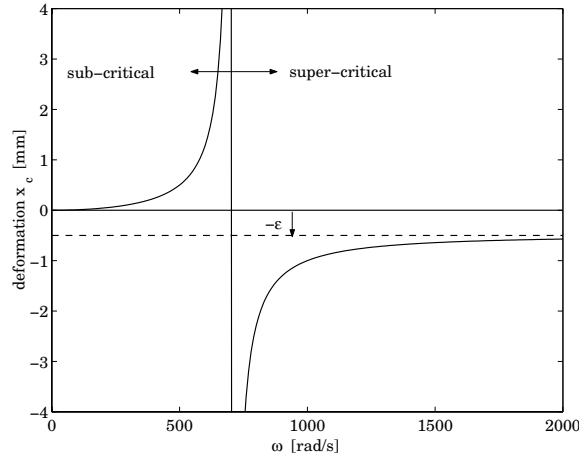
Figure 5.6: Deformation x_c as a function of the rotor speed, eccentricity ε=0.5 [mm], radial stiffness $C_{rad} = 5 \cdot 10^6$ [N/m], rotor mass m_f=10 [kg]

the super-critical speed range is clear: the deformation x_c tends to be equal to $-\varepsilon$ when the flywheel speed goes to infinity, *i.e.,* the system tends to rotate about its mass center instead of its geometrical center. Even though self-centering takes place, static and dynamic balancing of the rotor still have to be applied to a certain level to avoid excessive whirl motion of the bearing support. When the rotation axis of the flywheel is tilted in any direction, the flywheel will induce a gyroscopic moment $\vec{M}$ that will give an extra load on the bearings and its support

$$\vec{M} = J \vec{\omega} \times \vec{\Omega} \tag{5.12}$$

with J the moment of inertia of the flywheel about its spin axis and $\vec{\Omega}$ the tilting speed of the rotation axis. Using the flywheel in a vehicle, the position of the rotating axis and the rotation direction with respect to the direction of the vehicle speed have influence on the vehicle dynamics. The gyroscopic moment is proportional to the speed of the flywheel. However, given the energy content of the flywheel (see equation 5.8), it is seen that the gyroscopic moments can be reduced using a high speed, low inertia flywheel.

To prevent tilting of the rotation axis due to the motion of the surroundings, the flywheel including its bearings can be decoupled from these motions using a cardanic suspension. The rotation axis of the flywheel will keep its orientation and the bearing load due to gyroscopic moments is then reduced.

5.4.1 Flywheel containment

Since windage power losses increase with the third power of the speed, a closed housing around the flywheel and a vacuum system to reduce the air density inside the housing are necessary with super-critically operated flywheels. Too high windage losses would unacceptably decrease the system efficiency and overheat the flywheel. The vacuum housing or containment will also be used to provide a safety function. While high speed machinery, such as a super-critically operated flywheel, is always a potential source of danger, safety can be guaranteed by preventing any fragment penetration. This can be achieved by minimizing the radial clearance between the flywheel and its housing, by a modular rotor design (smaller fragment sizes) and by an appropriate strength of the containment itself. The practice of overlaying a thin metallic liner with a specified number of layers of bare Kevlar fibers has produced very effective and light containment structures, see [Genta, 1985]. It should be prevented that due to fatigue, creep or defects of the rotor material, debris can come out of the containment structure. Several causes can act together in order to bring about the failure of the flywheel. All possible causes of failure must be taken into account. For each cause a certain number of failure modes must be assessed together with their probability.

Although a complete flywheel containment results in a severe weight penalty, any failure of a flywheel system would drastically reduce the chance of acceptance by the public. Future demonstration of reliability to be equivalent to that accepted for other structures, would make a safety containment likely to disappear.

Chapter 6

Kinetic energy exchange: bottom-up design

Every design is made in view of certain system levels. In this thesis, the lowest system level considered is the flywheel, *i.e.*, the basic part of the kinetic energy exchange system, and the highest system level considered is the vehicle-road system. Linking the term bottom-up design to the lower and upper system levels, in this chapter it will be clear that the kinetic energy exchange system will be designed in view of the characteristics of the flywheel. The top-down design of the kinetic energy exchange system, made in view of the characteristics of the vehicle road system, is described in Chapter 8. There, the insights of the two different approaches come together and final system proposals are made. In this chapter the demands prescribed by the use of the system in a vehicle-road system will be neglected, to give freedom in finding the most suitable flywheel system(s). However, practical and economical constraints are determined in this design stage to achieve a design that has the potential of being used in a passenger car:

- compact system, with outer radius $R_o \leq 0.25$ [m] and rotor width $h_o \leq 0.15$ [m];

- weight $m_f \leq 20$ [kg], to avoid an increase in fuel consumption;

- power losses $P_{loss} \leq 750$ [W] (1% of the maximum engine power of 75 [kW]);

- low complexity;

- minimum costs in mass production (≤ 20 [euro/kW]);

- maximum safety and reliability.

Regarding the design criteria made, it can be stated that the design must aim at maximizing the specific energy with minimal power losses, within the given dimensional constraints. The complexity of the flywheel system (number of advanced components) and costs in mass production are greatly linked to sub- or super-critical operation of the flywheel system, see Chapter 5.3 and 5.4. For this reason two flywheel energy exchange systems will be conceived, one based on sub-critical and one based on super-critical operation, see Table 6.1. For the super-critical flywheel system a cardanic suspension to reduce the bearing load due to gyroscopical

COMPONENT/ FUNCTION	SUB-CRITICAL	SUPER-CRITICAL
Rotor	to be specified	to be specified
Bearings	rolling element bearings	rolling element bearings
Support	stiff (C_{rad}=10^8 [N/m])	flexible (C_{rad}=10^6 [N/m])
Damping	none	squirrel dampers
Vacuum	none	vacuum 1 [mbar]
Cooling	none	liquid cooling
Containment	housing	closed flywheel containment
Suspension	none	cardanic/none
Variator	mechanical	electrical (integrated)

Table 6.1: Flywheel energy exchange systems to be designed

forces will not be used as a result of the packaging constraints. In view of the efficiency, for both systems defined in Table 6.1, the mechanical variator seems to be preferred because of its high mechanical to mechanical efficiency (η_{mech}=85%) over the electrical variator (η_{elec}=75%) using synchronous PM motors, see Chapter 3. However, with a super-critical flywheel the electrical variator is favourable for many reasons:

- the electrical machine can be directly connected to the high speed rotor, where the mechanical variator needs a reduction gear in between them because the maximum speed of the mechanical variator is limited;

- the bearings of both rotors can be combined and a "complex" mechanical coupling can be left out when integrating the rotor and stator of the electric machine M1 in Figure 5.2 with the flywheel rotor and housing;

- the electrical CVT has an infinite ratio coverage, and is therefore able to match the super-critical speed of the flywheel with the speed of a load that is generally operated from zero speed. A mechanical variator would need a clutch or a power split device to create an infinite ratio coverage;

- when a cardanic suspension is used and the surroundings are moving, the mechanical variator would need a complex transmission between the flywheel and its surroundings. Using an electrical variator the electric cabling between the electric machines is flexible enough to follow the movements.

The efficiency of the electrical variator can be improved by splitting the power and transmitting one part mechanically and the other electrically. However, using a power split device, *e.g.,* a planetary gear set, the flexibility of placement of the electric machines is limited. It must be noted that the power level that can be transmitted with the electrical variator depends on the size of both electric machines. Because the mechanical variator is able to transmit 100 [kW] within a smaller volume and lower weight, the electrical variator shows definitely a great penalty here, see Chapter 3. Generally it can be stated that a super-critical flywheel needs the flexibility offered by the purely electrical variator, while a sub-critical flywheel can profit from the higher efficiency of the mechanical variator, although it is constraining the position of the flywheel.

6.1 Specific energy versus power loss

This section focuses on the relation between specific energy and power loss for the two rotor systems defined in Table 6.1. The variator is left out in this stage of the design. Figure 6.1 defines variables that will be used in the rotor system design optimization for both the sub- and super-critical flywheel system. The maximum specific energy of the flywheel rotor follows
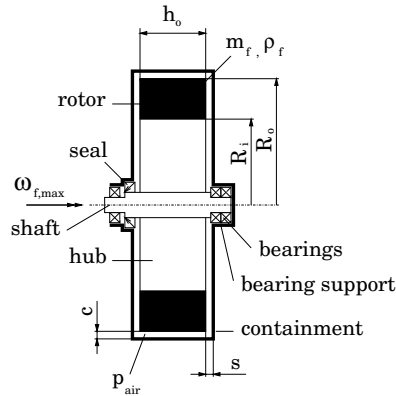
Figure 6.1: Rotor system design parameters

from equation 5.8 and 5.9 and equals

$$\frac{E_{\max}}{m_{\rm f}} = \tfrac{1}{4}\,R_{\rm o}^2(1 + \xi^2)\,\omega_{\rm f,max}^2 \tag{6.1}$$

From equation 6.1 it is seen that the maximum energy stored per unit of mass increases with increasing rotor radius $R_{\rm o}$, increasing maximum rotor speed $\omega_{\max}$ and increasing inner to outer radius ratio ξ. However there are several factors that limit or penalize the maximum specific energy:

- $E_{\max,\rm stress}$, see equation 5.5;

- $E_{\max,\rm subcr}$, see equation 5.10;

- power loss due to air friction at the sides and at the circumference of the rotor, bearing friction and, when a vacuum system is used, the vacuum pump power and seal friction.

The first two items are restrictions that limit the maximum specific energy. The third item shows a penalty on the specific energy. To be able to minimize the power loss of the rotor system, the design parameters have to be related to the power loss. In the next sections the friction losses are analyzed per component.

6.1.1 Rotor power losses

There are various ways to realize a rotor that is able to store a certain amount of energy. The maximum speed, the rotor mass and the material density all influence the final dimensions

of the rotor and so the air friction losses between the sides of the rotor and its housing. The relevant parameters in the analysis of the air friction loss are:

- material: density ρ_f;

- geometry: shape factor K, multi ring type (layered materials);

- dimensions: outer radius R_o, inner radius R_i, width h_o, side air gap s, circumferential air gap c;

- operational conditions: angular speed ω_f, air pressure p_{air}, air density ρ_{air}, air temperature θ_{air}, dynamic viscosity of air η_{air}.

The power loss due to air friction between the sides of the rotor and its housing, and between the circumference of the rotor and the housing are equal to (see [Kok, 1999]):

$$P_{side} = \tfrac{1}{2}\, \rho_{air}\, \omega_f^3\, R_o^5\, C_s(R_{e,s}\,,\, \frac{s}{R_o}) \tag{6.2}$$

$$P_{circ} = \tfrac{1}{2}\, \pi\, \rho_{air}\, \omega_f^3\, R_o^4\, h_o\, C_c(R_{e,c}\,,\, \frac{c}{R_o}) \tag{6.3}$$

where ρ_{air}, p_{air} and θ_{air} are related by (see [Genta, 1985]):

$$\rho_{air} = \frac{p_{air}}{287.2\, \theta_{air}} \tag{6.4}$$

The friction coefficients C_s and C_c are defined by [Schlichting, 1979]. Depending on the Reynolds number and the relative gap-width, four different regimes of airflow can be distinguished, being either laminar or turbulent in combination with converged or separate boundary layers, see [Kok, 1999]. The Reynolds numbers are given by

$$R_{e,s} = \frac{\omega_f\, R_o^2\, \rho_{air}}{\eta_{air}(\theta_{air})} \tag{6.5}$$

$$R_{e,c} = \frac{\omega_f\, R_o\, c\, \rho_{air}}{\eta_{air}(\theta_{air})} \tag{6.6}$$

When expressing the rotor width h_o in equation 6.3 in terms of rotor mass and rotor material density according to

$$m_f = \pi \rho_f\, h_o\, R_o^2 (1 - \xi^2) \tag{6.7}$$

equation 6.3 becomes

$$P_{circ} = \frac{\tfrac{1}{2}\, \rho_{air}\, \omega_f^3\, R_o^2\, m_f\, C_c(R_{e,c}\,,\, \frac{c}{R_o})}{\rho_f\,(1 - \xi^2)} \tag{6.8}$$

For a given rotor mass m_f and material density ρ_f, and a given ξ, it can be shown that an optimum for the sum of side and circumferential power loss exists for every required energy content. For example when increasing the rotor outer radius and subsequently decreasing the rotor speed the side power loss P_{side} increases and the circumferential power loss P_{circ} decreases. The optimized parameters are then the rotor speed, rotor outer radius and rotor width. An optimum also can be determined for the inner to outer radius ratio ξ, using the optimized outer radius and the former optimization constraints. For example when increasing ξ the power loss due to side air friction decreases (due to decreasing rotor speed) and the power loss due to circumferential air friction increases (influence of increasing rotor width is greater than influence of decreasing rotor speed).

hub design

The hub connects the flywheel rotor with its shaft. A general design target for a flywheel hub is to maximize the axial and bending stiffness with minimal mass. For disc shaped rotors (ξ=0), the flywheel and the hub can be made of the same material, which is mostly the case with steel rotors. In the case of fiber composite materials, to prevent delamination, a layered structure of different materials press fitted together is often used, [Thoolen, 1993]. When a ring type rotor is applied ($\xi \neq 0$), for steel rotors mostly the rotor will be made of one piece of material from which material on the inner side is removed. Special attention has to be paid to the connection of the hub with the rotor shaft to avoid high stresses at the connection. A good example is given by the Oerlikon Electrogyro, which combines a constant stress disc with an outer ring, [Genta, 1985]. Flywheel Energy Systems Inc. offers the combination of composite ring type rotors connected by spokes to the hub.

As far is known, flywheel rotors with spokes are not studied with respect to windage losses. For the calculation of the side air drag of ring type of rotors ($\xi \neq 0$) in this chapter it is assumed that the friction coefficient C_s is equal to the value for disc shaped rotors. After the realization of the designed flywheel it is of course possible to do a coast down test, to measure experimentally the drag torque coefficient.

shaft design

The shaft connects the hub with its bearings. A general design target for flywheel shafts is to maximize bending stiffness with minimal shaft diameters and minimal mass. Because the shaft end diameter mostly defines the minimum bearing diameter, for minimum bearing losses the shaft end diameter must be chosen as small as possible. If the driven and driving torque goes through the flywheel shaft, the maximum torque defines also the minimum shaft diameter. For determination of the minimal bearing diameter in the power loss calculations, the shaft is not considered to limit the minimal bearing size.

6.1.2 Bearing power losses

As defined in Table 6.1, rolling element bearings will be used for both sub- and super-critical flywheel systems because they are cost effective and show low friction coefficients. The relevant bearing design parameters are:

- type of rolling element bearings: ball, spindle, cylindrical, conical;

- configuration: various combinations of bearing types possible;

- dimensions and quality: outer diameter d_o, inner diameter d_i, static eccentricity e_0, pretension F_{pre}, contact angle ϕ, outer race radius r_o, inner race radius r_i, cross race radius r_r, contact element radius r_e, number of contact elements n_c;

- operational conditions: angular speed ω_f, speed dependent friction coefficient f_0, load dependent friction coefficient f_1, equivalent friction load P_0, kinematic viscosity of lubrication ν_{lub}, temperature difference within bearing θ_b.

The above parameters can be chosen to minimize bearing friction losses. The design target is to provide the required radial and axial stiffness for sub- or super-critical operation with minimal system power losses. The power loss in the bearings can be divided in load dependent losses P_{roll} and load independent losses P_{lub}, mainly caused by the lubrication of the bearings.

$$P_{\text{roll}} = f_1 \, d_{\text{m}} \, P_0(F_{\text{rad}}, F_{\text{ax}}) \, \omega_{\text{f}} \tag{6.9}$$

$$P_{\text{lub}} = 0.45 \, f_0 \, \nu_{\text{lub}}^{\frac{2}{3}} \, d_{\text{m}}^3 \, \omega_{\text{f}}^{\frac{5}{3}} \tag{6.10}$$

The mean diameter d_{m}, defined as

$$d_{\text{m}} = \frac{d_{\text{o}} + d_{\text{i}}}{2} \tag{6.11}$$

is very important especially for the power loss due to lubrication. For the power loss calculations the size of the bearings will be chosen such that the required radial and axial stiffness for sub-critical operation is obtained. For super-critical operation the bearing size could be chosen smaller if a cardanic suspension, to reduce the bearing load, is used. The required radial (bearing) stiffness is given by

$$C_{\text{rad,required}} = \frac{n}{n-1} \, m_{\text{f}} \, \omega_{\text{f,max}}^2 \tag{6.12}$$

The axial and radial bearing stiffness depend on the internal geometry of the bearing, the loads F_{pre}, F_{rad} and F_{ax} and the temperature difference between inner and outer ring:

$$C_{\text{rad,bear}} = func(F_{\text{pre}}, F_{\text{rad}}, F_{\text{ax}}, \phi, r_{\text{i}}, r_{\text{u}}, r_{\text{r}}, r_{\text{e}}, n_{\text{c}}, \theta_{\text{b}}) \tag{6.13}$$

$$C_{\text{ax,bear}} = func(F_{\text{pre}}, F_{\text{rad}}, F_{\text{ax}}, \phi, r_{\text{i}}, r_{\text{u}}, r_{\text{r}}, r_{\text{e}}, n_{\text{c}}, \theta_{\text{b}}) \tag{6.14}$$

The appropriate bearing type and size giving the required radial bearing stiffness is found using the bearing manufacturers data catalogue, [FAG, 1997]. For calculation of the equivalent friction load $P_0(F_{\text{rad}}, F_{\text{ax}})$ to determine the load dependent power loss, the radial bearing load is determined from the static and dynamic load

$$F_{\text{rad}} = m_{\text{f}} \sqrt{g^2 + n^2 \, e_0^2 \, \omega_{\text{f}}^4} \tag{6.15}$$

and the axial bearing force for the spindle bearings is assumed to be equal to the pretension required for the radial bearing stiffness

$$F_{\text{ax}} = F_{\text{pre}} \tag{6.16}$$

From equation 6.9 and equation 6.10 it is seen that with increasing rotor speed the bearing power loss increases, especially due to lubrication.

bearing support design

The bearing support connects the bearing with its housing. The design target for sub-critical operation is to maximize radial and axial stiffness with maintained roundness and position accuracy. Ball-bearings generally have an outer ring with low radial stiffness. So, the roundness of the bearing support is greatly responsible for the eccentricity of the rotating flywheel. Since most ball-bearings allow only a small tilting angle of the rotor shaft, the radial position accuracy of the bearings with respect to each other has a great influence on the bearing load. The bearing support design target for super-critical operation is to create proper stiffness characteristics to prevent or reduce structural vibrations below the maximum speed as well as to avoid critical speeds in the operational speed range, see [Thoolen, 1993]. For the power loss calculation it is assumed that the bearing support does not influence the bearing power loss.

containment design

As stated before, super-critical flywheel systems require an enclosure to maintain a vacuum or any other drag-reducing environment and to provide the required safety. For minimal air friction losses the axial and radial clearance between the flywheel and the housing must not be too small. According to [Kok, 1999] the ratio c/R_o of circumferential gap-width c and outer radius R_o must exceed 0.022 [-]. However enlarging the gap-width increases the systems volume and would result in higher reaction torques in case of a bouncing or broken rotor. The ratio s/R_o of side plane gap-width s and outer radius R_o shows a reasonable compromise for friction, packaging and safety at a value of 0.03 [-]. In the power loss calculations the ratios c/R_o and s/R_o are chosen at the mentioned values.

6.1.3   Vacuum system power losses

At very low air pressures within the flywheel housing ($p_{air} < 1$ [mbar]) and at low flywheel speeds, the power needed to maintain the air pressure may become higher than the reduction in air friction losses. Using commercially available vacuum pumps, the following relation between the vacuum pump shaft power and the final steady-state air pressure p_{air} is found by [Kok, 1999]

$$P_{pump,shaft} = \frac{A}{p_{air}} + B \qquad (6.17)$$

where A=6.0·10^3 [Pa.W] and B=75 [W]. In the power loss calculations it is assumed that the vacuum pump will be driven by an electric motor powered from the 12 [V] board net. The efficiency η_{drive} from the engines crankshaft to the shaft of the vacuum pump is estimated at a typical value of 0.5 [Bosch GmbH, Robert, 1996]. Then the power needed to maintain a given pressure within the housing becomes

$$P_{vac} = \frac{P_{pump,shaft}}{\eta_{drive}} \qquad (6.18)$$

The air leakage, caused by the rotary seal is assumed constant. The rotary seal introduces a friction torque that depends on the shaft diameter d_{shaft}. According to experimental data (see [Kok, 1999]), the power loss in the seal is given by

$$P_{seal} = 1.7\, d_{shaft}\, \omega_f \qquad (6.19)$$

The minimum seal/shaft diameter to be used is linked to the minimum inner bearing diameter according to Section 6.1.2.

6.1.4   Load conditions

The bearing load and, consequently, the bearing friction depend on both the internal and the external load resulting from the use of the flywheel system in a road vehicle. For the bottom-up design evaluation, the load conditions of both the sub- and super-critical flywheel systems are taken equal. The super-critical flywheel doesn't use a cardanic suspension as a result of the packaging limitations. The bearing size for both flywheel systems will be chosen with respect to the radial bearing stiffness needed for running safely below the first critical speed. The sum of gravitational, centrifugal, gyroscopical and acceleration forces as a result of driving a passenger car over a road appear to be negligible for the required bearing size, see [van Tilborg, 1999].

6.2 Design optimization strategy

The main idea of the design optimization is, to calculate for different rotor materials the optimum combination of outer radius R_o, speed ω_f and width h_o as function of the specific energy, to minimize the power loss in the total system P_tot, [van Druten *et al.*, 1999a].

$$P_\mathrm{tot} = P_\mathrm{side} + P_\mathrm{circ} + P_\mathrm{roll} + P_\mathrm{lub} + P_\mathrm{vac} + P_\mathrm{seal} \tag{6.20}$$

The rotor weight m_f=20 [kg] and inner to outer radius ratio ξ=0 are used as constraints in the first optimization step. The distinction between sub- and super-critically operated flywheels reveals itself in the value of the air pressure within the housing p_air and the material choices, suitable for the required energy density. In Figure 6.2 an example for one kind of material is given of the first optimization step. This figure shows the total power loss P_tot under ambient air pressure (a) and under vacuum conditions (b) as a function of the rotor radius R_o for different specific energies up to the maximum for the chosen rotor material. Both graphs show an optimum rotor radius with respect to the total power loss, due to the counteracting influence of rotor speed and rotor radius on the air friction losses. The steps in power loss seen in Figure 6.2, are the result of a discrete choice in bearing size to obtain the required radial bearing stiffness. Plotting the optimum power loss (marked with $*$) as a function of the specific energy for the different suitable rotor materials the sensitivity of specific energy to the optimum total power loss is found, see Figure 6.3. In Figure 6.3(a) it is seen that for a rotor

(a) ambient air pressure of 1 bar   (b) vacuum of 1 mbar
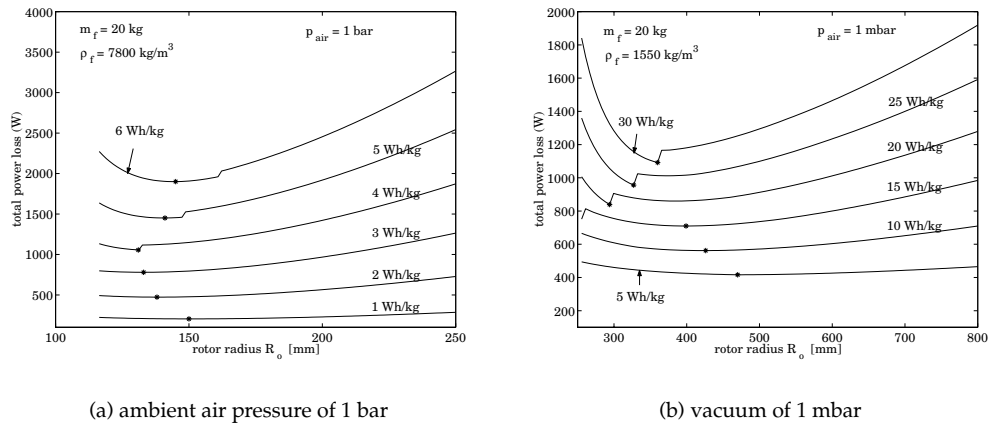
Figure 6.2: Total power loss as function of the combination of rotor radius, speed and width

in an environment with ambient air, a material with a high density such as steel is preferable with respect to minimum power losses. Contrary, in Figure 6.3(b) it is seen that for a rotor, rotating in a vacuum, no material is favourable with respect to minimum power losses. For both operational conditions the power loss increases with the specific energy and the maximum specific energies shown are limited by the maximum allowable stress in the material (limits are plotted for K=0.303 [-]). According to the maximum power loss constraint of 750 [W] the maximum specific energy for a flywheel under ambient air pressure equals approxi-

(a) ambient air pressure of 1 bar   (b) vacuum of 1 mbar
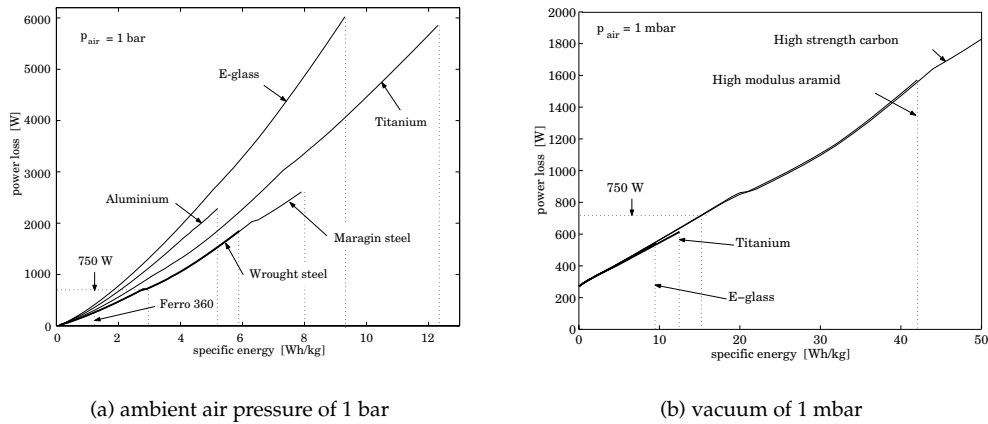
Figure 6.3: Total power loss as function of the specific energy (for a 20 [kg] rotor)

mately 3 [Wh/kg], whereas for a flywheel in vacuum 15 [Wh/kg] can be reached. Given the 3 [Wh/kg] limit in Figure 6.3(a), wrought steel shows best in minimal power losses. Its maximum energy capacity lies well above the amount that will be used. Given the 15 [Wh/kg] limit in Figure 6.3(b), the high strength or modulus fiber materials as aramid and carbon have to be used. *Generally it is seen that using the power loss constraint the rotor materials will be used well below their maximum energy storage capacity. For this application, the optimal flywheel design is found using power loss optimization instead of stress distribution optimization, generally applied to flywheel design.*

After establishing the maximum specific energy and having chosen the most suitable rotor material for both flywheel systems, the trade-off between rotor speed ω_f and rotor outer radius R_o can be made. In Figure 6.4 the total power loss, subdivided to air friction power loss P_{air}, bearing friction power loss P_b, vacuum pump power loss P_v and seal friction power loss P_s, is plotted as function of the flywheel speed for different rotor radii. As already seen in Figure 6.2 the power loss optimum appears to be flat and leaves some freedom in choosing the combination of rotor outer radius and maximum rotor speed.

The flywheel in ambient air with a maximum energy storage of 60 [Wh] (3 [Wh/kg], 20 [kg] rotor) will be operated sub-critical. It will be used in combination with a mechanical variator and therefore it is preferable to keep the speed of the flywheel as low as possible, reducing or even eliminate the reduction step between the flywheel and the variator. To reduce the maximum flywheel speed, in this case, the outer rotor radius R_o should be chosen larger than the optimum value of 133 [mm]. A radius of 200 [mm] in combination with a rotor speed of 1040 [rad/s] shows to be a good choice within the constraints.

The flywheel in vacuum with a maximum energy storage of 300 [Wh] (15 [Wh/kg], 20 [kg] rotor) will be operated super-critical and be used in combination with an electrical variator. With respect to packaging the optimum outer radius R_o has to be smaller than the optimum value of 400 [mm]. Choosing a radius of 250 [mm] the penalty to the total power loss is relatively small. The high rotor speed of 1860 [rad/s] evolving from this choice requests for

69

(a) ambient air pressure of 1 bar

(b) vacuum of 1 mbar
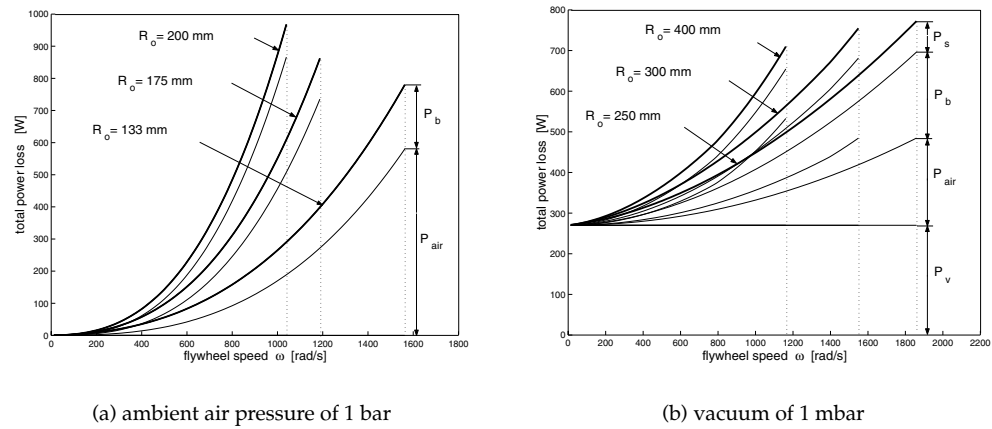
Figure 6.4: Power losses as function of rotor speed for different rotor radii

a direct coupling or integration of the electrical machine with the rotor. Given the maximum energy content of the flywheel systems and outer radius choices, the inner to outer radius ratio ξ leaves freedom for further reduction in power loss, or weight reduction. In Figure 6.5 the influence of ξ and the rotor mass to the total power loss is shown. A value of $\xi=0.8$ [-] for a flywheel in ambient air and $\xi=0.7$ [-] for a flywheel in vacuum shows to be optimal with respect to the total power loss, using a 20 [kg] rotor.

(a) ambient air pressure of 1 bar

(b) vacuum of 1 mbar
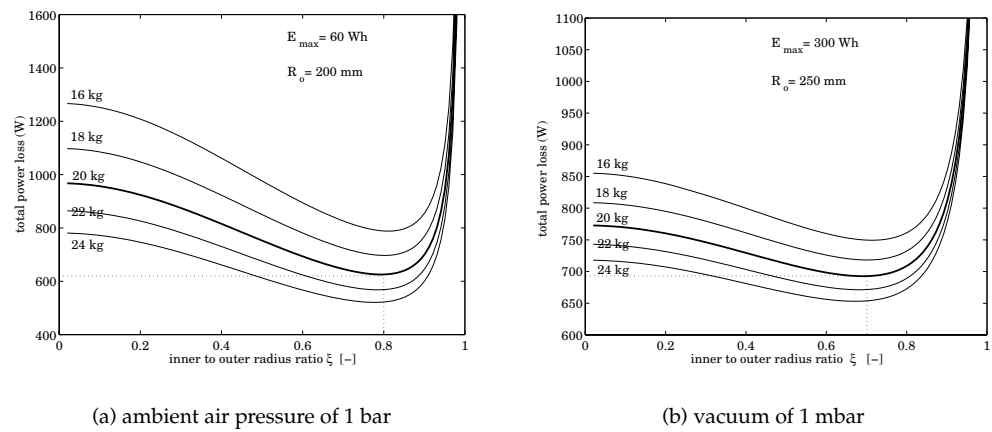
Figure 6.5: Power loss as function of the inner radius and mass sensitivity

6.3   Flywheel concepts for passenger car application

To exchange kinetic energy, a sub- or a super-critical flywheel system can be combined with either a mechanical or an electrical variator. The system and component requirements, such as rotor material, bearing support, vacuum system and safety containment, for sub-critically operated flywheels differ significantly from those for super-critically operated flywheels. Using the power loss optimization procedure two flywheel systems are conceived, see Figure 6.6. The super-critical flywheel inside a vacuum housing is able to contain five times more energy than the sub-critical flywheel operating in ambient air, having similar power losses. In Table 6.2 the specifications of both systems are compared.   Although the super-critical

(a) Sub-critical flywheel system (60 Wh)

(b) Super-critical flywheel system (300 Wh)
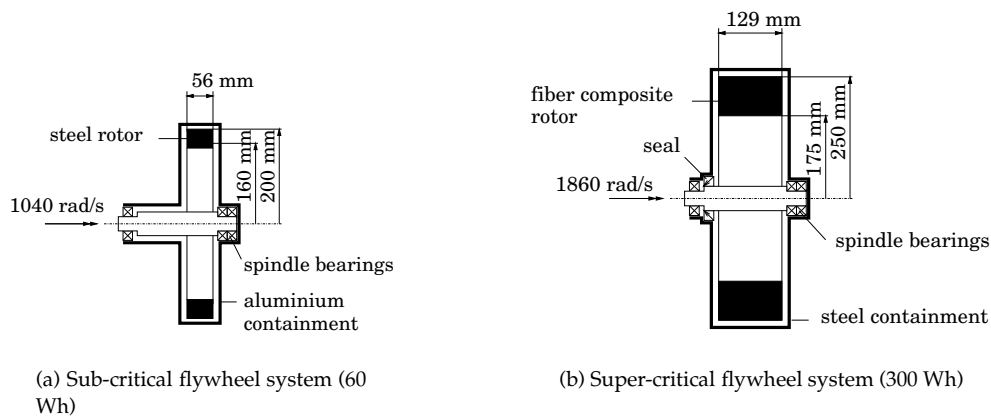
Figure 6.6: Flywheel concepts for passenger car application

flywheel system shows disadvantages over the sub-critical flywheel, it is mainly caused by the combination with the electrical variator. The design of a super-critical flywheel system in combination with a mechanical variator would give better overall system specifications and raises a challenging design case. A design that also could be considered is the combination of a sub-critical flywheel in a vacuum housing, using a mechanical variator and if necessary the use of advanced rotor materials, see [van der Graaf, 1995]. Looking at the weight and costs to be paid extra for the increase from 60 [Wh] to 300 [Wh] using an advanced flywheel system with electrical variator, five parallel steel rotors of 60 [Wh] in combination with a mechanical variator would provide better specific energy, energy density and lower costs. In a later design stage the additional weight should be canceled by an integrated design of flywheel system, transmission and engine because the weight/power ratio of the total powertrain should at least remain constant.

Commercial success of advanced flywheel systems for stationary and mobile applications is still limited. Costs, packaging and the not yet proven reliability are the most important factors that hamper widely spread application. While the efficiency benefits of these flywheel systems are staying ahead of storage devices such as electro-chemical batteries, and research to eliminate the drawbacks is going on, commercialization is likely to appear in niche-markets at first. For passenger car applications, the way to take advantage of the well-known prop-

COMPONENT / PROPERTY	SUB-CRITICAL FLYWHEEL SYSTEM	SUPER-CRITICAL FLYWHEEL SYSTEM
Energy storage capacity*	60 [Wh]	300 [Wh]
Max. stationary power loss	625 [W]	693 [W]
Air density within housing	1 [bar]	1 [mbar]
Rotor material	Wrought steel	Aramid/Carbon
Material density	7800 [kg/m^3]	1550 [kg/m^3]
Max. rotor speed	1040 [rad/s]	1860 [rad/s]
Outer rotor radius	200 [mm]	250 [mm]
Inner to outer radius ratio	0.8 [-]	0.7 [-]
Rotor width	56 [mm]	129 [mm]
Rotor weight	20 [kg]	20 [kg]
Rotor outside volume	7 [dm^3]	25.3 [dm^3]
Containment	aluminium housing	steel containment
Containment weight	5 [kg]	26 [kg]
Containment volume	10.7 [dm^3]	32.8 [dm^3]
Suspension	none	none
Variator	mechanical	electrical
Variator specific power	2 [kW/kg]	0.5 [kW/kg]
Variator power density	6 [kW/dm^3]	1 [kW/dm^3]
Variator efficiency	85 %	75 %
Total weight 75 [kW]	63 [kg]	196 [kg]
Total volume 75 [kW]	23.2 [dm^3]	107.8 [dm^3]
Total cost in mass production	€630	€3920

Table 6.2: Specification of two flywheel energy exchange systems. The energy storage capacity for both systems is limited by the maximum stationary power loss

erties of flywheels is not to extend the energy storage capacity with advanced materials and constructions, but to reduce the high energy storage request by a system integrated design. More specific, use the flywheel only because of its merits as a high power storage device, with a fast torque response, time independent behaviour, large lifespan (number of cycles), full charge depletion usage and high mechanical efficiency.

Chapter 7

Flywheel usage

7.1 Introduction

Flywheels are used for different purposes. One of the possible applications of flywheels is to smoothen the angular velocity of reciprocating machines like internal combustion engines. The design then aims at minimizing the changes of the stored energy of the flywheel. This will be discussed in some detail in Section 7.2. Another application, is to use a flywheel as an energy storage device. The design then aims at maximizing the exchange of stored energy (*e.g.*, the exchange of energy between two inertias). This will be the topic of Section 7.3 from which the results will be used in Chapter 8.

7.2 Minimizing changes of stored energy

Figure 7.1 gives a schematic representation of an internal combustion engine with a flywheel that is rigidly connected to the crankshaft. The inertia of the flywheel (including the other moving parts of the engine) is denoted by J and is assumed to be constant. The system is loaded by a load torque T_{load} which is also assumed to be constant. The individual combustions result in a periodical engine torque T_{e} at the crankshaft. This torque is approximated by the sum of a nominal, constant torque T_0 and a harmonic torque with amplitude A and angular frequency Ω, *i.e.*,

$$T_{\text{e}} = T_0 + A \sin(\Omega t) \tag{7.1}$$

From the equation of motion $J \dot{\omega} = T_{\text{e}} - T_{\text{load}}$ the angular velocity ω of the engine then follows as

$$\omega(t) = \omega_0 + \frac{T_0 - T_{\text{load}}}{J} t + \Delta\omega(t) \tag{7.2}$$

where $\Delta\omega(t)$ represents the harmonic part of the engine velocity

$$\Delta\omega(t) = -\frac{A}{J\Omega} \cos(\Omega t) \tag{7.3}$$

It is assumed that the load torque T_{load} is balanced by the nominal engine torque T_0, meaning that $\omega(t) = \omega_0 + \Delta\omega(t)$ and that the average speed is equal to the nominal speed ω_0. Furthermore, it is noted that the angular frequency Ω of the engine torque is proportional to this
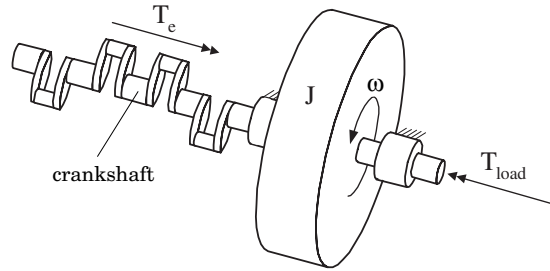
Figure 7.1: Flywheel connected to a crankshaft of an internal combustion engine

nominal speed ω_0. In formula $\Omega = p\,\omega_0$ where p depends on the engine type. For a four stroke engine with nc cylinders, p is equal to $nc/2$. With the nominal energy $E_0 = \frac{1}{2}J\,\omega_0^2$ and using $\Omega = p\,\omega_0$ it is seen that the relative amplitude $|\Delta\omega|/\omega_0$ of the oscillating part of the engine speed is given by

$$\frac{|\Delta\omega|}{\omega_0} = \frac{A}{2\,p\,E_0} \tag{7.4}$$

Hence, this relative amplitude decreases if the nominal energy increases, *i.e.,* if the inertia J or the nominal speed ω_0 are enlarged or the number of cylinders increases. In Figure 7.2 it is seen that the relative amplitude of the alternating engine speed as a result of the oscillating engine torque becomes smaller if the nominal energy E_0 increases with the engine speed. For passenger car applications, increasing the number of cylinders will increase the costs, increasing the engine inertia will increase the weight/volume of the inertia and also reduce the net engine power when speeding up the engine. Increasing the nominal speed of the engine is unfavourable for the the fuel consumption, see Chapter 3. Generally a compromise between the mentioned penalties is found for every type of engine-transmission-vehicle combination.

7.3 Maximizing energy exchange

Another application, is to use a flywheel as an energy storage device. This function usually aims at maximizing the exchange of stored energy. In Figure 7.3 an example of a kinetic energy exchange system with a mechanical variator is shown. Assuming that there are no resulting external torques on the system, the energy balance reads

$$E_1(t) + E_2(t) = C \tag{7.5}$$

where E_i (i=1,2) represents the kinetic energy of inertia i with angular velocity ω_i and moment of inertia J_i:

$$E_i(t) = \tfrac{1}{2}\,J_i\,\omega_i(t)^2, i = 1, 2 \tag{7.6}$$

Defining the ratio of the CVT r_{cvt} by

$$r_{cvt} = \frac{\omega_2}{\omega_1} \tag{7.7}$$
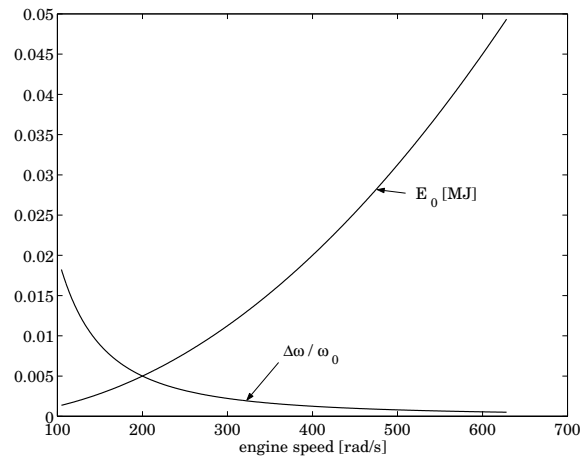
Figure 7.2: Relative amplitude of the alternating engine speed $|\Delta\omega|/\omega_0$ as function of the engine speed, *i.e.*, nominal stored energy E_0. Four cylinder four stroke engine (p=2) with torque amplitude A=100 [Nm] and engine inertia J=0.25 [kgm^2]
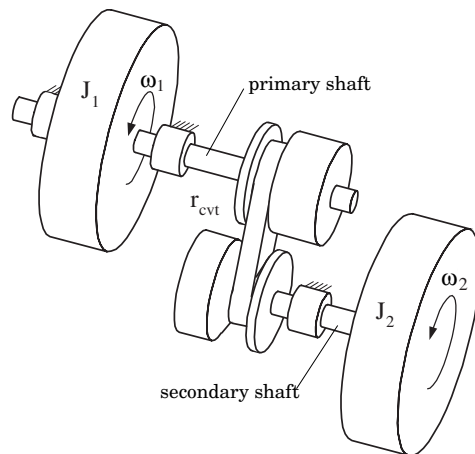
Figure 7.3: Two inertias J_1 and J_2 coupled by a mechanical continuously variable transmission

the angular velocities ω_1 and ω_2 are related to this ratio and to the total energy C by

$$\omega_1^2 = \frac{2\,C}{J_1 + r_{\text{cvt}}^2 J_2}; \quad \omega_2 = r_{\text{cvt}}\,\omega_1 \tag{7.8}$$

75

The possible ratios of a mechanical CVT are upper and lower bounded, *i.e.,*

$$0 < r_{\text{cvt,min}} \leq r_{\text{cvt}} \leq r_{\text{cvt,max}} < \infty \tag{7.9}$$

As a consequence, the velocities of both inertias are upper and lower bounded if the total energy is given.

$$\omega_{1,\text{max}}^2 = \frac{2C}{J_1 + r_{\text{cvt,min}}^2 J_2}; \quad \omega_{2,\text{min}} = r_{\text{cvt,min}}\, \omega_{1,\text{max}} \tag{7.10}$$

$$\omega_{1,\text{min}}^2 = \frac{2C}{J_1 + r_{\text{cvt,max}}^2 J_2}; \quad \omega_{2,\text{max}} = r_{\text{cvt,max}}\, \omega_{1,\text{min}} \tag{7.11}$$

For the so-called speed coverage $s_i = \omega_{i,\text{max}}/\omega_{i,\text{min}}$ of inertia i (i=1,2) it follows that

$$s_1^2 = \frac{J_1 + r_{\text{cvt,max}}^2 J_2}{J_1 + r_{\text{cvt,min}}^2 J_2}; \quad s_1 s_2 = R = \frac{r_{\text{cvt,max}}}{r_{\text{cvt,min}}} \tag{7.12}$$

with R named the *ratio coverage* of the CVT.

Using these results it can be shown that the ratio of $E_{1,\text{max}} = \frac{1}{2} J_1 \omega_{1,\text{max}}^2$ and $E_{2,\text{max}} = \frac{1}{2} J_2 \omega_{2,\text{max}}^2$ and the ratio of the inertias J_1 and J_2 are given by

$$\frac{E_{1,\text{max}}}{E_{2,\text{max}}} = \frac{1 - (\frac{1}{s_2})^2}{1 - (\frac{s_2}{R})^2} \tag{7.13}$$

$$\frac{J_1}{J_2} = (\frac{\omega_{2,\text{max}}}{\omega_{1,\text{max}}})^2 \frac{E_{1,\text{max}}}{E_{2,\text{max}}} \tag{7.14}$$

For a symmetric CVT with $r_{\text{cvt,min}} = 1/r_{\text{cvt,max}}$ the ratio of the maximum speeds becomes

$$\frac{\omega_{2,\text{max}}}{\omega_{1,\text{max}}} = \frac{s_2}{\sqrt{R}} = \frac{\sqrt{R}}{s_1} \tag{7.15}$$

In Figure 7.4 the ratio of $E_{1,\text{max}}$ and $E_{2,\text{max}}$ is shown as function of the secondary speed coverage s_2 for different CVT ratio coverages R. From this figure it is seen that the larger the speed coverage s_2, the larger the energy ratio $E_{1,\text{max}}/E_{2,\text{max}}$. Also seen from this figure is that the energy ratio, with constant speed coverage s_2, decreases with increasing ratio coverage R of the CVT.

When both speed coverages are the same, *i.e.,* $s_1 = s_2 = \sqrt{R}$, the maximum stored energies are equal. Even if $s_1 = s_2$, the maximum speed of both inertias can be different when using an asymmetric CVT, *i.e.,* a CVT with $r_{\text{cvt,min}} \neq 1/r_{\text{cvt,max}}$. This is illustrated in Figure 7.5. As a result of the logarithmic scale for the speeds on the vertical axis in this figure, an asymmetric CVT can be identified by the tilting of the dashed line, connecting the logarithmic mean speeds of both inertias. For construction reasons, however, mechanical CVTs are mostly symmetrical. When choosing different primary and secondary speed coverages, *i.e.,* $s_1 \neq s_2$, the maximum energy ratio is not equal to one anymore. In Figure 7.6 the maximum and minimum speeds of both inertias for unequal speed coverages are illustrated. As seen in equation 7.13, the energy ratio $E_{1,\text{max}}/E_{2,\text{max}}$ is independent of the symmetry or asymmetry of the CVT. The speed ratio $\omega_{2,\text{max}}/\omega_{1,\text{max}}$, on the other hand, depends on the symmetry or asymmetry of the CVT, as is illustrated in Figure 7.6. In Figure 7.7 the inertia ratio J_1/J_2 is shown for a symmetric CVT
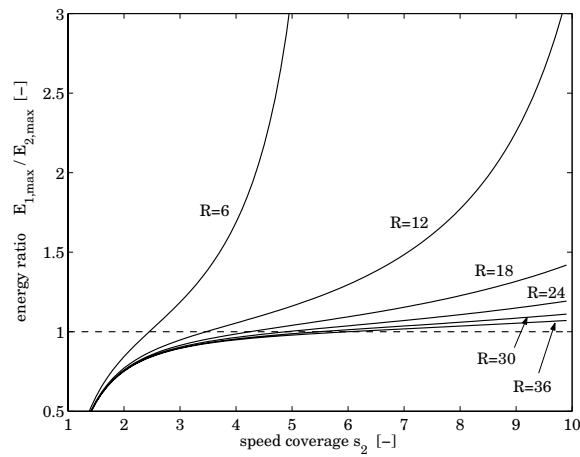
Figure 7.4: Energy ratio $E_{1,max}/E_{2,max}$ as function of the speed coverage s_2 for different CVT ratio coverages R

(a) Symmetric CVT   (b) Asymmetric CVT

Figure 7.5: Maximum and minimum speeds of two inertias connected by a mechanical CVT. Ratio coverage $R = 6$, equal speed coverages $s_1 = s_2 = \sqrt{6}$

as function of the speed coverage s_2 for different ratio coverages R. As can be seen from this figure the inertia ratio is one when the speed coverages are equal, *i.e.,* $s_2 = \sqrt{R}$.

In conclusion: to maximize the energy exchange between two inertias coupled by a symmetrical mechanical CVT with a finite ratio coverage R, *i.e.,* aiming for $E_{1,max}/E_{2,max} = 1$, the speed coverages of both inertias have to be equal $s_1 = s_2$. The speed coverages can be increased by enlarging the ratio coverage R of the CVT. Given a certain ratio coverage R of the CVT, the speed coverage of one inertia can be increased at the cost of increased energy content, *i.e.,* inertia, of the other. Using an asymmetric CVT the speed ratio $\omega_{2,max}/\omega_{1,max}$ can be altered, however the energy ratio $E_{1,max}/E_{2,max}$ remains unchanged.

(a) Symmetric CVT (b) Asymmetric CVT

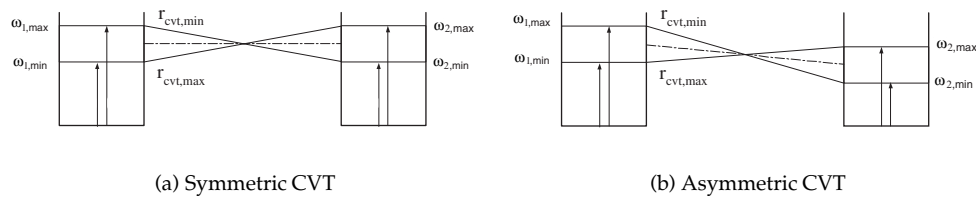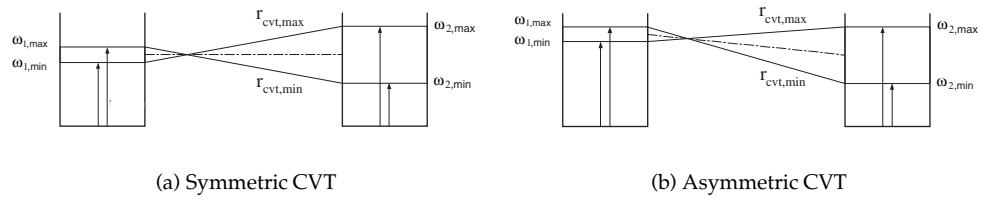Figure 7.6: Maximum and minimum speeds of two inertias connected by a mechanical CVT. Ratio coverage $R = 6$, unequal speed coverages $s_1 = 1.5, s_2 = 4$
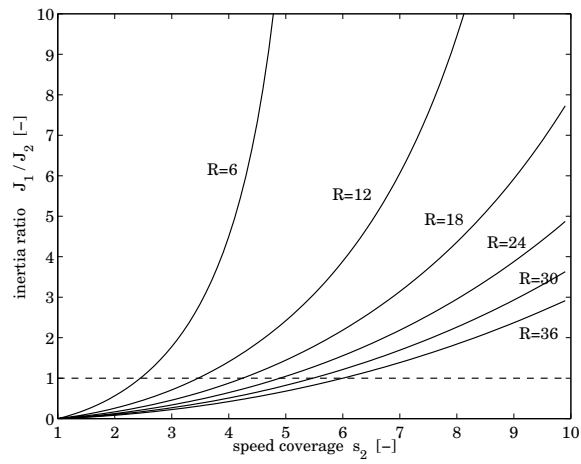
Figure 7.7: Inertia ratio J_1/J_2 as function of the speed coverage s_2 for different CVT ratio coverages R

Chapter 8

Kinetic energy exchange: top-down design

8.1 Introduction

The profit of a kinetic energy exchange system in an automotive powertrain must lie in the improvement of driveability and fuel economy. One of the possible applications is the exchange of kinetic energy between a flywheel and the vehicle mass. The design then enables to use the Start-Stop and Brake Energy Recovery fuel saving principles. The demands coming from the use of this kind of system in a passenger car will be investigated in Section 8.2. Another application, is to exchange kinetic energy between a flywheel and the engine's inertia. This application is aimed at using the E-line tracking and Stop-Go fuel saving principles. The demands to the kinetic energy exchange system for this application will be investigated in Section 8.3. In that section also the ZI and ZI-SG powertrain concepts are proposed.

8.2 Flywheel-vehicle energy exchange

One natural application of an extra flywheel in an automotive powertrain would be the exchange of kinetic energy between the flywheel and the vehicle mass. The mechanical variator (CVT), present between the engine and the wheels in many cars today, can be used for this application when the extra flywheel is connected to the primary shaft of the CVT, *i.e.,* when the engine's inertia is enlarged. In Figure 8.1 a schematic view of such a CVT driveline is given. The given system is a combination of Figure 7.1 and Figure 7.3 with added road load and brake torques at the wheel. Inertia J_2 represents the inertia of the vehicle (m_v) and of the wheels ($4J_w$). In practice a final drive reduction gear r_d is placed between the secondary shaft of the transmission and the wheel to adapt the speed and torque. In Figure 8.1 the final reduction gear is lumped into the inertia J_2 and the vehicle speed v_v.

$$J_2 = r_d^2(m_v\,R_w^2 + 4\,J_w) \tag{8.1}$$

$$v_v = r_d\,\omega_2\,R_w \tag{8.2}$$
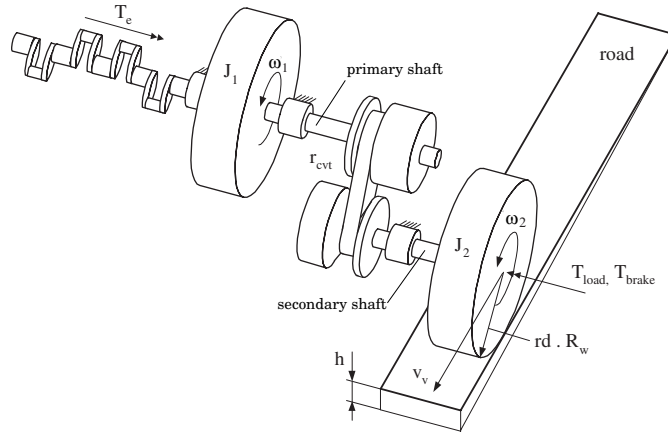
Figure 8.1: Kinetic energy between a flywheel and the vehicle mass. Driveline representation by two inertias coupled by a mechanical CVT

With the external torques T_e, T_{load} and T_{brake} on the two inertias, equation 7.5 becomes

$$\int_0^t [T_e\,\omega_1 - (T_{load} + T_{brake})\omega_2]dt = \tfrac{1}{2}\,J_1[\omega_1^2(t) - \omega_1^2(0)] + \tfrac{1}{2}\,J_2[\omega_2^2(t) - \omega_2^2(0)] + m_v\,g\,[h(t) - h(0)]$$

$$\text{(8.3)}$$

$$E_e - E_{load} - E_{brake} = E_1 + E_2 + E_p - C \qquad\qquad \text{(8.4)}$$

T_{load} represents the load torque at the secondary shaft, due to, *e.g.*, air drag, rolling resistance and bearing losses. T_{brake} represents the torque exerted by the brakes at the secondary shaft. The brake energy E_{brake} can be recovered in the flywheel J_1 by shifting the transmission to a lower ratio r_{cvt}. In practice no brake torque has to be applied for decelerating the vehicle on a flat road, except when the brake power exceeds the driveline specification and the rear or front wheels have to assist. The potential energy of the car E_p can not be recovered in practice. The amount of energy released when driving downhill and needed for driving uphill cannot be predicted. Also the order in energy requirement or release can not be predicted yet, for example when entering a parking lot it is not known before if you are going up or down. Moreover, the longer the time between the kinetic energy storage and usage the larger the energy loss caused by the friction of the flywheel system. Assuming a flat road and applying no external brake torque on the wheels, equation 8.4 becomes

$$E_e - E_{load} = E_1 + E_2 - C \qquad\qquad \text{(8.5)}$$

However, if equal hill climbing and descending performance with respect to a purely engine driven car is requested, the size of the internal combustion engine and the brakes can not be reduced. To enable kinetic energy exchange between the flywheel J_1 and the vehicle inertia J_2, the flywheel must be speeded up by the engine initially. The kinetic energy of the flywheel can then be used to reduce the energy demand of the engine in multiple ways:

1. kinetic energy exchange between the flywheel and the vehicle to accelerate or decelerate the vehicle, while the engine is operated continuously, just to compensate the external

loading;

$$E_1 + E_2 = C; \quad E_e = E_{\text{load}} \tag{8.6}$$

2. energy exchange between the flywheel and the vehicle to accelerate or decelerate the vehicle and to compensate the external loading. The engine is now operated intermittently, with a certain time interval, to overcome the friction losses.

$$E_1 + E_2 + E_{\text{load}} = C; \quad E_e = E_{\text{load}} \tag{8.7}$$

In principle, unlimited accelerations and decelerations can be performed, when over the total speed range of the vehicle kinetic energy can be exchanged with the flywheel. Only the shifting speed of the CVT and the maximum power that can be transmitted by the CVT will restrict the maximum performance of the vehicle. In Figure 8.2 the kinetic energy, exchanged over the total speed range of the vehicle, is shown. In the second method the speed (*i.e.,* kinetic
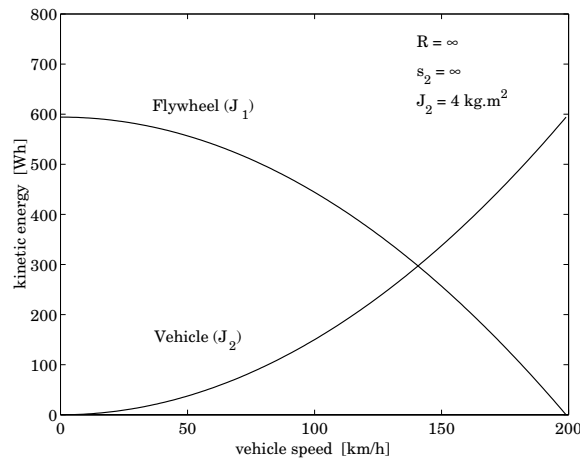
Figure 8.2: Kinetic energy exchange between a flywheel and the vehicle mass of a mid size passenger car. Ratio coverage R is not limited, J_2=4 [kgm^2], R_w=0.3 [m] and r_d=0.175 [-]

energy) of the flywheel is not directly related to the vehicle speed, since the kinetic energy in the flywheel is also used to overcome the friction losses. In this case a certain flywheel speed band has to be used. If the flywheel reaches the lower bound, the engine has to be started to speed up the flywheel till the upper bound is reached, after which the engine will be shut down again. The gain over the first method is that the engine is either shut down (no fuel consumption) or operated in or close to its best efficiency point. In this way the fuel consumption is improved more than 40% with respect to continuous operation of the engine in the first method [Kok, 1999]. The penalties of intermittent engine operation over the first method are the mode switches which require a lot of effort to ensure comfort, performance and proper thermal management, see Section 3.3.3.

For both engine operation strategies it is important to know the restrictions caused by the finite ratio coverage R of the CVT. In Figure 8.3 the flywheel speed ω_1, respectively engine speed, is shown in relation to the vehicle speed v_v for a ratio coverage R of 24 and 12. It is seen that the maximum vehicle speed $v_{v,max,kinetic}$, as far as energy can be exchanged between the flywheel and the vehicle, is limited by the maximum (overdrive) ratio r_{od} of the CVT. As a

(a) ratio coverage R=24   (b) ratio coverage R=12

Figure 8.3: Flywheel speed, limited by the ratio coverage of the CVT, as function of the vehicle speed for different maximum energy contents of the flywheel. The secondary speed coverage s_2 equals R/2

result of the minimal (low) ratio r_{low}, a clutch between the flywheel and the primary shaft of the CVT must be used to transmit the torque while launching the vehicle. By a small increase of the vehicle speed $v_{v,close}$, at which the clutch will be closed, the maximum vehicle speed $v_{v,max,kinetic}$ can be greatly increased. However the increase of $v_{v,close}$ means that the engine speed and thus the flywheel speed have to increase, resulting in a higher maximum energy level of the flywheel and a larger slip trajectory for the clutch.

The automotive V-belt variator of today has a maximum ratio coverage R of approximately 6. The ratio coverage can be enlarged using a power split device, but this will decrease the transmission efficiency, see [Mattsson, 1996]. Using mode switching, *i.e.,* using the ratio coverage of the CVT twice, a ratio coverage of R^2=36 can be reached, see [Höhn, 1994]. In Figure 8.4 the kinetic energy exchange using a conventional variator with a ratio coverage R of 6 is shown. As was seen in Figure 7.4 the use of the kinetic energy is maximal when both speed coverages are the same, *i.e.,* when the secondary speed coverage equals $\sqrt{R}$. To ensure a reasonable vehicle speed coverage given the relatively small ratio coverage of six, the vehicle speed coverage has to be chosen higher. In Figure 8.4 the trade off between maximum flywheel energy and vehicle speed coverage is shown.

The following aspects have to be taken into account when designing a driveline for a mid size passenger car using energy exchange between a flywheel and the vehicle mass:

- due to the unpredictable amount (and order) of potential energy release and require-

(a) ratio coverage R=6, vehicle speed coverage s_2=3

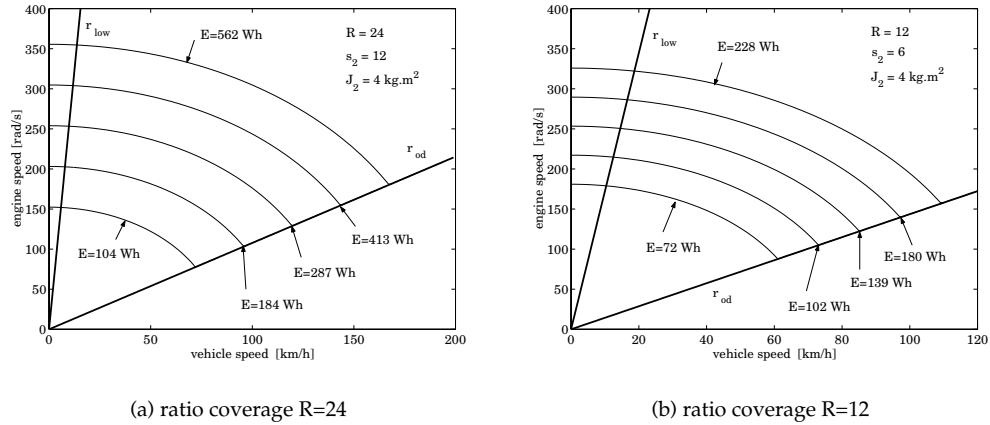(b) ratio coverage R=6, vehicle speed coverage s_2=4
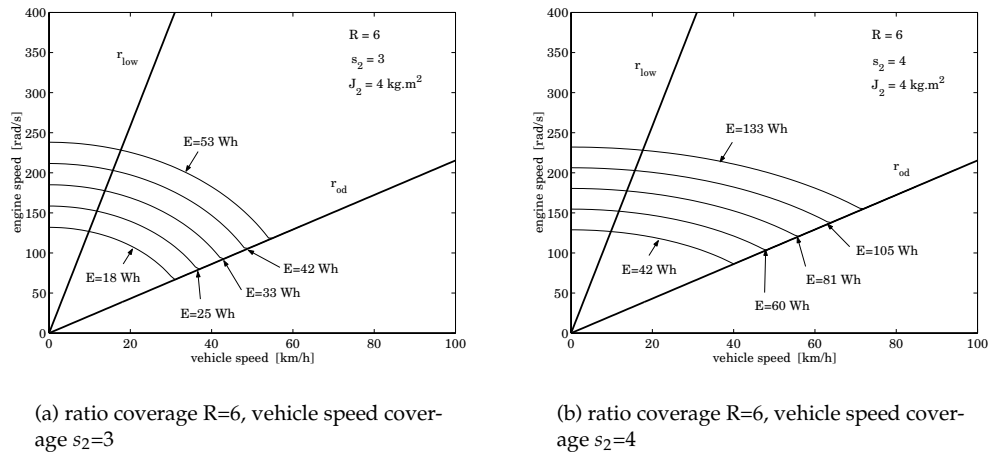
Figure 8.4: Flywheel speed, limited by the ratio coverage of the CVT, as function of the vehicle speed for different maximum energy contents of the flywheel ($s_2 > \sqrt{R}$)

ment, the energy exchange with a flywheel is limited to kinetic energy exchange only;

- the size of the engine and the brakes can not be reduced without limiting the use of the car (allowing hill climbing/descending and maximum vehicle speed);

- the vehicle speed range in which kinetic energy can be exchanged is limited by the storage capacity of the flywheel and the ratio coverage of the CVT;

- before initially launching the vehicle, the flywheel has to be speeded up by the engine;

- to exchange the kinetic energy over the full speed range of the vehicle, the ratio coverage R of the CVT must be larger than 24 and the flywheel must be able to store more than 400 [Wh];

- when limiting the vehicle speed range in which kinetic energy can be exchanged, the engine speed at the end of the speed range (CVT in overdrive) has to be sufficient for driving the vehicle;

- for kick downs close to or in overdrive, the flywheel must be decoupled to allow the engine to speed up fast to increase its power level;

- a decoupled flywheel has to be "picked up" when driving in the limited speed range again.

Regarding the above design aspects a prototype flywheel hybrid driveline for a passenger car was developed at the Technische Universiteit Eindhoven in the the years 1980-1998, see [van der Graaf, 1995] and [Kok, 1999]. In 1976, a Ford Pinto was equipped with a gasoline engine, flywheel and hydrostatic CVT at the University of Wisconsin, see [Frank and Beachley,

1980]. General Motors Research Laboratories also built a prototype engine-flywheel hybrid powertrain, see [Schilke *et al.*, 1984]. More recently, at the Swiss Federal Institute of Technology (ETH) a prototype of a flywheel hybrid driveline incorporating an electric machine is designed and tested, see [Dietrich *et al.*, 1999].

8.3 Flywheel-engine energy exchange

Contrary to the previous section, where energy exchange was considered between the flywheel and the vehicle inertia, now energy exchange between the flywheel and the engine is studied. The innovation values of this principle are Stop-Go and E-line tracking. The main idea is to speed up or down the engine inertia, using a secondary power source, *i.e.,* a flywheel. It will be seen that straightforward use of the variator, already present in the driveline, is not possible. New concepts, based on a conventional CVT powertrain will be proposed to meet the specific demands. In figure 8.5 a conventional CVT powertrain used in a passenger car is shown, with an, as yet unconnected flywheel. The inertia J_1 is the equivalent inertia of all
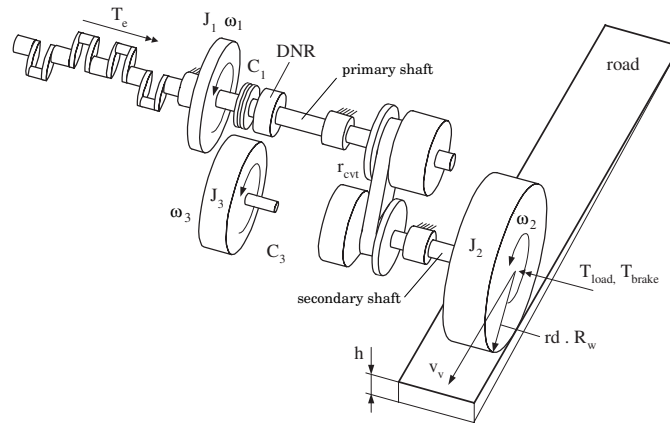
Figure 8.5: CVT driveline with engine inertia J_1, launch clutch C_1, Drive Neutral Reverse unit, push-belt CVT, equivalent vehicle inertia J_2 and to be coupled flywheel inertia J_3

rotating components on the primary side of the CVT. The clutch C_1, materialized as a torque-converter for most CVTs, is required for launching the vehicle because the CVT has no infinite ratio coverage. The vehicle mass, the wheels of the car and the rotating components, which are directly connected to the secondary shaft of the CVT, are represented by the equivalent inertia J_2. The inertia J_3 represents the flywheel inertia that is to be used for energy exchange with the inertia J_1. As for the exchange of energy between the flywheel and the vehicle mass, also here a variator is needed between the inertias. The demands on the variator are different for Stop-Go and E-line tracking.

With Stop-Go, the vehicle and engine initially have zero speed and an infinite ratio coverage of the variator between the flywheel and the engine is needed to start the engine. Furthermore, using stop-go the engine is shut-down automatically when the vehicle is stopped, and the driver will not accept a time delay between a kick-down of the accelerator pedal and

vehicle launch [Vroemen, 2001]. So, while starting the engine with the flywheel, a positive torque has to be applied to the vehicle inertia J_2.

With E-line tracking the engine is running, and its speed will be kept as low as possible for every stationary vehicle speed by controlling the CVT ratio in or close to overdrive. In this ratio the flywheel speed has to be high to enable energy exchange, *i.e.,* power assist. In contrary, when the engine speed is high, *i.e.,* the CVT ratio is low, no power assist from the flywheel is needed. The flywheel speed can thus be directly linked to the ratio of the CVT, *e.g.,* high flywheel speed in overdrive and low flywheel speed in the low CVT ratio. Thinking of using the mechanical CVT that is already present between the engine and the wheels, it could be considered to connect the flywheel directly to the secondary side of the CVT, see Figure 8.6. Then, however, the vehicle has to slow down when the flywheel is to be used to speed up the engine and vice versa. Decoupling the vehicle inertia J_2 from the secondary shaft of the CVT is also no option, as it results in a torque interruption at the wheels. Hence it seems
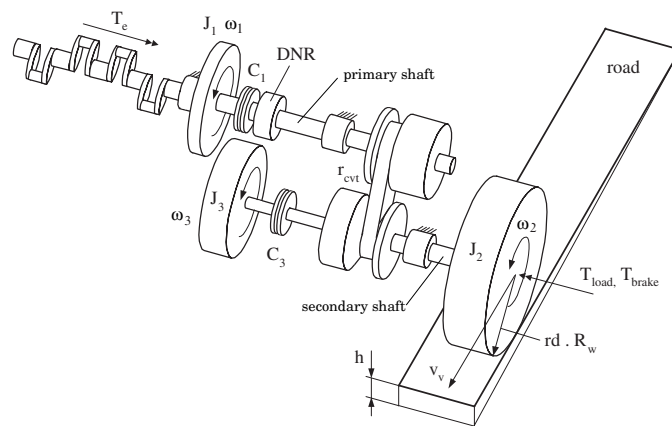
Figure 8.6: CVT driveline with clutch C_3 between flywheel and secondary side of the CVT

impossible to directly use the present CVT between the engine and the wheels. An additional CVT between the flywheel and the engine would give all the flexibility needed, but it would be a costly solution with severe packaging and weight penalties. Alternatively, one could think of two clutches and a fixed reduction gear between the flywheel and the engine, although with the 50% (average) efficiency of the clutches due to slip this would give a severe penalty to the fuel consumption reduction of E-line tracking. Of course criteria as size, weight, complexity and costs also are of great importance. In the following, first the design of the power assist application (E-line tracking) will be discussed. After that, Stop-Go will be considered in some detail.

8.3.1 Power assist specification

To track the E-line, a short duration (1-2 seconds), additional peak power of approximately 27 [kW] is needed to ensure responsive acceleration of the car, as argued in Chapter 3. In this section, the power assist specification is studied in more detail. The mentioned values of 27

[kW] and 18 [Wh] in Section 3.3.1 are based on a specific engine speed trajectory and a specific vehicle speed. It will be seen that the power assist specification greatly depends on the vehicle speed at which the assist is requested.

In Figure 8.7 a variogram of the reference vehicle is shown. Here, ω_{min} is the engine speed, required for a proper operation of the engine. Furthermore, ω_{max} is the maximum allowable engine speed. From Figure 8.7 it is seen that the possible engine speeds, given a vehicle speed v_v, are bounded by ω_{min}^* and ω_{max}^*, due to the finite ratio coverage $R = r_{od}/r_{low}$ of the CVT:

$$\omega_{min}^*(v_v) = max(\omega_{min}, \frac{v_v}{r_d\, r_{od}\, R_w}); \quad \omega_{max}^*(v_v) = min(\omega_{max}, \frac{v_v}{r_d\, r_{low}\, R_w}) \qquad (8.8)$$

The difference $\Delta\omega_{trans}(v_v)$ of $\omega_{max}^*(v_v)$ and $\omega_{min}^*(v_v)$ is called the maximum possible *speed transient* at vehicle speed v_v.
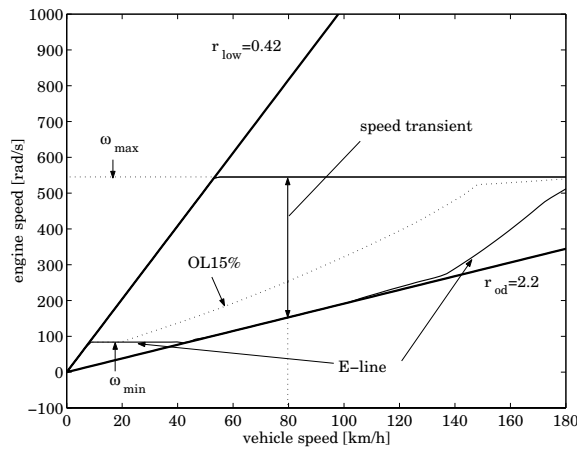
Figure 8.7: Variogram of the reference CVT powertrain a ratio coverage R=5.24, r_d=0.21, R_w=0.31 [m]

In Figure 8.7 also the engine speed as a function of the stationary vehicle speed v_v is drawn for E-line tracking and for OL15%-line tracking, using the vehicle parameters of Section 3.2.1 and the measured CVT efficiency according to [Vroemen, 2001]. From this figure it is seen that the maximum possible speed transient $\Delta\omega_{trans}(v_v)$ greatly depends on the vehicle speed, having a maximum around 55 [km/h]. The speed transient from the E-line to the maximum possible engine speed, $\Delta\omega_{trans}(v_v)$ at 80 km/h, is used as an example throughout this section.

In Figure 8.8, the required engine power for stationary driving $P_{stationary}$ and the engine power levels reached when fully opening the throttle, from three different operating lines, are plotted as function of the vehicle speed. The engine speeds at which the engine power reserve lines $P_{reserve,E-line}$, $P_{reserve,OL15\%}$ and $P_{reserve,low}$ are calculated, correspond with the E-line, OL15%-line and low-line respectively, indicated in Figure 8.7. The engine power reserve from the E-line, based on engine torque reserve only (ω_1=constant), does not exceed the 10 [kW] over the total vehicle speed range, also seen in Section 3.3.1. If, next to fully opening the throttle, the engine is speeded up instantly to its maximum value ω_{max}^*, the maximum engine power level P_{max} can be reached above 55 [km/h], while below this vehicle speed the maximum engine power level is limited by the low ratio $P_{reserve,low}$.

86
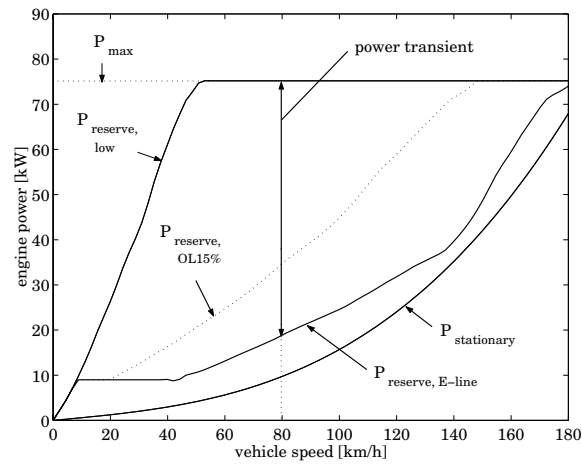
Figure 8.8: Stationary and maximum achievable engine power levels as function of the vehicle speed and operating line

The engine *power transient* indicated in Figure 8.8, shown at 80 [km/h], can only be made when the engine is speeded up according to the engine speed transient indicated in Figure 8.7. The power needed to make the speed transient, depends on the magnitudes of the engine's inertia and acceleration. If the indicated engine speed transient is performed within one second, the power request will penalize the driveability. If more time is taken to speed up the engine, the car will feel sluggish due to the created power gap. Using a power assist system the power gap can be filled up to accomplish a step-wise power transient. The required peak power of the power assist system is very near to the magnitude of the desired power transient, as is illustrated in Section 3.3.1. Assuming the driveability level reached with the OL15%-line acceptable in practice, from Figure 8.8 it can be seen that the magnitude of the required power transient, *i.e.,* the required peak power of the power assist system, increases with the vehicle speed between 20 and 140 [km/h]. Above 140 [km/h] the power requirement of the power assist system decreases, and below 20 [km/h] no power assist system is required to enable E-line tracking.

In contrary to the required peak power, the energy requirement is relatively low. In Figure 8.9 the required energy to speed up the engine from ω^*_{min} to ω^*_{max} as function of the vehicle speed is shown. In this figure the required energy when shifting to three different transmission ratios is shown, initiated from either the E-line or the OL15%-line. Below a vehicle speed of 55 [km/h] the maximum achievable engine power level is reached at the low ratio r_{low}, while above this vehicle speed the maximum power level is reached at higher transmission ratios. For example at 80 [km/h] the maximum engine power is found at a ratio r_{cvt} of 0.61. In Figure 8.9 it is seen that the required energy first increases with increasing vehicle speed, up to an amount of 10 [Wh] at 55 [km/h] for both E-line and OL15%-line, after which it decreases only slightly when departing from the E-line and substantial when departing from the OL15%-line. These net energy requirements are in shrill contrast with the energy demand for exchanging energy with the vehicle inertia, as depicted in section 8.2. Typically the required energy is 10 to 50 times less, and no accumulated energy is needed at stand still of the vehicle.
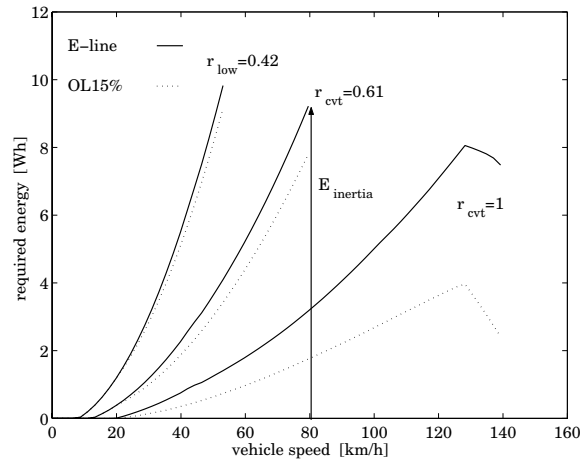
Figure 8.9: Required energy to perform the maximum possible speed transient $\Delta\omega_{\mathrm{trans}}(v_{\mathrm{v}})$ as function of the vehicle speed, using constant shifting speed, 2 [s] shifting time and an engine inertia J_1 of 0.25 [kgm²]

8.3.2 Zero Inertia concept

Looking at the system of Figure 8.5 again there are three inertias, *i.e.,* the engine, vehicle and flywheel, to be coupled together. The kinetic energy exchange between the engine inertia and the flywheel requires the flywheel to speed down when the engine is speeded up and vice versa, while the vehicle speed remains nearly constant. This speed relation between three components is also seen between the left and right wheel of a car and the speed of the car itself when cornering. For example, when making a turn to the left, the right wheel speeds up and the left wheel speeds down, while the vehicle speed remains constant. It is common to use a differential, *i.e.,* planetary gear set, between the driven wheels to transmit the drive torque equally to each wheel while cornering. Applying this principle to the current design problem, one could imagine the three inertias of Figure 8.5 connected to the members of a planetary gear set, *i.e.,* to the annulus, to the carrier and to the sun gear. Then the speeds of the three inertias are kinematically linked. In the so called 'Zero Inertia' concept, schematically depicted in Figure 8.10, the vehicle inertia is connected to the carrier, the flywheel is connected to the sun gear and the primary side of the driveline is connected to the annulus.

It seems a rather cost effective solution since only a planetary gear and a small flywheel (net 10 [Wh]) have to be added to the conventional CVT drive train. It remains to be seen whether the system works at all vehicle speeds, what is the maximum flywheel energy to be stored and what is the transient behaviour. Design and analyzing tools to optimize the system have been developed and will be discussed in Chapter 9.

8.3.3 Stop-go specification

As depicted in Chapter 3, it is seen that to accelerate the engine towards its idle speed (800 [rpm]) within 0.15 [s], the energy and power requirements are 0.26 [Wh] and 12.6 [kW] respectively. Table 8.1 contains the net requirements for additional vehicle launch under different
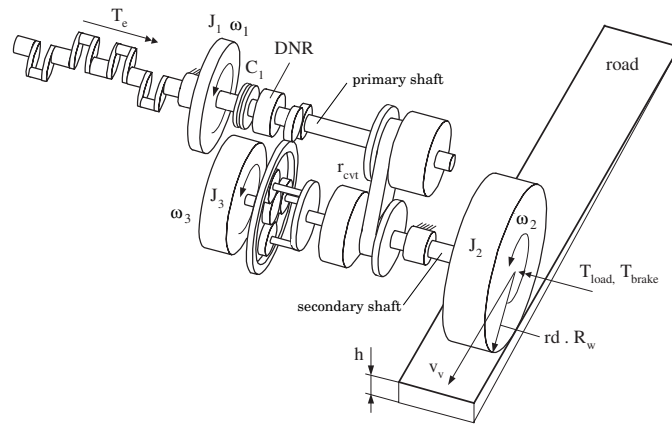
Figure 8.10: CVT driveline with epicyclic geared inertia J_3 "Zero-Inertia" concept

vehicle acceleration conditions. The values in this table are calculated for the reference vehicle with the CVT in low r_{low}, and assuming that the accelerations are constant. The highest acceleration level specified for every start condition is equally to the maximum acceleration of the reference vehicle with 1.6 liter engine. The acceleration on a flat road is limited to 4 $[m/s^2]$, and on a road slope of 30% the acceleration of the vehicle is limited to 1.5 $[m/s^2]$. The lower the vehicle acceleration level, the more time it takes to speed up the engine to 800 [rpm], and the more energy is lost due to friction losses. The higher the vehicle acceleration level the higher the power requirement, due to the shorter starting time. Starting the engine and the vehicle on a road slope additional potential energy is required.

START CONDITION	VEHICLE ACCELERATION $[m/s^2]$	START-TIME [s]	ENERGY [Wh]	POWER [kW]
idle-start	0	0.15	0.27	13
idle-start + vehicle launch with:	1	1.88	1.36	5.2
	4	0.47	1.03	15.8
idle-start + vehicle launch + 30% ramp with:	0.5	3.76	5.66	10.8
	1	1.88	3.29	12.6
	1.5	1.25	2.5	14.4

Table 8.1: Required net energy and net power for different start-stop conditions: J_1=0.25 $[kgm^2]$, J_2=4 $[kgm^2]$, $T_{drag.engine}$=15 [Nm], $T_{drag.load}$=55 [Nm], r_d=0.175 and r_{low}=0.42

8.3.4 ZI Stop-Go concept

Facilitating the Zero Inertia concept of Figure 8.10 with the Stop-Go functionality it has to be decided whether starting condition will be used. From the driveability point of view a direct launch of the vehicle, while starting the engine would be preferable. In practice, this strategy shows a wide variation in required energy, making it difficult to guarantee an engine start under all conditions.

According to the design specification a new stop-go concept has evolved, guaranteeing an engine start under all conditions and directly applying a torque to the wheels. This concept, based on the flywheel power assist concept in Figure 8.10, needs two additional clutches, and is shown in Figure 8.11. By closing clutch C_3 the flywheel, rotating at a certain speed, applies
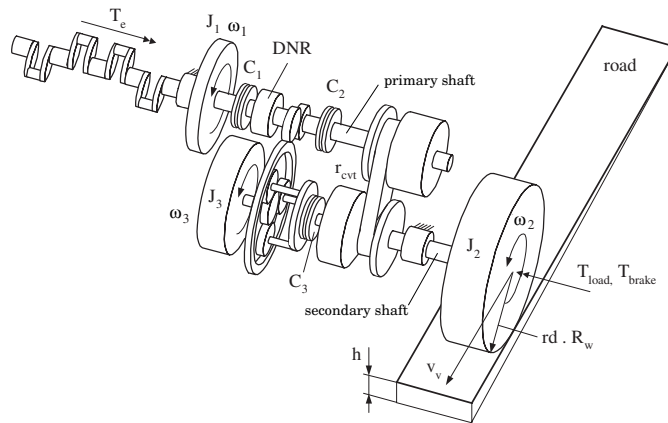
Figure 8.11: CVT driveline with epicyclic geared inertia J_3 and stop-go clutches C_2 and C_3, "ZI Stop-Go" concept

a torque at both the engine and the wheels via the planetary gear set. The additional clutch C_2 is needed to decouple the CVT from the driveline. In [Vroemen, 2001] the control strategy, using the additional clutches C_2 and C_3 and clutch C_1 and the drive and reverse clutch inside the DNR, is developed and experimental results with a the prototype Stop-Go transmission on a test-rig are presented. While the control strategy using the five clutches appears to be quite complex, the materialization takes only two additional clutches and the performance of both engine start and vehicle launch is well established.

90

Chapter 9

Driveline design tools

To analyze the proposed flywheel driveline concepts and to optimize the system parameters, the models as shown in Figure 8.10 and Figure 8.11 can be used. In this chapter a graphical representation of the kinematics and dynamics is developed. Using so called "translational driveline models" combined with a general representation of epicyclic gears, the essential phenomena within the proposed driveline concepts can be explained, [van Druten *et al.*, 1999b]. In Chapter 10 it will be seen that many insights in the functioning of a driveline and more specific of the ZI powertrain can be gathered using these translational models.

9.1 Translational driveline model

In this section a translational driveline model, that is equivalent to the rotational driveline model in Figure 8.5, will be derived. In the translational model angular velocities and moments of inertia are replaced by translational speeds and masses. The inertias J_1 (with angular velocity ω_1) and J_2 (with angular velocity ω_2) in Figure 9.1 are replaced by an equivalent engine mass m_e with linear speed v_e and an equivalent vehicle mass m_v with linear speed v_v, such that

$$m_e = \frac{J_1}{R_w^2}; \quad v_e = \omega_1 R_w \tag{9.1}$$

$$m_v = \frac{J_2}{R_w^2}; \quad v_v = \omega_2 R_w \tag{9.2}$$

where R_w is the wheel radius. From $\omega_2 = r_d r_{cvt} \omega_1 = r_{drive} \omega_1$ it then follows that $v_v = r_{drive} v_e$. Defining the equivalent engine force F_e by $F_e = T_e / R_w$ and the equivalent load force F_{load} by $F_{load} = T_{load} / R_w$, the power balance for the system in Figure 9.1 becomes:

$$m_v \dot{v}_v v_v = F_e v_e - m_e \dot{v}_e v_e - F_{load} v_v \tag{9.3}$$

For future analyzes it is beneficial to have a graphical representation of the kinematic relation $v_v = r_{drive} v_e$ and the dynamic equation 9.3. Such a representation is given in Figure 9.2. The displacements s_e and s_v are proportional to, respectively, v_e and v_v with proportionality constant α. Furthermore, the "damping" coefficients b_e and b_v are proportional to, respectively, m_e and m_v with proportionality constant $1/\alpha$. The constant a, *i.e.,* the distance a in Figure 9.2
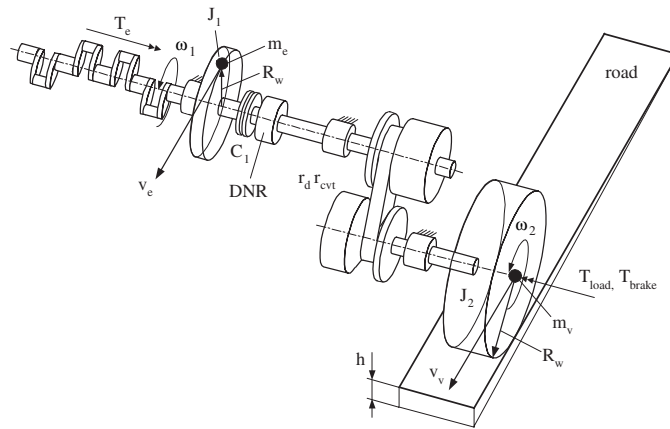
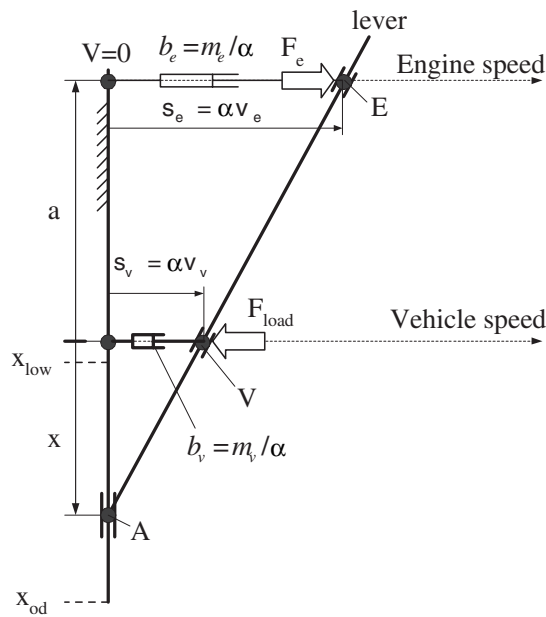Figure 9.1: Driveline model considering translational speeds of both engine and vehicle mass

Figure 9.2: Translational Driveline Model (TDM)

can be chosen arbitrarily. From Figure 9.2 it is seen that $(a + x)\, s_v = x\, s_e$. Hence, with $s_e = \alpha\, v_e$

and $s_v = \alpha\, v_v$ it follows that the distance x is related to r_{drive} by:

$$r_{\text{drive}} = \frac{x}{a + x} \qquad (9.4)$$

Since r_{drive} is limited by $r_{\text{drive,low}} = 0.09$ and $r_{\text{drive,od}} = 0.5$ it can be concluded that x can vary from $x_{\text{low}} = 0.1\,a$ to $x_{\text{od}} = a$. With the introduced quantities equation 9.3 can be rewritten as:

$$(a + x)(F_e - b_e\,\dot{s}_e) = x\,(F_{\text{load}} + b_v\,\dot{s}_v) \qquad (9.5)$$

This is exactly the equation for moment equilibrium of the lever with respect to hinge point A in Figure 9.2. Therefore, with an appropriate interpretation of the quantities in Figure 9.2, the system in this figure is equivalent to the kinematic relation $v_v = r_{\text{drive}}\, v_e$ plus the dynamic equation 9.3. It is fairly uncommon to use an analog of this type. However, it yields a model in which the speeds and the ratio are visualized. Later on, a similar Translational Driveline Model (TDM) will be used to analyze the driveline with an extra flywheel.

For an analysis of the acceleration response potential of a passenger car, the TDM in Figure 9.2 is used. The distance x (with $x_{\text{low}} \leq x \leq x_{\text{od}}$) of point A is an unique measure for the ratio between vehicle and engine speed. The angle between the lever and the vertical is a measure for the value of the engine and vehicle speed. When the engine force is not sufficient to achieve the required vehicle acceleration level (horizontal speed of the lever in point V), point A has to be shifted towards x_{low} for better leverage. It is seen that, due to the engine inertia (b_e in Figure 9.2), the vehicle acceleration response while shifting point A towards x_{low}, depends on the shift speed. If the shift speed $\dot{x}$ of point A is low, the lever is turning around point A, resulting in a slow acceleration of the vehicle. If $\dot{x}$ is high, the lever initially turns around a point between point V and point E, so an initial negative acceleration will follow.

9.2 General epicyclic gear representation

To represent the third inertia (see Figure 8.10) in the TDM, a translational model of the kinematics of an epicyclic gear has to be used. In Figure 9.3 different configurations of a single epicyclic gear are shown. In general a single epicyclic gear consists of three elements, rotating about a common axis, and one or more planet gears. The tangential speeds of the three elements are combined by the planet gear(s). The planet gear axles are fixed to the carrier, which is one of the three rotating elements. For the epicyclic gear of Figure 9.3(b), the planet gear speeds are shown in Figure 9.4. The relation between the speeds v_1, v_2 and v_3 and the radii R_{p1} and R_{p2} of the planet gear is given by

$$v_3 = \frac{R_{\text{p1}}}{R_{\text{p1}} + R_{\text{p2}}}\, v_2 + \frac{R_{\text{p2}}}{R_{\text{p1}} + R_{\text{p2}}}\, v_1 \qquad (9.6)$$

Another relationship exists between the radii of the three elements R_1, R_2, R_3 and the planet gear radii R_{p1}, R_{p2}, given by

$$R_3 = \frac{R_{\text{p1}}\, R_2 + R_{\text{p2}}\, R_1}{R_{\text{p1}} + R_{\text{p2}}} \qquad (9.7)$$

The radii R_1 and R_2 can be equal. Usually this is true for a differential gear. Using equation 9.6, equation 9.7 and $v_n = \omega_n\, R_n$ it is seen that

$$\omega_2 = (z + 1)\,\omega_3 - z\,\omega_1 \qquad (9.8)$$
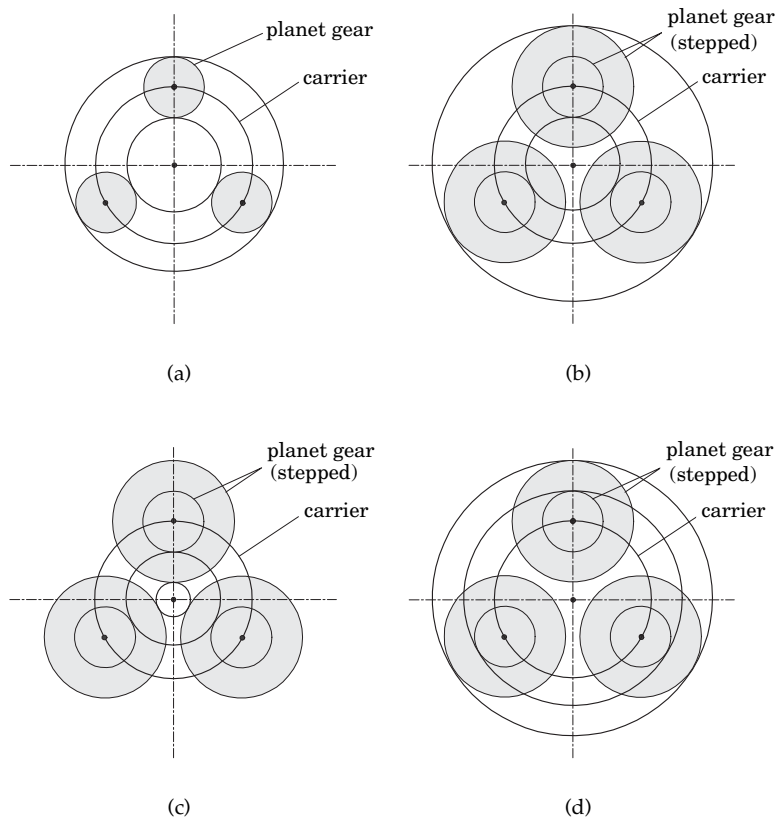
Figure 9.3: Epicyclic gear configurations

with epicyclic gear ratio z, given by

$$z = \frac{R_{\mathrm{p2}}}{R_{\mathrm{p1}}} \frac{R_1}{R_2} \tag{9.9}$$

An epicyclic gear with $R_1 = R_2 = R_3 = \beta$ and the planet radii normalized with R_{p1} is shown in Figure 9.5. The circumferential speeds in Figure 9.5 all are based on the radius β, and thus are proportional to the angular speeds of the three elements.

9.2.1 Fixed reductions

Taking into account fixed reductions connected to the planetary gear $\omega_{\mathrm{n}} = \omega_{\mathrm{n}}^*/r_{\mathrm{n}}$, equation 9.8 becomes

$$\frac{k}{r_2} \omega_2^* = k \frac{(z+1)}{r_3} \omega_3^* - k \frac{z}{r_1} \omega_1^* \tag{9.10}$$
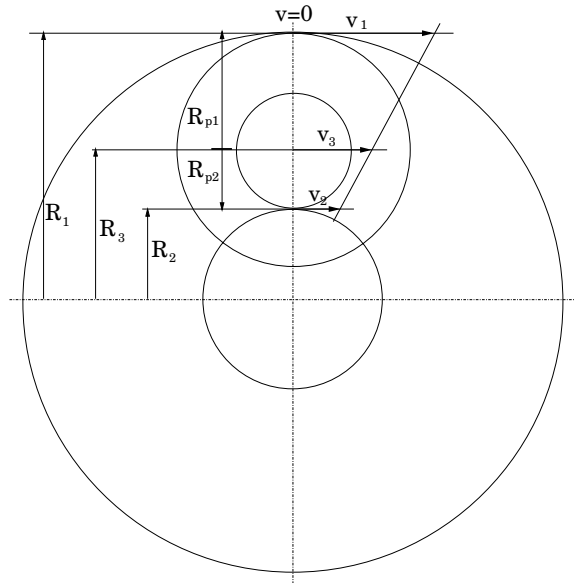
Figure 9.4: Speed balance on planet gear
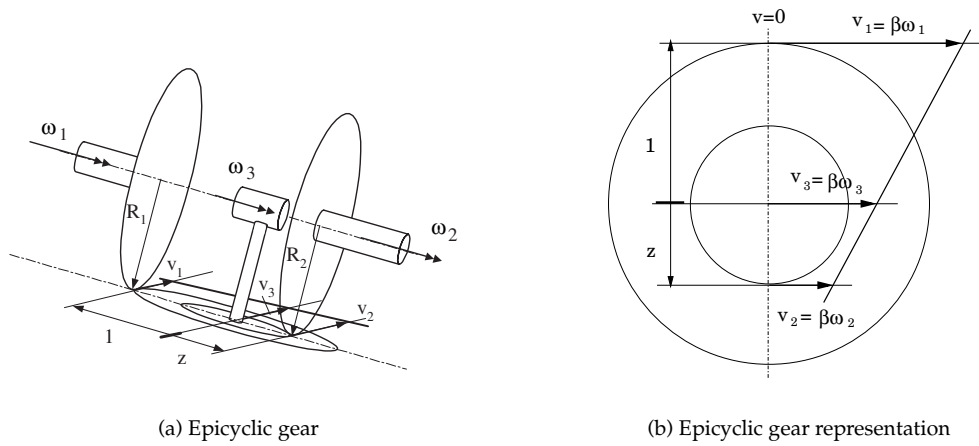
(a) Epicyclic gear

(b) Epicyclic gear representation

Figure 9.5: General epicyclic gear representation

where a factor k is introduced to establish the original form of equation 9.8 also for the case with reductions. This means that k has to satisfy

$$k \frac{(z+1)}{r_3} = k \frac{z}{r_1} + 1 \tag{9.11}$$

95

$$k = \frac{1}{\frac{z+1}{r_3} - \frac{z}{r_1}} \tag{9.12}$$

Then equation 9.10 can be written as

$$\kappa\,\omega_2^* = (z^* + 1)\,\omega_3^* - z^*\,\omega_1^* \tag{9.13}$$

where κ and z^* are given by:

$$\kappa = \frac{k}{r_2} = \frac{1}{(\frac{z+1}{r_3} - \frac{z}{r_1})\,r_2} \tag{9.14}$$

$$z^* = \frac{1}{\frac{z+1}{r_3}\frac{r_1}{z} - 1} \tag{9.15}$$

If z^* is the required kinematic ratio, it is seen that with the use of fixed reductions, this ratio can be realized with different epicyclic gear ratios z. Figure 9.6 gives a visual representation of equation 9.13. When fixed reductions are connected to the epicyclic gear one speed will be scaled with the factor κ.

(a) Epicyclic gear   (b) Epicyclic gear representation
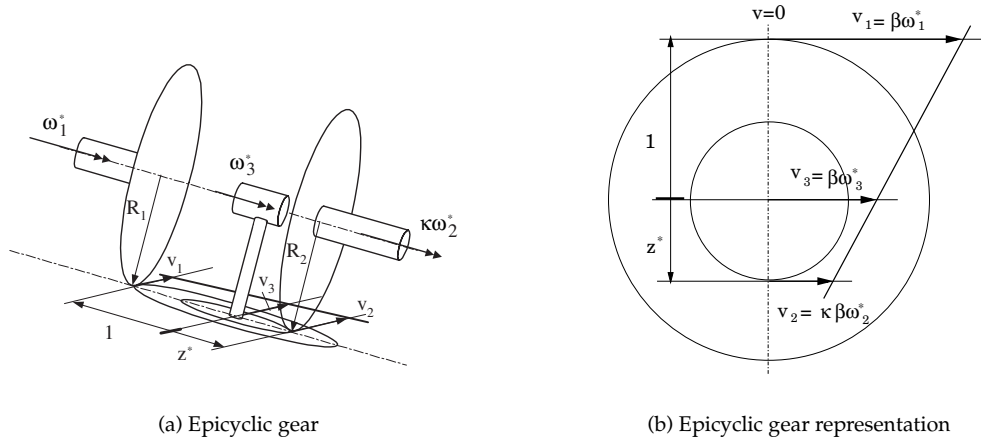
Figure 9.6: General epicyclic gear representation with fixed reductions

9.3 Extended translational driveline model

Comparing the epicyclic gear representation with fixed reductions of Figure 9.6 with the ZI concept shown in Figure 8.10, it is seen that ω_1^*, ω_3^* and ω_2^* are corresponding with the engine speed ω_e, the wheel speed ω_v and the flywheel speed ω_f, respectively. Hence equation 9.13 can be written as

$$\kappa\,\omega_f = (z^* + 1)\,\omega_v - z^*\,\omega_e \tag{9.16}$$

Mapping the epicyclic gear representation of Figure 9.6 onto the earlier given TDM of Figure 9.2, a translational model for a driveline with an epicyclic gear and a flywheel can be made.
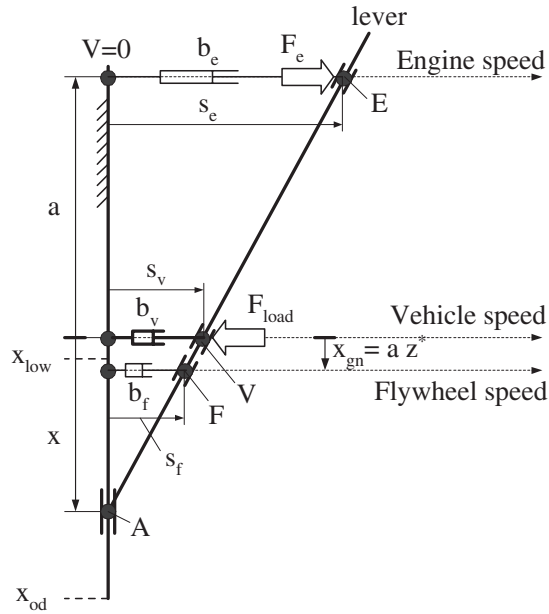
Figure 9.7: Extended Translational Driveline Model (ETDM)

This Extended TDM (ETDM) is shown in Figure 9.7. The meaning of the quantities F_e, a, s_e, s_v, b_e, b_v and x in Figure 9.7 is the same as in Figure 9.2. The displacement s_f and the "damping" coefficient b_f are proportional to, respectively, ω_f and J_f and are defined by

$$s_f = \alpha \, \kappa \, R_w \, \omega_f \tag{9.17}$$

$$b_f = \frac{J_f}{\alpha \, \kappa^2 \, R_w^2} \tag{9.18}$$

where α is equal to the proportionality factor for the TDM in Figure 9.2. The radius indicated with β in Figure 9.6 becomes equal to R_w. It is noted that the ETDM in Figure 9.7 is equivalent to the equation of motion 9.3 plus the kinematic relations $v_v = r_{drive} v_e$ and 9.16. Comparing Figure 9.7 and Figure 9.6, the relation for the epicyclic gear ratio z^* becomes:

$$z^* = \frac{x_{gn}}{a} \tag{9.19}$$

When the transmission ratio r_{drive} (indicated with x in Figure 9.7) is equal to $r_{drive.gn}$ (indicated with x_{gn}) the flywheel is not rotating. Therefore this specific transmission ratio is indicated with "geared neutral".

$$r_{drive.gn} = r_d \, r_{gn} = \frac{x_{gn}}{a + x_{gn}} = \frac{z^*}{1 + z^*} = \frac{r_3}{z + 1} \frac{z}{r_1} \tag{9.20}$$

In Figure 9.7 it is seen that there are only two parameters, namely z^* ($r_{\text{drive,gn}}$) and b_{f} which determine the kinematics and dynamics of the extra flywheel in the powertrain. The functional design is therefore directed towards optimization of only these two parameters with respect to the reference CVT driveline. Using the ETDM in Figure 9.7 it will be shown that the flywheel positively influences the transient behaviour of the vehicle while shifting for $x > x_{\text{gn}}$ (*i.e.*, $r_{\text{drive}} > r_{\text{drive,gn}}$).

Chapter 10

Zero-inertia powertrain design

The insights gained from the ETDM of Figure 9.7 in Section 9.3 show that only two indepen-
dent parameters influence the functionality of the epicyclic geared flywheel. These parameters
are optimized in a functional design optimization in this chapter. The outcome of this opti-
mization is the starting point for a constructive optimization. Finally a proposal is given for
the constructive realization of the mechanical power assist driveline.

10.1   Functional design: parameter optimization

The only two parameters which determine the functioning of the mechanical torque assist are
the gear ratio z^* and the coefficient $b_f = J_f / \alpha \, \kappa^2 \, R_w^2$, as shown in Figure 9.7). Using equation
9.16, the flywheel speed can be written as

$$\omega_f = \frac{\omega_v}{\kappa} \left(z^* + 1 - \frac{z^*}{r_{\text{drive}}} \right) \tag{10.1}$$

and hence, the energy stored in the flywheel equals

$$E_f = \tfrac{1}{2} \, b_f \, \alpha \, R_w^2 \, \omega_v^2 \left(z^* + 1 - \frac{z^*}{r_{\text{drive}}} \right)^2 \tag{10.2}$$

The flywheel speed depends on the kinematic factor κ (see equation 10.1), but the energy
content of the flywheel turns out to be independent κ. While the ratio z^* is directly linked to
$r_{\text{drive.gn}}$, the value of the factor b_f influences the energy content of the flywheel E_f, and can be
seen as a scaled flywheel inertia. The two parameters z^* and b_f together determine the energy
content of the flywheel as a function of the vehicle speed and the drive ratio, see equation
10.2. The factor κ manifests itself as a fixed reduction between the flywheel and the planetary
gear and thus gives freedom of choice in the trade off between flywheel speed and flywheel
inertia. Using the ETDM of Figure 9.7 the following insights can be gathered:

- while shifting fast from overdrive to low without the flywheel attached, the lever will
  have a center of rotation between point V and point E and thus the vehicle speed will
  initially decrease (jet-start principle described in Section 3.3.1);

- attaching the flywheel, the rotation point of the lever, while shifting fast from overdrive to low, changes towards point F. If $b_f \gg b_e$ the lever will turn around a point between point F and point V, resulting in a positive initial acceleration of the vehicle (positive speed of point V) when making a fast shift towards low (ZI principle);

- the magnitude of the scaled flywheel inertia b_f has to be dimensioned such that the lever will have a center of rotation just below point V, *i.e.,* ensuring a positive acceleration when shifting towards low and ensuring a negative acceleration when shifting towards overdrive;

- if x_{gn} is chosen close to x_{low}, the flywheel will be a negligible part of the load when the vehicle acceleration is large at low vehicle speeds;

- the larger x_{gn}, the more effective the flywheel will be. However, a large value of x_{gn} limits the shifting range of point A in which the flywheel will give a positive force to the driveline. If x (point A) crosses x_{gn} towards x_{low} the flywheel b_f will swing over to the opposite direction and then will have a negative contribution to the acceleration of the vehicle;

- the optimum for x_{gn} will be found between x_{low} and x_{med};

- at vehicle halts the energy content of the flywheel is negligible. The energy increases with increasing vehicle speed, according to the required energy content for power assist, as seen before in Figure 8.9.

The ETDM of Figure 9.7 can be used to determine the influence of changing the parameters x_{gn} and b_f. An analytical study, performed by [Serrarens, 2001], leads to the introduction of another kinematic ratio, called "zero-inertia" ratio or ZI ratio r_{zi}, here to be expressed as

$$r_{\text{drive,zi}} = r_{\text{drive,gn}} \left(1 + \frac{J_e}{(z^*)^2} \frac{\kappa^2}{J_f} \right) \tag{10.3}$$

For drive ratios between the zero-inertia ratio $r_{\text{drive,zi}}$ and the overdrive ratio $r_{\text{drive,od}}$, unlimited shifting speeds are allowed without compromising driveability. Between $r_{\text{drive,zi}}$ and $r_{\text{drive,gn}}$ the flywheel contributes positively to the driveline dynamics, but the acceptable shifting speeds are not unlimited. Between $r_{\text{drive,gn}}$ and $r_{\text{drive,low}}$ the flywheel absorbs power from the powertrain. Using equation 5.8 and using equation 10.1 the factor κ^2/J_f in equation 10.3 can be written as

$$\frac{\kappa^2}{J_f} = \frac{\omega_v^2}{2E_f} \left(z^* + 1 - \frac{z^*}{r_{\text{drive}}} \right) \tag{10.4}$$

Using equation 10.3 and equation 10.4, and given the engine inertia J_e=0.234 [kgm^2] the relation between $r_{\text{drive,zi}}$, $r_{\text{drive,gn}}$ and the maximum stored energy $E_{f,\text{max}}$ is found. From the ETDM of Figure 9.7 it is seen that the maximum energy in the flywheel $E_{f,\text{max}}$ will be reached at the maximum possible vehicle speed in overdrive or at top-speed of the vehicle. As can be seen in Figure 8.7, the maximum flywheel energy will be reached between 140 and 180 [km/h], depending on the ratios z^* and κ. For the next considerations it is assumed that the flywheel will reach its maximum speed at 180 [km/h], resulting in $r_{\text{drive}} = 0.32$ and $\omega_{v,\text{max}}$=163 [rad/s] corresponding with the maximum energy in the flywheel $E_{f,\text{max}}$. The relation between the two ratios and the maximum energy to be stored in flywheel is shown in Figure 10.1. An increase of the ZI ratio $r_{\text{drive,zi}}$ penalizes the ratio range in which power assist to the wheels is limited only by the shift speed, and an increase of the geared neutral ratio $r_{\text{drive,gn}}$ penalizes the
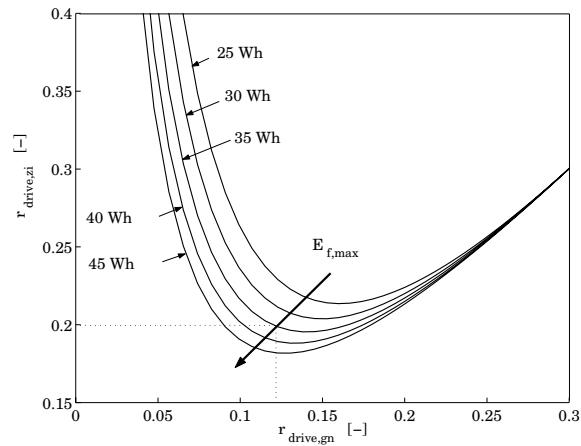
Figure 10.1: Zero-inertia drive ratio as function of the geared-neutral drive ratio for different maximum flywheel energies

maximum launch performance. The maximum energy to be stored has to be kept as low as possible to reduce weight, costs, volume and power losses of the flywheel system. With the insights gathered and with the results of many simulations (see [Serrarens, 2001]), an optimal choice is made for the parameters, see Table 10.1. In Figure 10.2 the four special drive ratios

PARAMETER	VALUE
$E_{f,max}$ (top-speed)	34 Wh
$r_{drive,gn}$	0.123
$r_{drive,zi}$	0.2

Table 10.1: Functional parameters of the ZI powertrain

$r_{drive,low}$, $r_{drive,gn}$, $r_{drive,zi}$ and $r_{drive,od}$ are shown as a function of the ratio z^*. It is seen that the characteristic of the zero-inertia powertrain is determined by the choice of either two of the parameters noted in Table 10.1.

10.1.1 Characteristic of the Zero Inertia powertrain

Given the energy content $E_{f,max}$=34 [Wh] of the flywheel and the ratio $z^* = 0.14$, the coefficient b_f can be determined from equation 10.2. The ETDM of Figure 9.7 can now be used to demonstrate the characteristics of the powertrain. Although not a functional parameter, the factor κ has to be chosen to define the horizontal speed scale of the flywheel. In equation 10.1 it is seen that κ can be determined if the maximum flywheel speed $\omega_{f,max}$ at maximum vehicle speed $\omega_{v,max}$ is known. Using the power loss optimization of Section 6.2 with the maximum energy content of 34 [Wh] as input, an optimum for the flywheel dimensions and the maximum flywheel speed will evolve for given flywheel mass and given ratio ξ. The outcome of the constructional optimization for a proof of concept transmission design (see Section 11.2)
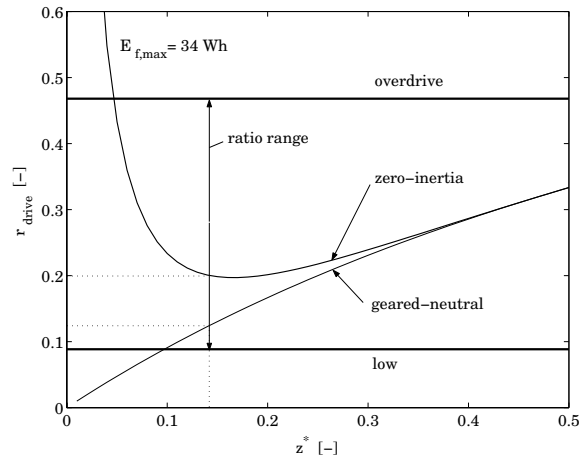
Figure 10.2: Drive ratios as function of the ratio z^*

shows a maximum speed of the flywheel of 782 [rad/s], resulting in κ=0.146. Using this value for κ and the functional parameters of Table 10.1 the behaviour of the zero-inertia powertrain is illustrated with the use of the ETDM of Figure 9.7. Before doing this, the characteristic of the ZI-powertrain is considered from the point of view of the power and energy demands defined in section 8.3.1. As an example, Figure 10.3(a) shows the engine speed transient at 80 [km/h] while shifting from overdrive r_{od} to r_{zi}. In Figure 10.3(b) the corresponding flywheel speed transient is shown, illustrating the opposite speed direction while shifting. Shifting through r_{gn} it is seen that the flywheel speed changes sign, *i.e.,* the flywheel runs in opposite direction. Looking at the engine power transient corresponding with the engine speed transient, in Figure 10.4(a) it is seen that the indicated ZI-power transient exceeds the power reserve from the OL15%-line. The different "power reserve" lines indicated with r_{zi}, r_{gn} and r_{low} show the final power level that is reached at the indicated ratio with wide open throttle. The engine power reserve lines $P_{reserve,E-line}$ and $P_{reserve,OL15\%-line}$ illustrate the power level that is reached when the engine speed is operated at the corresponding operating line, and the throttle is fully opened without changing the engine speed.

The "power reserve" to the zero-inertia ratio r_{zi} could be compared with the engine power reserve lines, since speeding up the engine while shifting towards r_{zi} requires no energy, as shown in Figure 10.4(b). When shifting further down towards r_{gn} it is seen that even with the ZI powertrain, net energy is required, however far less than without the assisting flywheel, see the line indicated with r_{drive}=0.13 in Figure 8.9. It can be concluded that, even though the net energy requirements of the flywheel are relatively small (<10 [Wh]), it is hard to meet the energy demand below the zero-inertia ratio. Nevertheless the ZI power transient surpasses the power reserve of the OL15%-line, associated with comfortable driving.

10.1.2 0 to 100 [km/h] acceleration

One of the design criteria for a powertrain is the time for acceleration from stand still to 100 [km/h] after a kick-down. While the ZI powertrain is not intended to assist the launch of

(a) engine speed trajectories

(b) flywheel speed trajectories
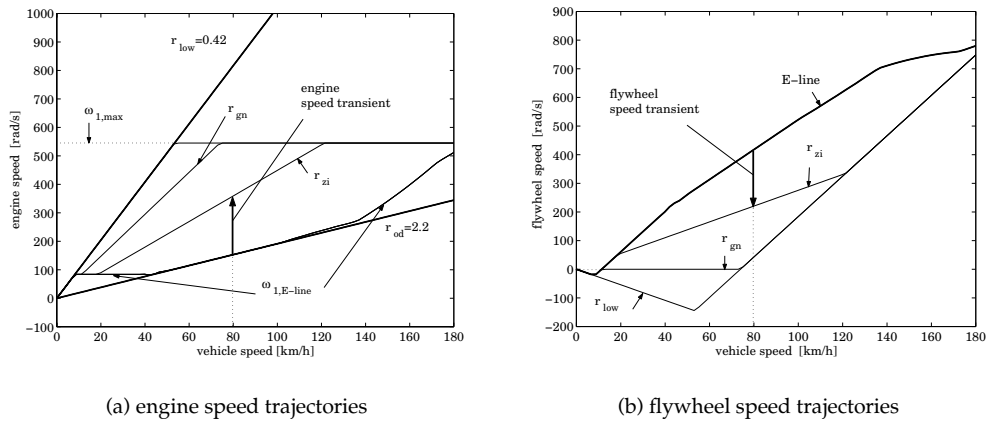
Figure 10.3: Engine and flywheel speed as function of the vehicle speed: R=5.2, r_d=0.21, R_w=0.31 [m]

(a) engine power reserve

(b) energy requirement
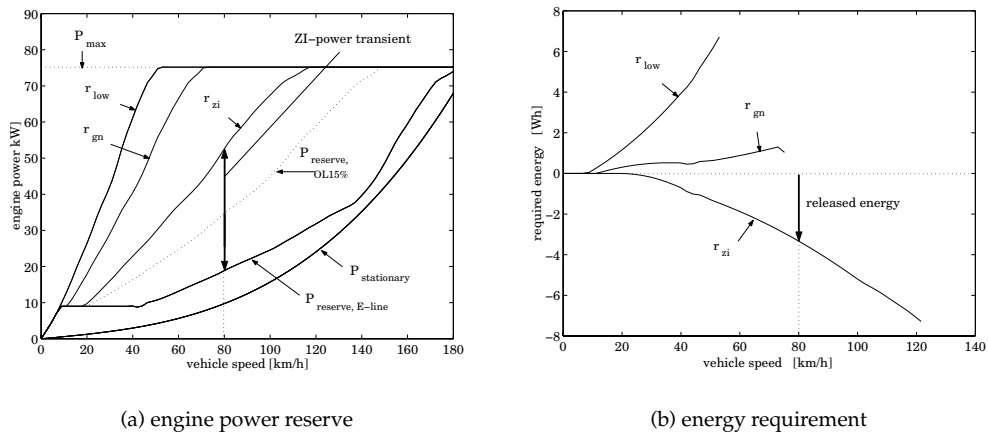
Figure 10.4: Stationary and maximum achievable engine power levels as function of the vehicle speed and energy requirements, using constant shifting speed (proportional shifting time) and an engine inertia J_1 of 0.25 kgm^2

the vehicle, it may not or hardly penalize the maximum launch performance. For maximum launch performance the torque converter lock-up is open during the initial acceleration. In Figure 10.5 the ratio between the primary pulley speed and the engine speed, *i.e.,* the torque converter speed ratio, during launch is shown. In Figure 10.6 the lever is used to illustrate
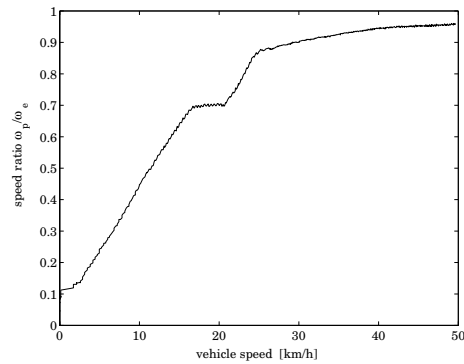
Figure 10.5: Speed ratio ω_p/ω_e while launching the vehicle with open torque converter (measured data)

the speeds of the engine, vehicle and flywheel as well as to show the torque amplification by the transmission. The slip of the torque converter (clutch C_1 in Figure 8.10) results in a higher engine speed with respect to the primary pulley. To distinguish the engine speed and the primary pulley speed in Figure 10.6, the engine speed is indicated with an open circle when the lock-up is open. In Figure 10.6(a) the start situation before launch is shown. The engine
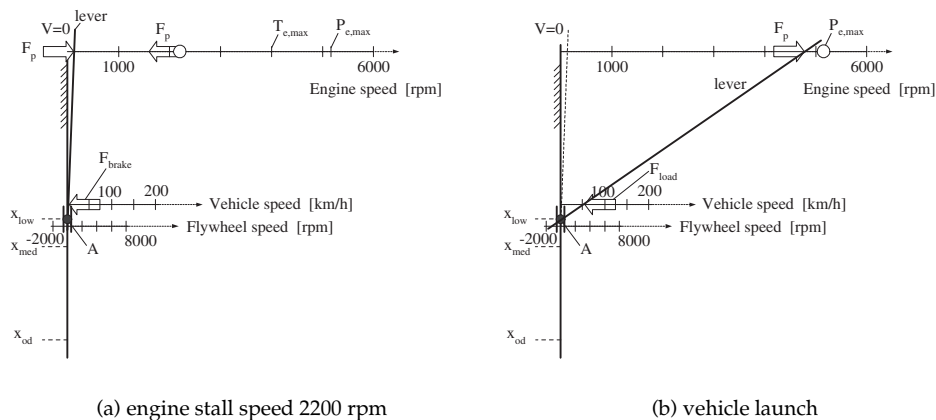
(a) engine stall speed 2200 rpm   (b) vehicle launch

Figure 10.6: Functional illustration of the vehicle launch with open torque converter (ZI powertrain)

runs at 2200 [rpm], the so called "stall speed", and the engine torque (F_e in Figure 10.6) is amplified by the torque converter resulting in a higher torque at the primary shaft (F_p working at the lever in Figure 10.6). The vehicle is held at zero velocity by the brakes, and the flywheel is not rotating in this situation. By releasing the brakes and kicking down the drive pedal

104

the vehicle is launched in the lowest transmission ratio (x_{low} in Figure 10.6), *i.e.,* with highest torque magnification, as illustrated in Figure 10.6(b). The engine reaches its maximum power level (at 5160 [rpm]) when the vehicle speed equals approximately 50 [km/h]. The slip over the torque converter is now reduced to only 4% as shown in Figure 10.5. During the initial vehicle launch the flywheel is accelerated in negative direction up to 1300 [rpm]. The energy stored in the flywheel at this time amounts to 1 [Wh] only. When the engine has reached its maximum power level, the transmission has to be shifted towards a higher ratio (direction of x_{med}) to accelerate the vehicle to higher speeds. In Figure 10.7(a) this is illustrated for a closed torque converter. During this shifting it is seen that first the flywheel is accelerated to zero (the flywheel speed increases from -1300 to 0 [rpm]), and next it is accelerated to 1800 [rpm] (equal to 1.9 [Wh]). As a result of the chosen value for x_{gn} between x_{low} and the value for x

(a) up-shift   (b) up-shift
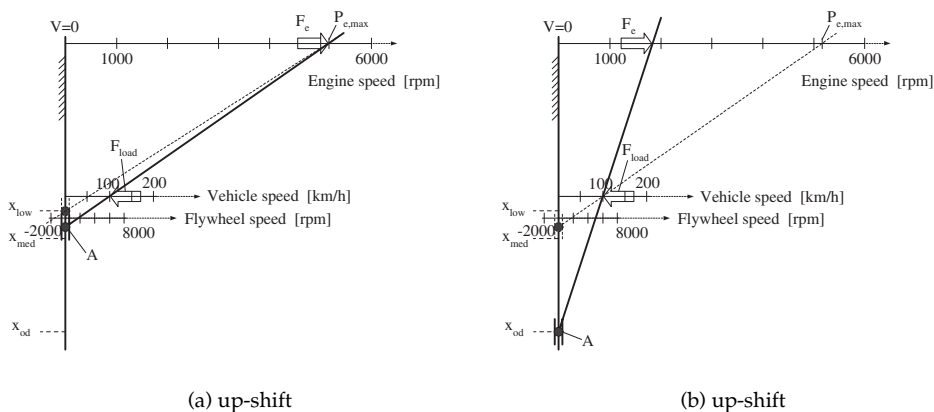
Figure 10.7: Functional illustration of the vehicle launch (ZI powertrain)

when the vehicle reaches 100 [km/h] from a kick-down, the energy fluctuation in the flywheel (penalty for launch performance) is minor compared to the energy stored in the vehicle (150 [Wh] at 100 [km/h]). Simulations show a penalty of only 0.4 [s] on the total acceleration time of 12.2 [s] for the reference CVT powertrain, see [van Druten *et al.*, 2001].

In Figure 10.7(b) it is seen that when the driver releases the drive pedal to establish a constant vehicle speed, the flywheel is "charged" while shifting the transmission towards its maximum ratio (x_{od}). During this shift, kinetic energy is exchanged between the engine and the flywheel. The response in this phase is greatly improved because the kinetic energy of the engine is not exchanged with the vehicle as happens with a conventional CVT powertrain. Driving stationary at 100 [km/h] with the engine operated a close as possible to the E-line, it is seen in Figure 10.7(b) that the flywheel rotates with 5000 [rpm], ready to exchange its energy (15 [Wh]) for further acceleration.

10.1.3 80 to 120 [km/h] acceleration

The main criterium for power assist is the improvement of acceleration response of the vehicle at higher vehicle speeds, as depicted in [van Druten *et al.*, 2001]. A typical acceleration perfor-

mance test is the 80 to 120 [km/h] "elasticity" test, in which the required acceleration time is measured. Although power assist is not directed towards improvement of acceleration time, the 80 to 120 [km/h] acceleration will be used to show that the epicyclic geared flywheel can greatly improve the acceleration response. In Figure 10.8 (a) the stationary situation driving fuel economically at 80 [km/h] with the transmission ratio in overdrive, is illustrated. It is seen that the flywheel is rotating at 4000 [rpm].

(a) 80 km/h stationary driving   (b) down shift (at kick-down)
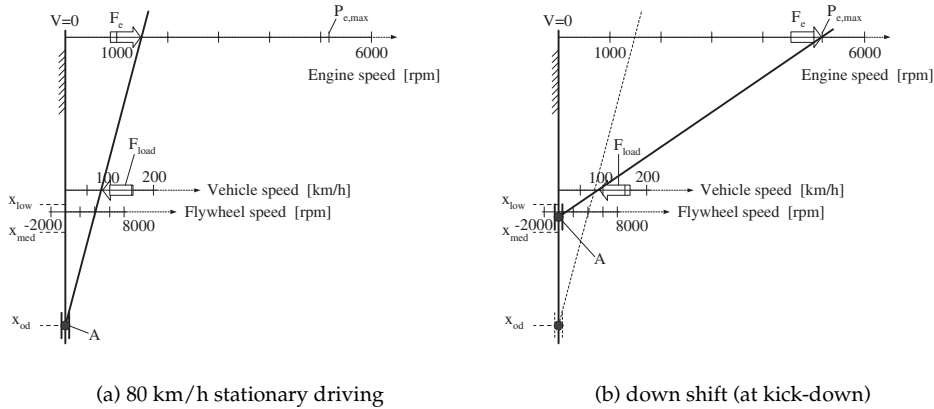
Figure 10.8: Functional illustration of the 80 to 120 [km/h] acceleration (ZI powertrain)

In Figure 10.8(b) the kick-down is initiated by the driver and the transmission prescribes to speed up the engine and to speed down the flywheel. While shifting, kinetic energy is exchanged from the flywheel to the engine, while the surplus of flywheel energy is directly used to accelerate the vehicle. The transmission is shifted back to a drive ratio of approximately 0.14, just in between the geared neutral and zero-inertia ratio, see Figure 10.2. To further accelerate the vehicle with the engine at maximum power level an up-shift is requested, as shown in Figure 10.9(a). In this figure it is seen that the flywheel will be accelerated along with the vehicle to reach the speed of 120 [km/h]. The transmission is shifted up towards a drive ratio of approximately 0.2, speeding up the flywheel towards 3100 [rpm].

Because the up-shift in Figure 10.9(a) is relatively slow compared to the down-shift in Figure 10.8(b), and because the flywheel speed is relatively low (<3100 [rpm]) the acceleration level and total acceleration time are only marginally affected, see [van Druten *et al.*, 2001]. In Figure 10.9(b) the up-shift towards the overdrive ratio to drive fuel economically at 120 [km/h] is shown. Having the immediate power assist from the flywheel, comfortable cruising of the vehicle with an engine speed of just 2200 [rpm] is possible.

10.1.4 Deceleration from 120 [km/h]

The power assist system, designed for exchanging energy between the engine and the flywheel, it is not able to recover brake energy. For full brake energy recovery a 10 times higher flywheel storage capacity and a four times wider ratio coverage would be required. To explain the normal braking strategy, in Figure 10.10 three lines are shown. The dotted line shows the

(a) up-shift (b) up-shift
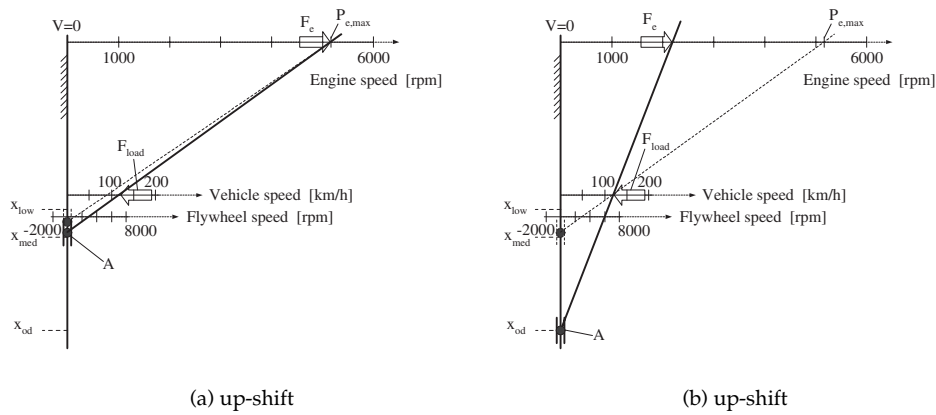
Figure 10.9: Functional illustration of the 80 to 120 [km/h] acceleration (ZI powertrain)

stationary driving situation at 120 [km/h] with the transmission in overdrive. During braking, two stages can be distinguished. In the first stage the engine and the flywheel will decelerate along with the vehicle, while keeping the transmission in overdrive. When the engine reaches a minimum speed (here 1200 [rpm]), expressed by the thin line, the first phase ends. During this phase the flywheel virtually enlarges the vehicle inertia with 10%. In the second phase the engine speed is kept constant whereas the vehicle slows down by shifting the transmission to lower ratios. During this phase the flywheel enlarges the vehicle inertia with less than 10%. At the end of this phase, expressed by the thick line, the torque converter has to be opened to allow further deceleration until the vehicle is stopped. Since the brake feeling is constant and the phase change doesn't involve a large inertia change, the conventional brake system doesn't have to be adapted. Actually, wheel slip is in most cases limiting the maximum deceleration (*i.e.*, for an emergency stop).
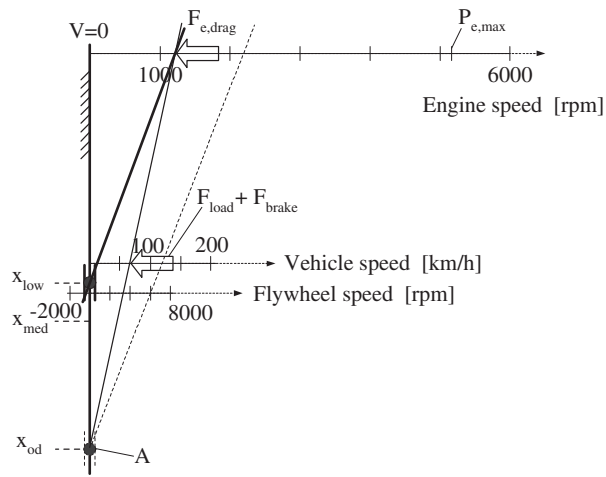
Figure 10.10: Functional illustration of deceleration from 120 km/h (ZI powertrain)

Chapter 11

Proof of concept transmission design

Before a transmission is ready for mass production, four evolving design steps have to be made. The first step is to design a so-called "Proof of Concept" (PoC) transmission, able to demonstrate the functionality of the concept. This design is the subject of this chapter. The second step is to design a prototype transmission with sufficient life span, to be proved by endurance tests. The third step is to design a pre-production transmission, aiming at optimal material usage and recyclability, ease of assembling, minimal weight and volume and adaptability to a range of engines. The last step is to take into account the production method, production machines and the material used in mass production, optimizing every single detail of each individual component, material and production machine.

11.1   Design approach

To demonstrate the practical applicability of the ZI concept and of the Stop-Go facility two prototype transmissions are built. These transmissions are highly similar, mainly differing in the presence of two wet-plate clutches for the stop-go facility. In this chapter the design choices, some construction aspects and the design of the transmissions itself is discussed.

The design criteria for a PoC transmission have to account for flexibility, allowing design changes during the test-program and enabling measurements of various speeds, pressures, temperatures and vibrations within the transmission. Therefore, in the realization of the PoC transmission flexible CNC production machines, operated by skilled persons, may be used instead of fully automated stamping and bending machines. The cost of a single prototype transmission can exceed the cost of a mass produced transmission by a factor of 100 or more. Despite all CAD programs and rapid prototype facilities, the design of a PoC transmission can not be passed over since it gives vital physical information.

One of the most important criteria for a PoC transmission is that it shows the merits of the concept. To minimize the chance of a mal-functioning component, proven and available CVT components are used as much as possible. This also helps to reduce the development time from concept to materialization which was restricted to one year for two engineers. Another criteria for the PoC transmission is the possibility to test the system with and without the flywheel and to add the clutches for Stop-Go in a later stadium. When one could easily

decouple the flywheel or remove it, the transmission could be tested step by step, revealing the changing driveability of the powertrain. To accomplish the PoC design according to the mentioned criteria the following design steps are made:

1. define the functional parameters, using the insights gained from the ETDM of Chapter 10 and using simulations of the dynamic behaviour of the powertrain [Serrarens, 2001];

2. optimize the planetary gear lay-out and the extra fixed reductions with respect to minimal friction losses during stationary drive situations, minimal number of components and packaging;

3. modular add-on design of the planetary gear set, flywheel and housings using mock-ups to investigate vehicle implementation;

4. modular design of the clutches for Stop-Go;

5. checking the procedure of assembling and dismantling and designing special tools for these activities;

6. detailed design of transmission components and housings;

7. manufacturing of components by dedicated specialists to speed up deliverance and to ensure proper quality;

8. checking, measurement and test of sub-assemblies prior testing the total assembly.

The first point, *i.e.,* the functional parameter optimization, is outlined in Chapter 10 and discussed in [Serrarens, 2001]. In the following sections the constructive optimization, *i.e.,* point 2, 3 and 4, will be described. Points 5 till 8 are not considered in this thesis.

11.2 Constructive optimization

The output of the functional optimization, see Chapter 10 is the input for the constructive optimization, being the kinematic ratio $z^* = 0.14$ and the energy content of the flywheel $E_{f.max}=34$ [Wh] at vehicle top-speed. The output of the constructive optimization is the maximum flywheel speed, gear-layout and dimensions. In the following sections the design choices are explained in detail.

11.2.1 Rotor weight versus rotor speed

For the constructive optimization, the first step is to determine the optimal trade-off between flywheel inertia and flywheel speed. Using the power loss optimization according to chapter 6.2 with the maximum energy content of 34 [Wh] as input, an optimum for the flywheel dimensions and the maximum flywheel speed can be found for given flywheel mass and ratio ξ. In Figure 11.1 different alternatives are given.

Since the form and speed of a flywheel do not affect the functional behaviour, additional constraints have to be found in construction, manufacturing, packaging, weight and safety requirements. For the PoC transmission it is chosen to reduce the flywheel speed, *i.e.,* power loss, in favour of reducing the rotor weight. The total power loss in Figure 11.1 doesn't include the friction losses caused by the bearings of the planetary gear and fixed reductions. After the
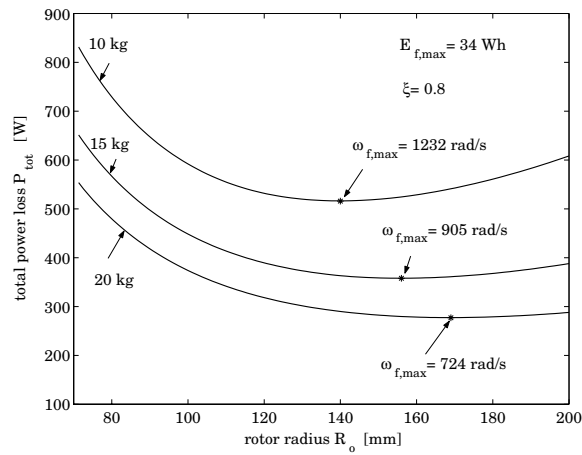
Figure 11.1: Steel flywheel alternatives for 34 [Wh] maximum energy storage

gear lay-out is determined, the power loss optimization is applied again to find the new trade-off between rotor mass and power loss. The final outcome of the constructional optimization for the PoC design shows a maximum speed of the flywheel of 782 [rad/s], resulting in a value for the kinematic ratio κ of approximately 0.15 [-]. For the pre-production version the trade-off between power loss and weight should be reconsidered while the weight penalty increases.

11.2.2 Topology

In Chapter 10 it is assumed that the engine, the flywheel and the wheels are connected to respectively component 1, 2 and 3 of the planetary gear. In this section it is shown that changing this topology doesn't affect the characteristics of the planetary gear, but gives extra freedom in choosing the planetary gear ratio z. Having determined both ratios z^* and κ according to the functional optimization, the fixed reductions r_1, r_2 and r_3, the topology and the planetary gear ratio z can be chosen, subject to various constraints. In equation 9.14 and 9.15 the relation between the mentioned parameters is given for the specific connection between the components of the planetary gear and the reductions shown in Figure 11.2(b).

Using the definition for z^* and κ, Figure 11.2(a) is equivalent to Figure 11.2(b), meaning that the ratio z' is equal to the kinematic ratio of the planetary gear z. By changing the connections, the ratio z' can be changed. In Table 11.1 the influence of the topology on z' is shown. From this table, it can be concluded that changing the topology gives extra freedom to accomplish the required ratio z'. Combining equation 9.14 and 9.15, with z being the required ratio z', the following expression for z' can be found

$$z' = \frac{r_1 z^*}{r_2 \kappa} \tag{11.1}$$

111

(a) General epicyclic gear representation

(b) Layer structure
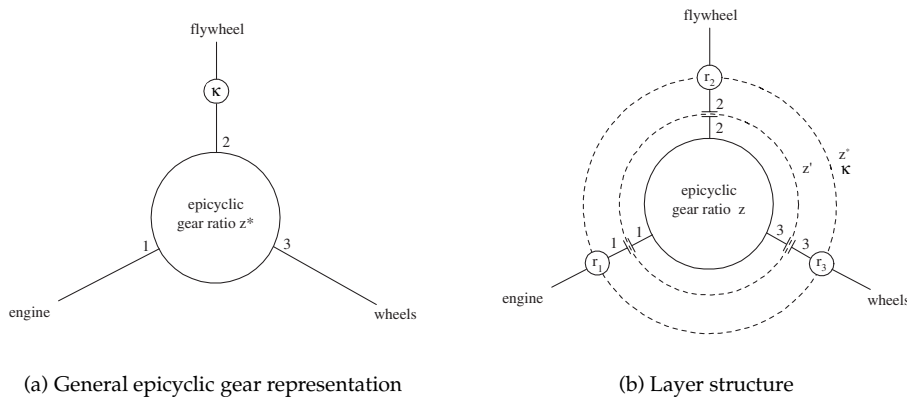
Figure 11.2: Topology of epicyclic gear and fixed reductions

and the relation between the fixed reductions becomes

$$r_3 = \frac{r_1 z^* + r_2 \kappa}{z^* + 1} \tag{11.2}$$

According to Table 11.1, equation 11.1 and equation 11.2 one can choose freely the gear lay-out and reduction sizes to realize the functionality of the ZI-powertrain.

ENGINE	FLYWHEEL	WHEELS	z'
1	2	3	[-]
1	2	3	z
1	3	2	-z/(z+1)
2	1	3	1/z
2	3	1	-(z+1)/z
3	1	2	-1/(z+1)
3	2	1	-(z+1)

Table 11.1: Relation between the kinematic ratio z' and the planetary gear ratio z when changing the topology

11.2.3 Gear lay-out and reduction size

Using Table 11.1 and equation 11.1 and 11.2, a gear lay-out with minimal number of gears, each running at a minimal speed, is found. To establish this, first the most suitable position of the flywheel with respect to the primary and secondary pulley is investigated. Since for the proof of concept transmission the flywheel unit is designed as an add-on, the space especially in axial direction is limited, as shown in Figure 11.3. Therefore it is preferable to

112
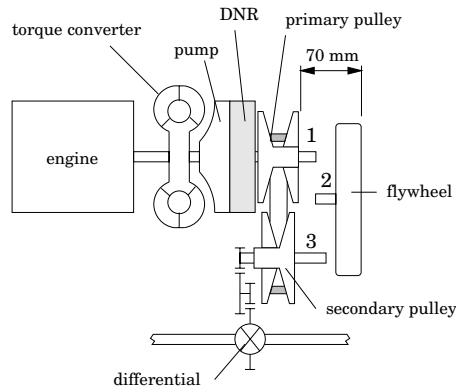
Figure 11.3: Front view of the conventional CVT with to be connected flywheel
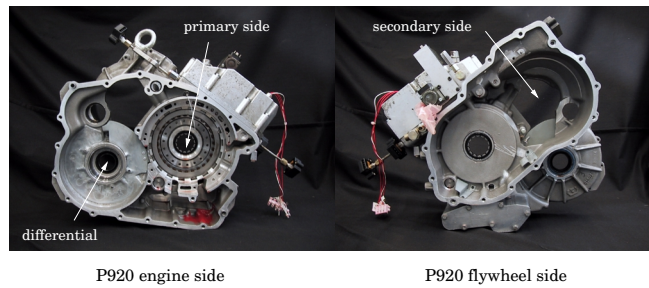
Figure 11.4: Left and right view of the P920 transmission housing

position the planetary gear in parallel with the primary and secondary pulley to make it possible to position the flywheel in axial direction as close as possible to the primary pulley. In Figure 11.4 the transmission housing of the CVT to be used for this project, is illustrated. It is a pre-production version (type P920), designed in 1992 by Van Doorne's Transmissie. The CVT consists of a torque converter (to be locked above 20 [km/h]), a roller-vane oil pump (to be used either single or double sided), a Drive Neutral Reverse unit (DNR), a standard Van Doorne V-belt (type 30/12) with a ratio-coverage of 5.3 and a final reduction gear with a total ratio of 0.21. Within the given space of approximately 70 [mm] (see Figure 11.3) the flywheel including a planetary gear connecting the shafts 1, 2 and 3 has to be fitted.

To minimize the number of reductions and the number of bearings, it is favourable to connect the flywheel directly to a member of the planetary gear. Furthermore the planetary gear set should be kept as simple as possible, without stepped or additional planet gears, for ease of construction and manufacturing. Therefore, the reduction gear r_2 must be left out ($r_2=1$) and the planetary gear ratio z must be in the range from 1.5 to 5, see Figure 11.5.

Without changing the topology (*i.e.*, $z' = z$), assuming $r_2=1$ and renaming the reduction between the annulus (ring) gear of the planetary gear and the primary pulley (engine) shaft

(a) z=1.5   (b) z=5
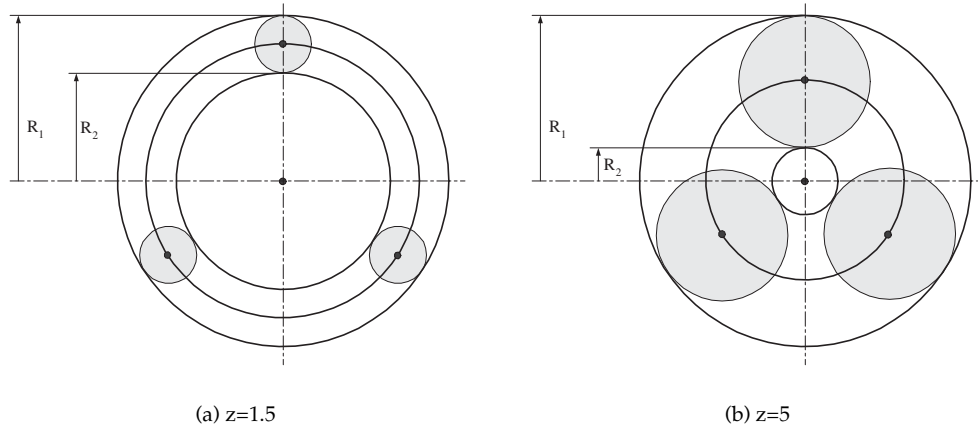
Figure 11.5: Ratio range of single stage planetary gear sets

from r_1 in r_a, equation 11.1 becomes

$$z = \frac{r_a z^*}{\kappa} \tag{11.3}$$

Writing r_3, the total reduction between the carrier of the planetary gear and the wheels, as

$$r_3 = r_d r_c \tag{11.4}$$

with r_d being the final drive reduction ratio and with r_c the reduction ratio between the carrier and the secondary pulley shaft, equation 11.2 becomes

$$r_c = \frac{r_a z^* + \kappa}{r_d(z^* + 1)} \tag{11.5}$$

Since z^* and κ are almost equal, it is seen from equation 11.3 that the planetary gear ratio z and the annulus reduction r_a are of the same order of magnitude. This means that if z is chosen in the middle of the range from 1.5 to 5, so $z \approx 3$, the ring gear speed will be reduced by a factor of 3 with respect to the primary pulley speed. This is advantageous while driving at stationary vehicle speeds because the power losses in the planetary gear set are reduced then. Using the final reduction ratio r_d of the standard transmission and $r_a=z=3$, the carrier reduction r_c becomes 2.3, reducing the speed of the carrier with respect to the secondary pulley speed.

Using the proposed gear lay-out, optimized with respect to the number of reduction gears, simplicity of planetary gear construction and reduction of planetary gear speeds, the final gear lay-out is shown in Figure 11.6. The sizes of the gears of the annulus and carrier reduction are chosen such that the flywheel shaft could be positioned in parallel to pulleys, shown in Figure 11.7. The number of teeth of the reduction gears are listed in Table 11.2.

114

RATIO	NUMBER OF TEETH	VALUE
z	62/22	2.82
r_a	94/32	2.94
r_c	85/37	2.30
r_d	25/33 & 16/57	0.21

Table 11.2: Number of teeth of the chosen reduction gears
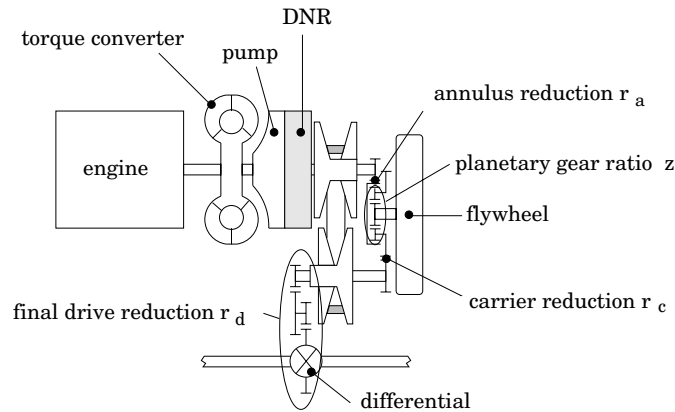
Figure 11.6: Front view of the gear lay-out

11.3 Planetary gear design

The first aspect concerning the design of the planetary gear set is to determine the exact number of teeth of the annulus, planet and sun gear within the geometrical constraints. The planet gears should be evenly spaced around the sun gear and inside the annulus. It is chosen to have three planet gears, enabling one element of the planetary gear set to center itself, ensuring a balanced force distribution through the planetary gear set. It is chosen to give the annulus gear the radial freedom with respect to the other gears in the planetary gear set. Figure 11.8 shows cross sections of subassemblies of the final planetary gear design.

The annulus gear, shown in Figure 11.8, is connected via a spline with the primary gear. The carrier, shown in the middle is made out of two pieces bolted together and aligned with alignment pins. The planet axles are enclosed between the separate carrier parts, and support the needle bearings and the axial thrust bearings of the planet gears. The bearings of the primary gear are mounted on the carrier, which reduces the bearing power loss further and requires less axial space. The bearings of the carrier are fitted left and right (not shown) and are supported by the transmission housing. The axial tooth angle and tooth direction on all gears is chosen such that the net bearing load is reduced. The lubrication path for the oil is chosen to start from the inside, *i.e.,* from the sun gear to the outside gears.

115
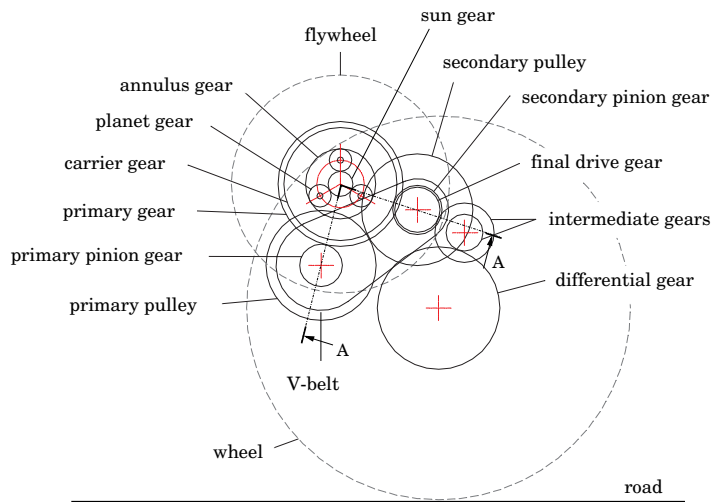
Figure 11.7: Side view of the gear lay-out
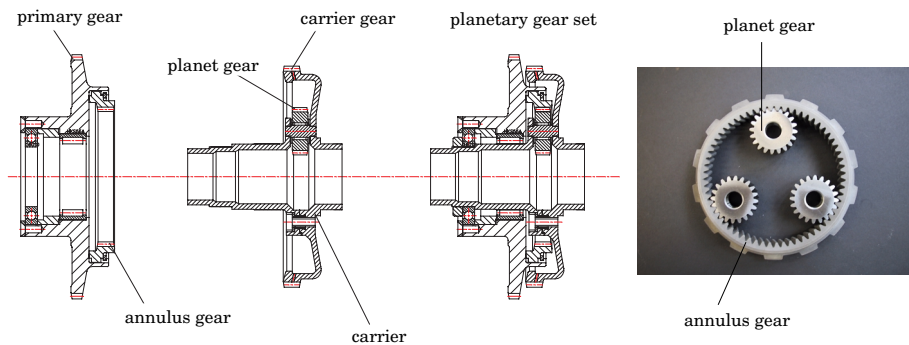
Figure 11.8: Construction of the planetary gear set

11.4 Flywheel design

The flywheel design is based on the optimization to reduce air drag and bearing losses given the required energy content of the flywheel, as described in Chapter 6. For the PoC transmission design the optimization resulted in a ring shaped steel flywheel with inertia J_f=0.4 [kgm^2], rotating at 782 [rad/s] when driving at maximum vehicle speed. There is no need for a vacuum system to reduce the air drag. With these specs, a steel flywheel is preferable

because of the high mass density, low material cost and good manufacturing properties. The
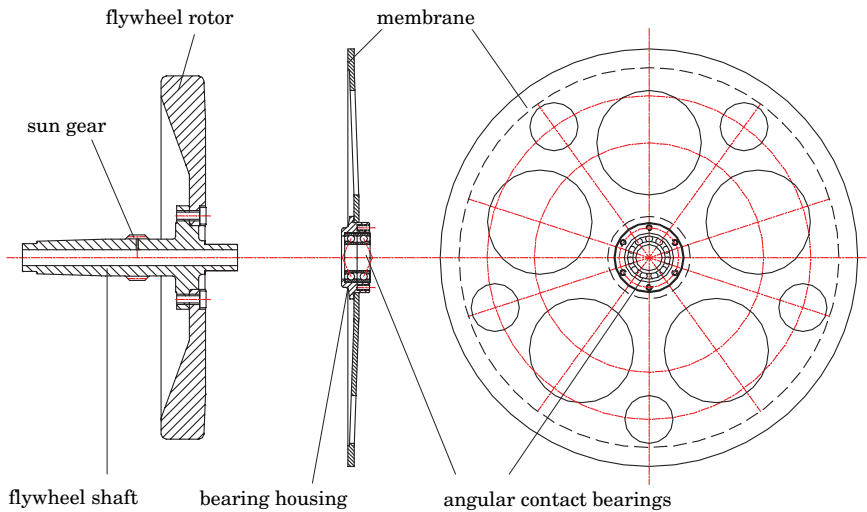
Figure 11.9: Cross-section of the flywheel construction

final flywheel construction, as shown in Figure 11.9 in cross section, can be divided into three separate parts: the flywheel shaft, the rotor and the bearings with its support. The sun gear of the planetary set is machined directly into the flywheel shaft. The flywheel shaft and rotor are made separately for ease of manufacturing and to allow the sun gear to be ground after the hardening heat treatment. The bearing configuration, with a cylinder roller bearing on the left side (not shown) and a pair of spindle bearings on the right side, is one of many alternatives investigated by [van Tilborg, 1999]. This configuration shows beneficial, since in this set up the shaft is allowed to grow thermally while all axial forces are supported by the spindle bearings. The pair of spindle bearings was chosen because, under pre-tension, it guarantees stiffness and has no play in radial and axial direction. The size of the bearings is chosen as small as possible in order to reduce the bearing losses. Apparently, the minimum bearing diameter was limited by the minimal flywheel shaft diameter required for proper bending stiffness and not by the life span requirements. In Figure 11.10 the cross-section of the flywheel assembly is shown. The pair of spindle bearings with a contact angle of 25 degrees are placed in an 'o'-configuration, as shown in Figure 11.10. The pre-tension is established by closing the axial gap of 4 to 5 [μm] between the inner bearing rings with the M25 nut. The bearing cap enables the outer bearing rings to be stiffly connected via an axial support rod (seen in Figure 11.12) with the transmission housing in axial direction. To support the flywheel in radial direction, the cylinder roller bearing on the left is directly mounted into the transmission housing and the pair of spindle bearings is radially supported by a steel membrane, as shown in Figure 11.10.
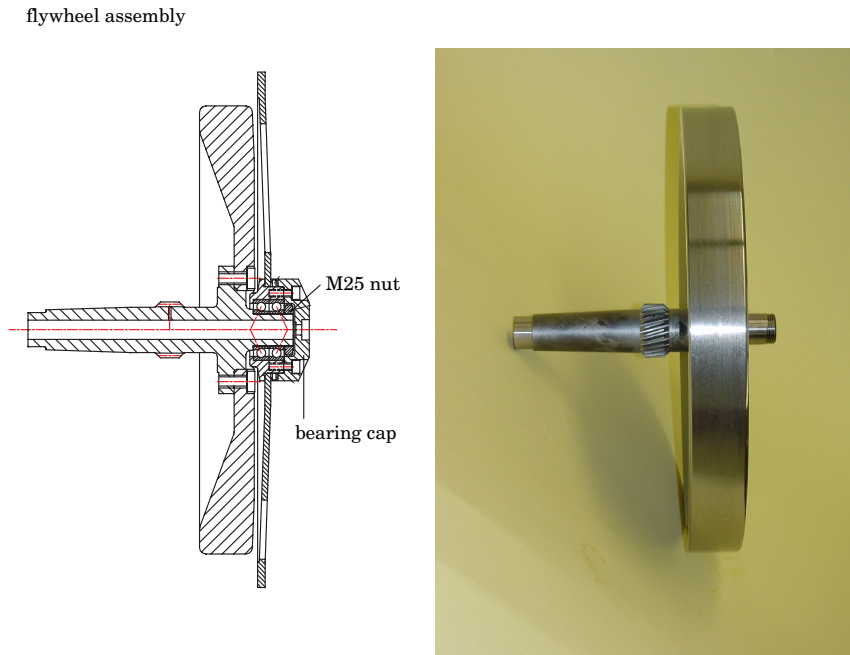
flywheel assembly

Figure 11.10: Cross-section of the flywheel assembly

Separating the axial and radial support by using a rod and a membrane, the flywheel has a lightweight, stiff support in both directions and the construction requires less axial space.

In the PoC transmission, the flywheel will rotate at speeds between 0 and 800 [rad/s] without resonance appearing. This requires a first eigenfrequency of the construction well above 800 [rad/s]. In order to meet this demand, a study has been made on the eigenmodes and frequencies of different flywheel constructions in which the construction is simplified to a serial connection of three stiffness: the shaft, the bearings and hub stiffness, see [van Druten *et al.*, 2000]. For the construction of flywheel, hub and bearings as shown in Figure 11.10, the first eigenfrequency is 1100 [rad/s]. To avoid noise production by the membrane, the pair of spindle bearings is set in a 'o'-configuration to provide angular stiffness to the center of the membrane, and holes are made in the membrane to reduce the surface area that could produce sound.

11.5 Transmission housing design

For the PoC transmission design it is chosen to have a modular construction that enables testing with or without planetary gear set and flywheel. To accomplish this, the assembly is made with two sub-assemblies: a flywheel housing in which the planetary gear set and secondary pinion gear are fixed in axial direction, see Figure 11.11, and the flywheel itself with spindle bearings and membrane as shown in Figure 11.10. The two sub-assemblies can be mounted

118

and removed easily without rebuilding other parts of the CVT. This makes it possible to investigate the functioning of the added assemblies separately whilst maintaining the conventional CVT behaviour as a reference. The flywheel housing is mounted to the pulley housing, as

flywheel housing

primary pulley bearing

planetary gear set

secondary pinion gear
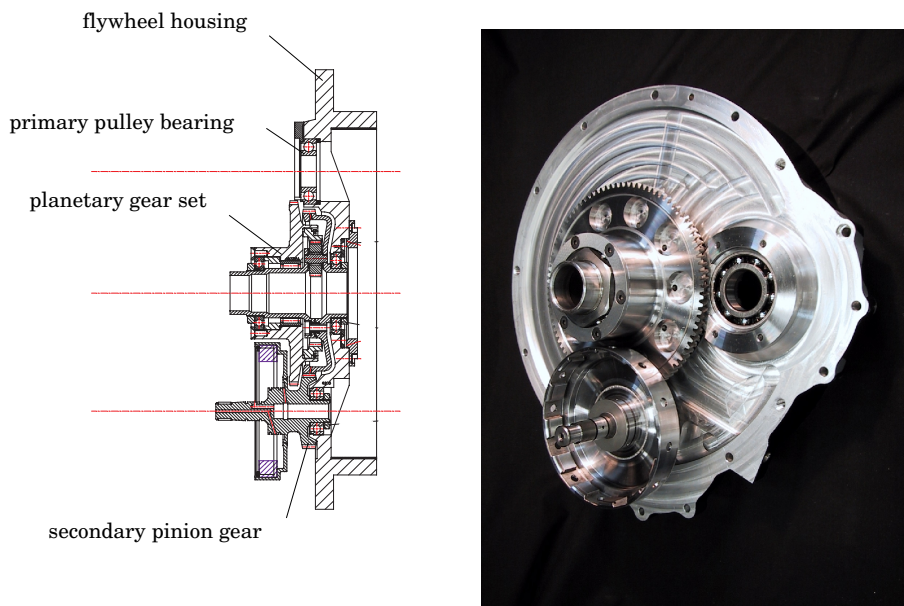
Figure 11.11: Cross-section A-A of flywheel housing

shown in Figure 11.12, which in turn is mounted to the standard P920 housing. The cross-section shown is section A-A in Figure 11.7 and it must be noted that the distance between the pulleys in reality is only 0.3 [mm]. The pulley housing replaces the back cover of the P920 transmission and is equal in axial length. According to the specification of approximately 70 [mm] extra length of the transmission, the combination of flywheel housing and membrane is designed such that it fits within this limited space.

For Stop-Go functionality it is chosen to use the pre-production P943 pulley set which enables the secondary pulley to be decoupled from the secondary shaft (the torque shaft in Figure 11.12). The P943 pulley set was designed to fit in the P920 housings and only minor design changes of the torque shaft were needed to adapt it to the secondary pinion gear. The primary pulley of the P943 variator, was changed in a later stadium to make the replacement of the primary pinion gear by a spacer easier.

To test the ZI functionality, the two clutches, which enable decoupling of the secondary pulley and the secondary pinion gear from the torque shaft, are locked with aluminium spline rings over the full width. To test the ZI Stop-Go functionality, both aluminium rings are replaced by a set of wet-clutch plate discs, and cylinders to hydraulically actuate the clutches

spacer

pulley housing

primary pinion gear

flywheel housing

primary pulley

rod

secondary pulley

final drive gear

spline rings

torque shaft
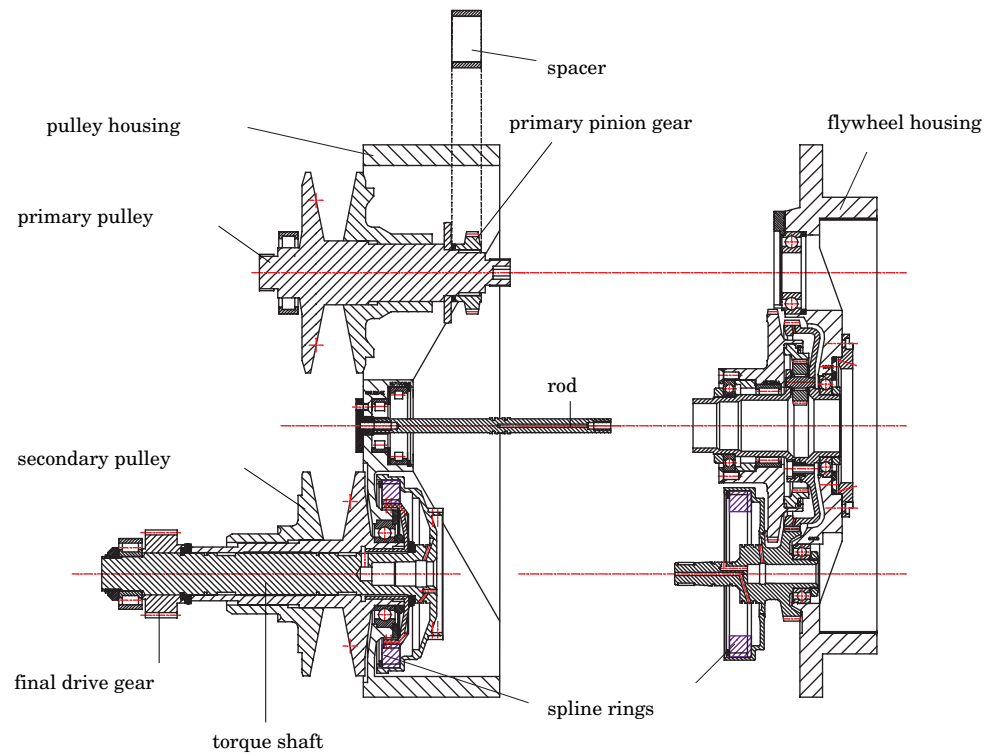
Figure 11.12: Cross-section A-A of flywheel and pulley housing

are mounted. Two oil channels starting from the flywheel housing are leading towards the cylinders. Oil chambers are designed opposite to the cylinders to compensate for the centrifugal force due to the oil centrifuging outwards. Without these compensation chambers it is difficult or even impossible to open the clutches at high rotational speed.

Figure 11.13 shows the pulley and flywheel housing mounted together and the flywheel assembly separately. The pulley housing supports the secondary pulley and the flywheel housing supports the primary pulley. The axial distance between the pulley shafts has to be aligned accurately (20 [μm]) to guarantee the lifespan of the variator. To allow less accurate machining of all parts that influence that distance, an alignment ring located under the primary pinion gear can be adjusted after measuring the axial distance between the fixed pulley discs. When the flywheel assembly is mounted, the membrane covers the flywheel housing as shown in Appendix A.

pulley housing + flywheel housing   flywheel assembly
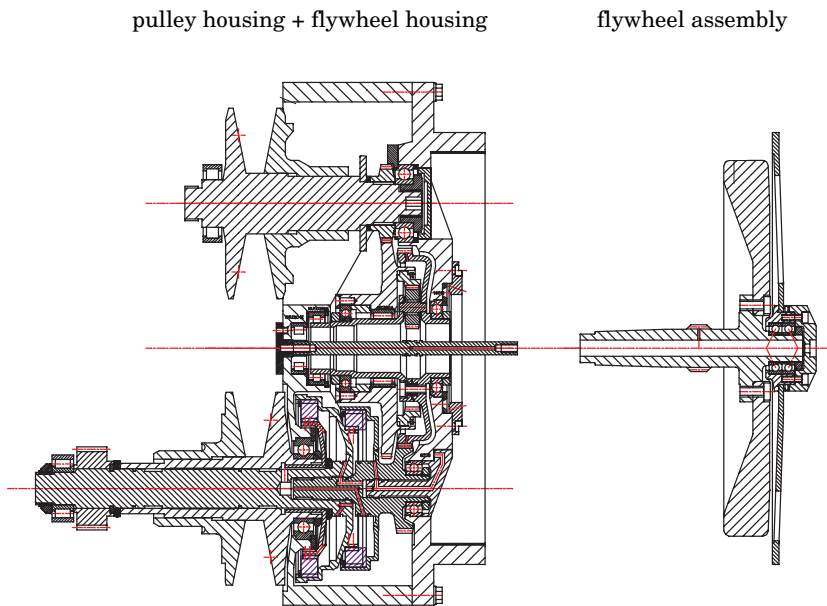
Figure 11.13: Modular assembly

11.6 Transmission efficiency

The flywheel rotates in its housing under ambient air pressure. No vacuum pump in combination with a sealed flywheel housing to reduce the air pressure within the housing is needed. As a result of the low speed flywheel operation (5000 [rpm] driving at 100 [km/h]), the decrease in air friction power loss is less than the increase in power loss due to the vacuum pump and the seal.

In Figure 11.14(a) the calculated stationary power loss in the flywheel system P_{fly}, consisting of air drag of the rotor and bearing friction of all additional bearings is plotted as function of the stationary vehicle speed while the engine speed tracks the E-line. To have an indication of these power losses with respect to the stationary driving power P_{load}, in Figure 11.14(b) the power loss ratio $P_{\text{fly}}/P_{\text{load}}$ is shown. From this figure it is seen that the stationary power loss within the flywheel system is less than 1% with respect to the driving power P_{load}.

The difference between the transmission efficiency without flywheel system $\eta_1 = P_{\text{load}}/P_{\text{in}}$ and the transmission efficiency with flywheel system $\eta_2 = P_{\text{load}}/(P_{\text{in}} + P_{\text{fly}})$ is related to the power loss ratio $P_{\text{fly}}/P_{\text{load}}$ by

$$\eta_1 - \eta_2 = \frac{P_{\text{fly}}}{P_{\text{load}}} \, \eta_1 \, \eta_2 \tag{11.6}$$

From equation 11.6 it becomes clear that the reduction in transmission efficiency due to the flywheel system is less than $P_{\text{fly}}/P_{\text{load}}$ due to the efficiency of the transmission itself. In Figure

11.15 the total transmission efficiency of the CVT with flywheel (η_2), measured on a test-rig, as function of the stationary vehicle speed is shown.

(a) power loss in the flywheel system P_{fly}

(b) power loss ratio $P_{\mathrm{fly}}/P_{\mathrm{load}}$
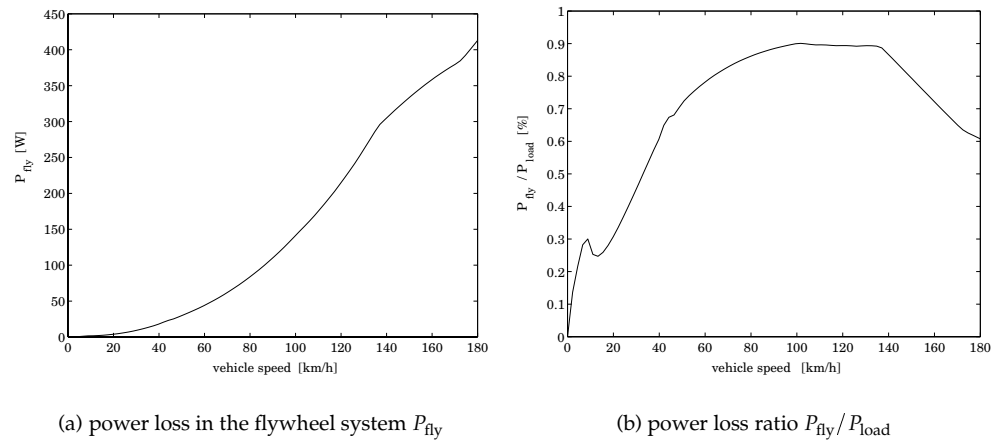
Figure 11.14: Absolute and relative power loss in the flywheel system as function of the stationary vehicle speed, while the engine speed tracks the E-line (calculated)
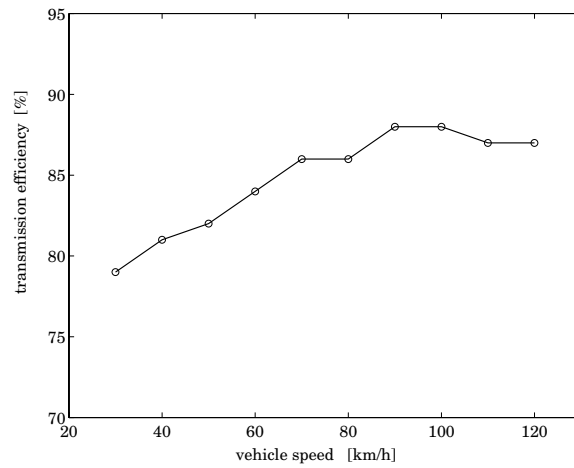
Figure 11.15: Transmission efficiency of the CVT with flywheel system (η_2) as function of the stationary vehicle speed, while the engine speed tracks the E-line (measured)

122

11.7 Test-rig and vehicle implementation

The PoC transmission is first tested without an internal combustion engine on a test-rig, see Figure 11.16. The tests comprise the effectivity of the mechanical power assist, the efficiency of the total transmission, the CVT control and the driveline management system, see [Serrarens, 2001] and [Vroemen, 2001]. After the transmission and the CVT control were proved to be reliable and part of the driveline management was tested, the PoC transmission was built in a mid-size passenger car with 1.6 *l* otto engine. Figure 11.17 shows the engine compartment of the test-car with engine/transmission system to be mounted. The second test
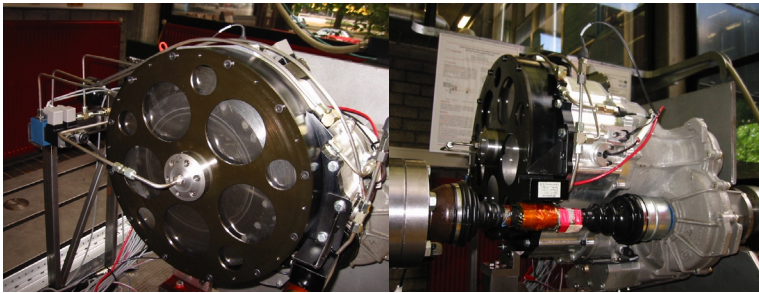
Figure 11.16: Zero-inertia transmission on test-rig

program was focused at the driveability aspects of the test vehicle and at the fuel consumption measurements. The acceleration responses of the vehicle, equipped with either a 4-AT, CVT or ZI transmission, are measured, showing a considerable driveability advantage for the ZI transmission (see Figure 8.20 in [Serrarens, 2001]). The actually obtained fuel savings on the NEDC using only ZI were measured at 9.0% and 11.0% with respect to 4-AT and CVT in 'performance mode', respectively, as reported in [Serrarens, 2001]. The third test program

Figure 11.17: Engine compartment of the VW Bora test-car with built in ZI-CVT

performed by [Vroemen, 2001] focused on the evaluation of the Stop-Go functionality on the test-rig, showing promising first results. The theoretically derived fuel saving for Stop-Go (not implemented yet) gives an additional 8%. Consequently, the combined fuel saving for ZI Stop-Go is near 18%.

Part III

Closure

Chapter 12

Conclusions

This chapter draws conclusions based on the research covered in this thesis and general conclusions of the EcoDrive ZI project. The organization is as follows. In Section 12.1, overall conclusions regarding the EcoDrive ZI project are presented. The conclusions which are specifically related to this thesis, are given in Section 12.2. The last section gives directions for future research, based on this thesis and more general directions based on the combined outcome this thesis, [Vroemen, 2001] and [Serrarens, 2001].

12.1 Overall conclusions: EcoDrive ZI

A novel automotive transmission concept, designated the *Zero Inertia* (ZI) powertrain, has been proposed. This powertrain, combining a Continuously Variable Transmission (CVT), a low-speed flywheel and a planetary gear set, enables a substantial reduction of fuel consumption while maintaining a high level of *driveability*, *i.e.,* longitudinal vehicle response and comfort. The improvement in fuel economy is obtained by operating the engine at very low speeds, where the engine efficiency is generally high (*E-line tracking*). The sluggish vehicle behaviour, that would normally result from such engine operation, is effectively counteracted by the flywheel which acts as a mechanical power assist source. The acceleration response of the vehicle, equipped with either a 4-AT, CVT or ZI transmission, is measured, showing a considerable driveability advantage for the ZI transmission (see Figure 8.20 in [Serrarens, 2001]).

Augmenting the ZI concept with two clutches created the *ZI Stop-Go* powertrain which makes it possible to shutdown the engine during vehicle standstill, and hence save an additional amount of fuel. The challenge in that was to guarantee a simultaneous restart of vehicle and engine without a noticeable delay. To show the potential of the ZI and ZI Stop-Go concepts as means to save fuel, an overview of fuel saving principles and associated efforts (development, costs, packaging, etc) has been presented. The fuel savings for ZI Stop-Go on the NEDC driving cycle were predicted to amount up to 21%.

The target of the EcoDrive ZI project was set at saving 25% fuel consumption on the NEDC driving cycle, with respect to a 4-speed automatic transmission (4-AT) vehicle, and without loss of driveability. As predicted in Part I, achieving this target was deemed nearly possible, *i.e.,* a fuel saving of 21% was projected. The actually obtained fuel savings on the NEDC using only ZI were measured at 9.0% and 11.0% with respect to 4-AT and CVT in

'performance mode', respectively, as reported in [Serrarens, 2001]. The theoretically derived fuel saving for Stop-Go gives an additional 8%. Consequently, the combined fuel saving for ZI Stop-Go is around 18%. This value is actually quite close to the theoretically predicted fuel saving of 21%, but somewhat below the initial target. In the overview of fuel saving principles, other methods were shown to have more fuel saving potential, but also to be far more complex. It is therefore believed that the chosen solution offers a fair trade-off between achieving the initially set targets and the objective to actually realize the ZI and ZI Stop-Go powertrains in a test vehicle and on a test rig, respectively, within a time frame of less than four years.

Apart from the research outcome described in this thesis, the EcoDrive project yielded a lot of knowledge on driveability notions, powertrain modeling, coordinated powertrain control, and controller implementation [Serrarens, 2001], as well as alternative hydraulic actuation leading to increased performance and robustness of the CVT. This aspect is covered in [Vroemen, 2001], where also control development for and experimental testing of the hydraulically actuated CVT is shown. Furthermore, the development, modeling and testing of the Stop-Go extension upon ZI is illustrated there.

12.2 Transmission design: kinetic energy exchange

Two passenger car transmissions, using kinetic energy exchange to enable the engine to run more fuel efficiently and to assist the engine in power transients, are designed and realized. Different approaches to the design problem were made to finally realize the transmissions, resulting in the following insights.

In Chapter 3 it was concluded that an additional power source is needed when changing the engine operation point to improve fuel economy substantially. Four fuel saving principles were defined, each demanding different energy and power levels of the secondary power source. Especially the energy demand appears to differ greatly for the different principles, up to a factor of 20 (*e.g.,* 20 [Wh] for power assist and 400 [Wh] for start-stop), while the power demand for all principles is merely the same, ranging from 10 to 30 [kW].

For all principles, the secondary energy source must be re-chargeable, either to exchange energy with the engine inertia or with the vehicle inertia. A re-chargeable energy/power source that is already present in today's passenger cars is the lead acid battery in combination with the starter and alternator. Functional integration of this system with the additional power source is unlikely, because the maximum power level of these devices is limited to 1 to 2 [kW]. Even with the oncoming 42 [V] board net, integrated starter-alternators and alternative battery systems, the maximum power level will generally be insufficient.

Since the secondary power source is an additional component in the powertrain, the costs, weight and volume should be kept as low as possible. In Chapter 3 it is seen that the power density of a purely mechanical system is ten times higher than for a purely electrical system with equal performance, resulting in a significant cost, weight and volume benefit for a mechanical power assist system embodied as a flywheel and mechanical variator. The mayor limitation of such a kinetic energy exchange system is the poor energy density of the flywheel, restricted by either the maximum stresses in the rotor (rotor speed), the maximum rotor size and weight (rotor inertia), or the power losses in the system.

Using the proposed flywheel design optimization of Chapter 6 it is seen that the maximum allowable stationary power loss restricts the energy density of the flywheel system for the passenger car application. Given a maximum for the stationary power loss of 750 [W] and given weight and volume limitations, two flywheel energy exchange concepts with dif-

ferent complexity are conceived, see Section 6.3. The system with lowest complexity is able to store 60 [Wh] and is made up of a sub-critical steel flywheel in ambient air combined with a mechanical variator. The more complex system is able to store 300 [Wh] and is made up of a super-critical fiber wound flywheel operating in vacuum and combined with an electrical variator. For efficiency, weight, volume and cost reasons it would be preferable to use a mechanical variator in combination with a super-critical flywheel system, however this leads to several additional design problems.

Having determined the maximum performance of alternative flywheel energy exchange systems that can potentially be used in a passenger car, in Chapter 8 the required specification of the flywheel energy exchange system according to its functionality in the powertrain is discussed. A distinction is made between energy exchange with the vehicle inertia and with the engine inertia. Exchanging energy with the vehicle inertia requires both a large ratio-coverage of the mechanical variator (R=24 [-]) and a high flywheel energy demand (up to 400 [Wh]). In contrary, energy exchange with the engine requires a net energy of the flywheel of just 10 [Wh]. Relating the two energy exchange principles with the four principles in saving fuel, it was seen that E-line tracking and Stop-Go can be performed by exchanging energy with the engine while intermittent engine operation in the point of best efficiency (Start-Stop) and brake energy recovery (BER) require energy exchange with the vehicle.

Since an energy demand higher than 60 [Wh] requires substantially higher design efforts to make it cost effective, as was concluded in Chapter 6, E-line tracking and Stop-Go are in principle ideal to be combined with kinetic energy exchange. Although the project goal for fuel saving can only be met partially, it was chosen to search for solutions in this direction while the potential for improving the driveability appears to be very high.

The design problem to be solved for exchanging energy with the engine inertia concentrates especially on the variator that has to be added to the driveline. Using a standard CVT transmission between the engine and the wheels, a low cost and efficient add-on transmission between the flywheel and the transmission is designed. This transmission, being a planetary gear set in parallel of the CVT, enables energy exchange between the engine and the flywheel while shifting the CVT. In first sight it was not clear whether the system was able to assist the engine sufficiently in engine power transients at all vehicle speeds. In Chapter 9 newly developed design tools are presented giving the required insights to design the system for a specific speed range. For E-line tracking the epicyclic geared flywheel should be able to compensate the inertial forces during shifting, especially at vehicle speeds between 30 and 120 [km/h]. For Stop-Go the flywheel should be able to start the engine while applying a torque at the wheels at zero vehicle speed.

Directing the design of the epicyclic gearing to enable E-line tracking, two additional clutches appeared to be needed to enable Stop-Go with the same transmission configuration. The optimization of the design of the so called Zero Inertia transmission was therefore aimed at assisting the engine within the mentioned vehicle speed range. From the design tools, being a combination of a general translational drive line model and a general epicyclic gear representation, a distinction between parameters that influence the functionality of the powertrain and the construction of the transmission could be made. Only two mutually independent parameters influence the functionality of the ZI powertrain, being the energy content of the flywheel and the geared-neutral transmission ratio of the planetary gear set. A trade-off between those parameters, influencing the effectiveness of the system is made and the functioning of the ZI powertrain under various conditions is illustrated in Chapter 10.

A proof of concept transmission, able to demonstrate the practical applicability of the concept of mechanical power assist, is made. Therefore a constructive optimization was carried out, using the outcome of the functional optimization as an input. The flywheel mass and

129

speed are chosen in favour of the stationary power losses due to air drag and bearing friction, so no vacuum system to reduce the air drag was necessary. The planetary gear set can be connected in six ways between the engine, vehicle and flywheel respectively. Given the functional constraints, the topology of the planetary gear set is chosen such that the speeds within the planetary gear set were reduced to improve efficiency furthermore. Altogether resulting in a highly efficient flywheel system in which the stationary power loss compared to the road load power is less than 1% over the total vehicle speed range.

The gear lay-out, bearing lay-out and dimensions of the individual components are chosen to fit within the limited axial design space. Especially for the support of the flywheel spindle-bearings a compact, lightweight and stiff solution is found by separating the axial and radial support using a rod and a membrane respectively. The flywheel design itself needed only limited attention while it is operated safely below the first eigenfrequency and at low material stress (< 100 [N/mm^2]). The design of the transmission housings is made such that the power assist and engine start functionality can be tested step by step. The design enabled to test the planetary gear set, the flywheel and the clutches for Stop-Go in consecutive order, resulting in a high reliability during testing.

Finally it is concluded that with the use of additional proven, low cost transmission technology (only gears, bearings and a plain steel rotor) the standard CVT design can be upgraded to improve both fuel economy and driveability.

Known power assist devices based on storage and conversion of mechanical power to and from the electrical power domain are likely to see competition from mechanical devices as described in this thesis, which can offer identical functionality in a much smaller volume, at a fraction of the cost.

12.3 Directions for future research

The directions for future research proposed in this section are based on this thesis, and more general directions based on the combined outcome this thesis, [Vroemen, 2001] and [Serrarens, 2001]:

1. in Chapter 1, the EcoDrive project organization was outlined in Figure 1.1. EcoDrive existed of two parts, the results of which can in principle be combined to some extent. The part of EcoDrive not described in this thesis, termed EcoDrive SI, resulted in a number of design and control modifications aiming at improvement of the (CVT) transmission and engine efficiency, [Veenhuizen and van Spijk, 2000]. The most important improvement was due to the integration of a so-called *torque fuse* in the CVT. This torque fuse allows a very small slip speed in the (secondarily positioned) drive clutch and as such safeguards the push belt of the CVT during torque shocks. Hence, the pulley clamping force can be substantially reduced, improving the CVT efficiency in part load especially. Given the layout of the ZI Stop-Go transmission, see Figure 4.6, the 'secondary pulley clutch' may be used as a torque fuse;

2. furthermore, in EcoDrive SI, a CVT with a ratio coverage of 6.55 was developed, which is large, even compared to the ratio coverage of 5.17 of the CVT used in the ZI transmission. Incorporating this transmission into the ZI configuration can reduce the engine speed even more with apparent fuel economy benefits;

3. additionally, a chain driven binary displacement pump was designed for the EcoDrive SI transmission, to enable a simultaneous high pressure oil supply (for pulley clamping

and clutches) and low pressure oil supply (for the torque converter, lubrication and cooling). Integration of the EcoDrive SI transmission modifications into the ZI design can be expected to improve the fuel economy by about 5%;

4. alternatively, one may choose to leave out the hydraulics partly or even entirely. In [van Tilborg, 2001], by applying part of the pulley clamping force electro-mechanically, the pump losses can be reduced;

5. in order to validate the functionality and performance of the ZI Stop-Go transmission, further implementation and validation of the controllers on the test rig is required. From this point on ZI Stop-Go may be implemented in a test vehicle to demonstrate the driveability and fuel economy. In the latter case, extensive modifications to the engine management must be undertaken in order to automate fuel injection and ignition without increasing the emissions;

6. also the emission control for normal ZI operation should be optimized for engine operation at very low speeds;

7. further improvement of the overall control and powertrain performance might require a reconsideration of the set point generation for CVT and engine, by taking their dynamics into account more explicitly. Coordinated and component control respectively described in [Serrarens, 2001] and [Vroemen, 2001], would be more intertwined then;

8. on the component control level, the development and implementation of alternative model based CVT controllers may be given more attention;

9. a number of research topics is proposed, involving more rigorous adaptations to the current ZI and ZI Stop-Go powertrains. The increasing popularity of the diesel engine in Europe, combined with its appreciable fuel economy, argues for investigating the combination of this engine with the ZI (and ZI Stop-Go) concept. Because the diesel engine has other torque and speed characteristics than the petrol engine, this would involve a modification of the transmission parameters;

10. next, the torque converter which is normally used to facilitate vehicle launch, might be omitted from the ZI Stop-Go powertrain if the flywheel indeed proves to enable an acceptable vehicle launch;

11. probably the most rigorous future research topic is to conceive and develop a mechanical full hybrid powertrain. From Chapter 3, it was concluded that such a hybrid powertrain has a large fuel saving potential combined with relatively low manufacturing costs. On the other hand, research efforts are quite challenging. In fact, a few solutions in this direction were already proposed, see [Kok, 1999] and [Dietrich *et al.*, 1999]. Searching for a combination of such concepts and the ZI functionality to solve driveability issues, while always aiming for minimal weight and complexity, seems well worth the investigation.

Bibliography

Adcock, I. "Stop-go systems get the green light". *European Automotive Design*, pp. 24–26, 1998.

An, F. and Ross, M. "Model of fuel economy with applications to driving cycles and traffic management". *Transportation Research Record*, no. 1416, pp. 105–114, 1993.

Baumann, B., Rizzoni, G., and Washington, G. "Intelligent control of the Ohio State University hybrid-electric vehicle". In Proc. of the 2nd IFAC Workshop on Advances in Automotive Control, pp. 123–128. Mohican State Park (OH), 1998.

Bosch GmbH, Robert. "Automotive handbook, fourth edition". ISBN 1-56091-918-3, 1996.

von Burg, P. "Schnelldrehendes schwungrad aus faserverstärktem kunststoff". Ph.D. thesis, Technischen Hochschule Zürich, 1996.

Bürger, K.G., Gröter, H.P., Lutz, H.J., Meyer, F., and Schleuter, W. "Alternators in Automotive Applications–State of the Art and Development Trends (translation from German text)". In Proceedings Symposium Nebenaggregate im Fahrzeug. Haus der Technik Essen, 1994.

Colotti, A., Reichert, K., and von Burg, P. "Design of an electrical machine with integrated flywheel". *SAE Transactions*, vol. EVS, no. 15, 1998.

Delsey, J. "How to Reduce Fuel Consumption of Road Vehicle." In Proceedings OECD/IEA Informal Expert Panel on Low Consumption Low Emission Automobile. Rome, 1991.

Dietrich, P., Eberle, M. K., and Hörler, H. U. "Results of the ETH-hybrid III—Vehicle project and outlook". *SAE Technical Paper Series*, no. 1999-01-0920, 1999.

Dietrich, Th. "Ultracapacitors—Power for innovative automotive applications (in German)". *VDI Berichte 1565*, pp. 731–735, 2000.

DOE and EPA. "Energy Technology and Fuel Economy". U. S. Departement of Energy, U. S. Environmental Protection Agency, http://www.fueleconomy.gov/feg/atv.shtml, 2001.

DoT, 1994. "Transport Statistics Great Britain 1994". Department of Transport, HMSO, London, 1994.

van Druten, R. M., Kok, D. B., and Vandewal, R. J. J. L. "Design optimization of a compact flywheel system for passenger cars". *VDI Berichte 1459*, pp. 331–343, 1999a.

van Druten, R. M., Serrarens, A. F. A., Vroemen, B. G., van den Tillaart, E., and de Haas, J. "Mild hybrids with CVT: Comparison of electrical and mechanical torque assist". *VDI Berichte 1610*, pp. 331–345, 2001.

van Druten, R. M., Serrarens, A.F.A., Vroemen, B.G., Veenhuizen, B., and Musseaus, M. "Transmission system, especially for a motor vehicle (patent WO09956039A2)". World Intellectual Property Organization, 1998.

van Druten, R. M., van Tilborg, P., Rosielle, P. C. J. N., and Schouten, M. J. W. "Design and construction aspects of a Zero Inertia CVT for passenger cars (F2–A058)". In Proc. of FISITA'00. Seoul, Korea, 2000.

van Druten, R. M., Vroemen, B. G., Rosielle, P. C. J. N., Veldpaus, F. E., and Schouten, M. J. W. "Design of a powertrain for optimal performance and fuel economy using a CVT and a flywheel". In Proc. of the Internat. Congress on Continuously Variable Power Transmission (CVT'99), pp. 231–237. 1999b.

Evans, L. "Driver behavior effects on fuel consumption in urban driving". *Human Factors*, vol. 21, no. 4 pp. 389–398, 1979.

FAG. "High-precision bearings catalogue", 1997.

Frank, A.A. and Beachley, H.H. "Continuously variable transmission requirements for high performance flywheel energy storage automobile". *SAE paper*, 1980.

Gabrys, C.W. "Design, Fabrication, and Testing of Advanced Composite Energy Storage Flywheels". Ph.D. thesis, The Pennsylvania State University, 1996.

Genta, G. Kinetic energy storage. Butterworth & Co., Great Britain, 1985.

Genta, G. Vibration of structures and machnines. Springer-Verlag, 1993.

van der Graaf, R. "Ein Hybrid-Antrieb mit Schwungrad und stufenlosem Getriebe für Pkw". *VDI Berichte 1175*, pp. 637–653, 1995.

Greve, P. and Liesner, W. P. "Der neue VW Golf Ecomatic". *Automobiltechnische Zeitschrift (ATZ)*, vol. 95, no. 9 pp. 438–446, 1993.

Guo, Z. Y., Yang, X. C., Yang, D., and Frank, A. A. "On obtaining the best fuel economy and performance for vehicles with engine-CVT transmissions". *SAE Technical Paper Series 881735*, 1988.

Healey, J. R. "VW Lupo: Rough road to fuel economy". USA Today, 1999.

Heavenrich, R.M., Murrell, J.D., and Hellman, K.H. "Light-duty Automotive Technology and Fuel Economy Trends Through 1991". Tech. rep., Control Technology and Applications Branch, EPA/AA/CTAB/91-02, Ann Arbor,MI: U.S. Environmental Protection Agency, 1991.

Hofmann, L., Petersen, R., Adamis, P., and Brunner, H. "Improvement of CVT's for light passenger cars—Fuel economy versus driveability—a solveable conflict? (in German)". *VDI Berichte 1418*, pp. 549–567, 1998.

Höhn, B.-R. "Konzepte weit gespreitzter stufenloser Getriebe". *Konstruktion*, vol. 46 pp. 359–364, 1994.

Höhn, B.-R. "Alternative Getriebesysteme". *VDI Berichte 1610*, 2001.

Junio, M., Roesgen, A., and Corvasce, F. "Rolling resistance of tires". *VDI Berichte 1505*, pp. 255–298, 1999.

Kluger, M. A. and Long, D. M. "An overview of current automatic, manual and continuously variable transmission efficiencies and their projected future improvements". *SAE Technical Paper Series*, no. 1999-01-1259, 1999.

Kok, D. B. "Design optimisation of a flywheel hybrid vehicle". Ph.D. thesis, Technische Universiteit Eindhoven, Eindhoven, The Netherlands, 1999.

Lechner, G. and Naunheimer, H. Automotive transmissions, pp. 135–136. Springer, 1999.

Lehna, M. "Audi Duo, ein Hybridfahrzeug für die City-Logistik". *VDI Berichte 1378*, pp. 119–128, 1998.

Machida, H. "Traction drive CVT up to date". In Proc. of the Internat. Congress on Continuously Variable Power Transmission (CVT'99), pp. 71–769. Eindhoven, The Netherlands, 1999.

Matsuo, I., Nakazawa, S., Maeda, H., and Inada, E. "Entwicklung eines Hybridantriebsystems mit CVT". In Proceedings Aachener Kolloquium Fahrzeug- und Motorentechnik, VDI, pp. 1299–1312. Aachen, Germany, 1999.

Mattsson, P. "Continuously variable split-power transmissions with several modes". Ph.D. thesis, Chalmers University of Technology, Sweden, 1996.

MITI. "Changes in fuel efficiency of Japanese passenger cars (10 mode fuel efficiency)". http://www.eccj.or.jp/databook/1998e/p95.html, source: Ministry of International Trade and Industry, Japan, 1996.

Müller, F. and Köhle, S. "Hybrid electric vehicles—Discussion of different configurations". In Proc. of the 2000 Global Powertrain Congress, pp. 54–63. Detroit (MI), 2000.

Office of Technology Assessment. "Advanced automotive technology: Visions of a super-efficient family car". Tech. rep., DOE, 1995.

Oppenheim, A. K., Maxson, J. A., and Shahed, S. M. "Can the maximization of fuel economy be compatible with the minimization of pollutant emissions". *SAE Technical Paper Series*, no. 940479, 1994.

Paefgen, F.-J. and Lehna, M. "Der Audi Duo–das erste serienmässige Hybridfahrzeug". *Automobiltechnische Zeitschrift (ATZ)*, vol. 99 pp. 316–320, 1997.

Reik, W. "Startergenerator im Antriebsstrang". In LuK Fachtagung: E-Maschine im Antriebsstrang, pp. 37–64. 1999.

Riezenman, M. J. "Engineering the EV future". *IEEE Spectrum*, vol. 35, no. 11 pp. 18–20, 1998.

Schilke, N.A., Dehart, A.O., Hewko, L.O., Matthews, C.C., Pozniak, D.J., and Rohde, S.M. "The design of an engine-flywheel hybrid drive system for a passenger car". *SAE paper*, , no. 841306, 1984.

Schlichting, H. Boundary Layer Theory. McGraw-Hill Book Company, 1979.

Seiffert, U. and Walzer, P. Automobiltechnik der Zukunft, pp. 146–147. VDI Verlag, 1989.

Serrarens, A. F. A. "Coordinated control of the Zero Inertia powertrain". Ph.D. thesis, Technische Universiteit Eindhoven, Eindhoven, The Netherlands, 2001.

Serrarens, A. F. A. and Veldpaus, F. E. "A Management System for a Flywheel Hybrid Driveline". In Proc. of the 4th International Symposium on Advanced Vehicle Control, pp. 159–164. Nagoya, Japan, 1998.

Tenberge, P. "E-Automat: Automatikgetriebe mit Esprit". *VDI Berichte 1610*, pp. 455–479, 2001.

Thoolen, F. J. M. "Development of an advanced high speed flywheel energy storage system". Ph.D. thesis, Technische Universiteit Eindhoven, Eindhoven, The Netherlands, 1993.

van Tilborg, P.G. "Ontwerp van een vliegwielunit voor een hybride aandrijflijn in een personenvoertuig". Master's thesis, Technische Universiteit Eindhoven, 1999.

van Tilborg, P.G. "Development of a concept electromechanical clamping system for a Van Doorne pushbelt variator". Master's thesis, Technische Universiteit Eindhoven, Eindhoven, The Netherlands, 2001.

Veenhuizen, P. A. and van Spijk, G. "General background of the application of the CVT by example of the VDT EcoDrive transmission". In Proc. CVT-Tagung 2000. Haus der Technik, Essen, 2000.

van der Voort, M. C., Dougherty, M.S., and van Maarseveen, Martin. "A new generation fuel-efficiency support tool". *Transportation Research Part C*, vol. 9, no. 4 pp. 279–296, 2001.

Vroemen, B. G. "Component control for the Zero Inertia powertrain". Ph.D. thesis, Technische Universiteit Eindhoven, Eindhoven, The Netherlands, 2001.

Waters, M.H.L and Laker, I.B. "Research on fuel conservation for cars". Tech. Rep. 921, Transport and Road Research Laboratory, Crownthrone, England, 1980.

Yamamoto, K. and Aoki, T. "Analysis of the influence on fuel economy by transmission type and the estimation of fuel economy". In Proc. of FISITA'00, F2000 A148. 2000.

Zeyen, K.-P. and Pels, Th. "ISAD—A computer controlled integrated Starter-Alternator-Damper-System". *SAE Technical Paper Series 972660*, 1997.

Appendix A

2D transmission lay-out

(see next page)

oil supply
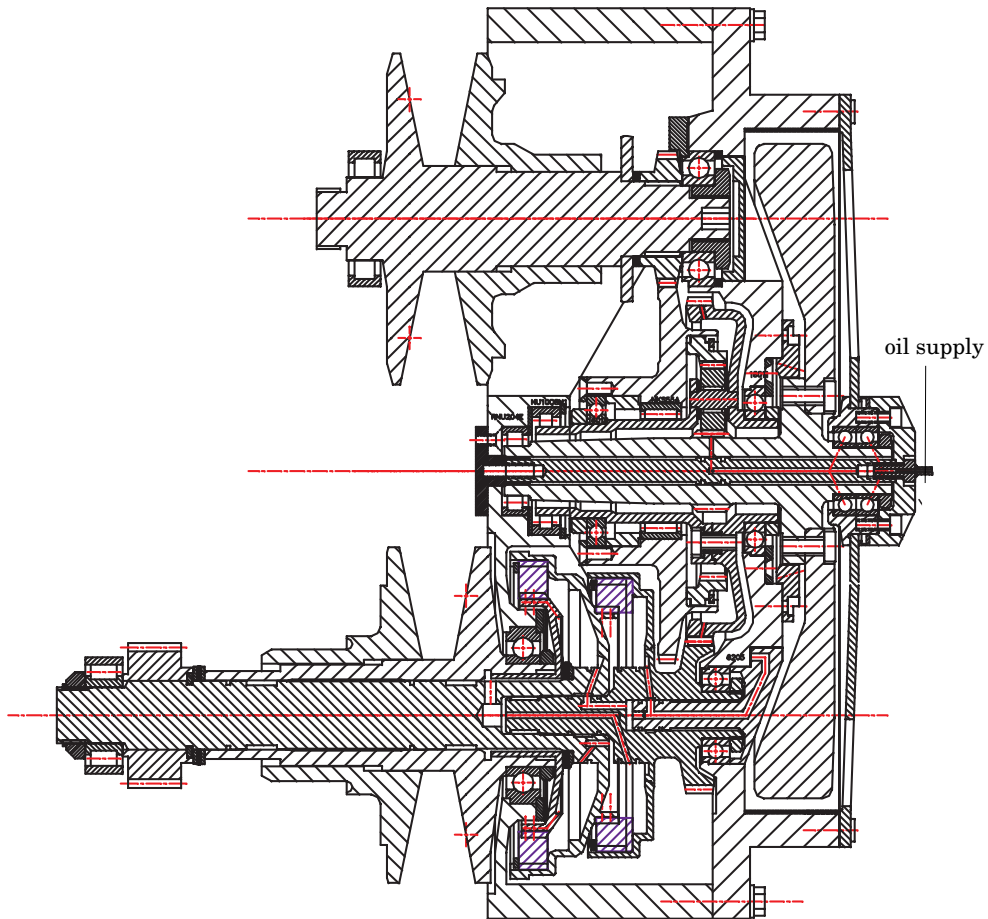
Figure A.1: Proof of concept transmission design

Appendix B

Nomenclature, Acronyms and Definitions

B.1 Acronyms

SYMBOL	DESCRIPTION
AMT	Automated Manual Transmission
AT	Automatic Transmission
BE	Break Even
BER	Brake Energy Recovery
BSFC	Brake Specific Fuel Consumption [g/kWh]
CSA	Crankshaft Starter Alternator
CVT	Continuously Variable Transmission
DNR	Drive-Neutral-Reverse
DPC	Double Primary Cylinder
E-line	collection of fuel-optimal engine operating points
EM	Electric Motor
ETDM	Extended Translational Driveline Model
FESS	Flywheel Energy Storage System
GDI	Gasoline Direct Injection
GN	Geared Neutral
HYZEM	HYbrid technology approaching efficient Zero Emission Mobility
IC	Integrated Circuit
IMA	Integrated Motor Assist
ISAD	Integrated Starter Alternator Damper
ISG	Integrated Starter Generator
Li-ion	Lithium ion
M1, M2	electro motor-generator
MT	Manual Transmission
NEDC	New European Driving Cycle
NiMH	Nickel Metal Hydride

OD	OverDrive
$OL_{x\%}$	operating line with $x\%$ higher BSFC than E-line
PM	Permanent Magnet
SA	Starter Alternator
SG	Stop-Go
SOC	State Of Charge
SS	Start-Stop
SS, DS	Single-Sided, Double Sided pump mode
T	Transmission
TC	Torque Converter
TDM	Translational Driveline Model
UD	UnderDrive
WOT	Wide Open Throttle
ZI	Zero Inertia
ZI-SG	Mechanical Stop-Go system, based on ZI

B.2   Symbols

SYMBOL	DESCRIPTION	VALUE [UNIT]
a	distance	[m]
A	amplitude of harmonic torque	[Nm]
α	proportionality constant	[s]
b_e, b_f, b_v	coefficient, proportional to the inertia of engine, flywheel and vehicle, respectively	[kg/s]
β	normalized gear radius	[m]
c	gap width between the circumference of the rotor and its housing	[m]
C	total energy within specified system	[J]
$C_{ax,bear}$	axial bearing stiffness	[N/m]
C_c	air friction coefficient between the circumference of a rotor and its housing	[-]
C_{rad}	total radial stiffness	[N/m]
$C_{rad,bear}$	radial bearing stiffness	[N/m]
$C_{rad,required}$	total radial stiffness required	[N/m]
C_s	air friction coefficient between the side of a rotor and its housing	[-]
d_i	inner diameter of bearing	[m]
d_m	mean diameter of bearing	[m]
d_o	outer diameter of bearing	[m]
d_{shaft}	flywheel shaft diameter at the position of the seal	[m]
e_0	static eccentricity of bearing	[m]
E_0	nominal kinetic energy in flywheel inertia	[J]
E_{brake}	energy absorbed by the brakes	[J]
E_e	energy delivered by the engine	[J]
E_f	kinetic energy of flywheel inertia	[J]

140

$E_{\text{f,max}}$	maximum stored kinetic energy in flywheel inertia	[J]
E_i	kinetic energy of inertia i, with i=1,2	[J]
E_{load}	energy required for driving the load	[J]
E_{max}	maximum stored kinetic energy	[J]
$E_{\text{max,subcr}}$	maximum stored kinetic energy in flywheel inertia limited by the constraint of sub-critical operation	[J]
E_p	potential energy in vehicle inertia	[J]
ε	eccentricity between the bearing axis and the center of mass of a rotor	[m]
f_0	speed dependent bearing friction coefficient	[-]
f_1	load dependent bearing friction coefficient	[-]
$f_{\text{OL}_{15\%}}$	fuel consumption using $\text{OL}_{15\%}$	[g]
f_{SS}	Start-Stop fuel consumption	[g]
F_{ax}	axial bearing load	[N]
F_e	engine force proportional to engine torque	[N]
F_{load}	load force proportional to load torque	[N]
F_p	primary pulley force proportional to primary pulley torque	[N]
F_{pre}	bearing load due to pre-tension	[N]
F_{rad}	radial bearing load	[N]
g	gravity constant (9.81)	[m/s^2]
G	quality grade for balancing	[mm/s]
γ	angle between dW_2 and neutral line	[rad]
h_o	width of flywheel rotor	[m]
η_1	transmission efficiency without flywheel system	[%]
η_2	transmission efficiency with flywheel system	[%]
η_{air}	dynamic viscosity of air	[Ns/m^2]
η_{cvt}	CVT efficiency	[%]
η_{elec}	efficiency of electrical variator	[%]
η_g	efficiency of the gear train parallel to the CVT	[%]
η_{mech}	efficiency of mechanical variator	[%]
η_{oil}	dynamic coefficient of viscosity, ATF @ 80°C (10^{-2})	[Ns/m^2]
η_t	transmission efficiency	[%]
η_{II}	efficiency of secondary power path	[%]
J	inertia	[kgm^2]
J_1, J_2	inertia of flywheel on the primary and secondary shaft of the variator, respectively	[kgm^2]
J_f	inertia of flywheel rotor around the z-axis (spin axis)	[kgm^2]
J_i	inertia of flywheel rotor i, with i=1,2	[kgm^2]
J_t	inertia of flywheel rotor around the x- or y-axis	[kgm^2]
J_w	inertia of one wheel of the vehicle around its spin axis	[kgm^2]
k	constant factor	[-]
K	shape factor of flywheel rotor	[-]
κ	kinematic factor equivalent to a fixed reduction ratio	[-]
m_e	equivalent engine mass at the primary shaft of the variator, proportional to the primary inertia	[kg]
m_f	mass of flywheel rotor	[kg]
m_v	equivalent vehicle mass at the secondary shaft of the variator, proportional to the secondary inertia	[kg]

141

$\vec{M}$	vector of gyroscopic moments	[Nm]
n	load factor (dynamic load/ static load)	[-]
nc	number of cylinders	[-]
n_c	number of contact elements in a bearing	[-]
ν_{lub}	kinematic viscosity of lubrication (16)	[mm^2/s]
p	proportionality factor	[-]
p_{air}	air pressure within flywheel housing	[Pa]
P_0	equivalent friction load on bearing	[N]
P_{air}	air friction power loss	[W]
P_b	bearing friction power loss	[W]
P_{circ}	power loss due to air friction between the circumference of the rotor and its housing	[W]
$P_{e.max}$	maximum engine power	[kW]
P_{fly}	power loss in additional flywheel system	[W]
P_{lub}	load independent power loss in bearings caused by lubrication	[W]
$P_{pump,shaft}$	vacuum pump shaft power	[W]
P_{roll}	load dependent power loss in bearings	[W]
P_{seal}, P_s	power loss due to friction between the seal and rotating shaft	[W]
P_{side}	power loss due to air friction between the sides of the rotor and its housing	[W]
P_{tot}	total power loss in the flywheel system	[W]
P_{vac}, P_v	required power to drive a vacuum pump transmission	[W]
P_{assist}	power from additional power assist source	[kW]
$P_{combustion}$	engine combustion power	[kW]
P_{cycle}	required wheel power on certain drive cycle	[kW]
$P_{desired}$	desired (engine) power	[kW]
P_e	engine power	[kW]
$P_{e.total}$	$P_{combustion} + P_{inertia}$, total engine power	[kW]
P_{in}, P_{out}	input and output power	[kW]
$P_{inertia}$	power absorbed by engine inertia	[kW]
P_{loss}	power loss	[kW]
P_{th}	threshold power for Start-Stop operation	[kW]
P_{ss}	power level in the sweet-spot	[kW]
P_w	wheel power	[kW]
P_E	power of primary source	[kW]
P_M	power of secondary motor	[kW]
P_G	power of secondary generator	[kW]
P_W	power at wheels	[kW]
Θ_{air}	air temperature	[K]
Θ_b	temperature difference within bearing	[K]
r_1, r_2, r_3	reduction ratio linked to engine, flywheel and vehicle speed, respectively	[-]
r_a	annulus reduction ratio	[-]
r_c	carrier reduction ratio	[-]
r_{cvt}	variator reduction ratio	[-]
$r_{cvt,max}$	maximum variator reduction ratio	[-]

$r_{\text{cvt,min}}$	minimum variator reduction ratio	[-]
r_{d}	final drive reduction ratio	[-]
r_{drive}	reduction ratio between engine and wheels $r_{\text{drive}} = r_{\text{d}}\, r_{\text{cvt}}$	[-]
$r_{\text{drive,gn}}$	specific geared-neutral reduction ratio between engine and wheels	[-]
$r_{\text{drive,low}}$	lowest reduction ratio between engine and wheels	[-]
$r_{\text{drive,od}}$	highest reduction ratio between engine and wheels	[-]
$r_{\text{drive,zi}}$	specific zero-inertia reduction ratio between engine and wheels	[-]
r_{e}	contact element radius of bearing	[-]
r_{i}	inner race radius of bearing	[-]
r_{low}	lowest ratio of the variator	[-]
r_{od}	highest ratio of the variator	[-]
r_{o}	outer race radius of bearing	[-]
r_{r}	cross race radius of bearing	[-]
R	ratio coverage of the variator $r_{\text{cvt,max}}/r_{\text{cvt,min}}$ or $r_{\text{od}}/r_{\text{low}}$	[-]
$R_{\text{e,s}}, R_{\text{e,c}}$	Reynolds number related to the side and the circumference of the rotor, respectively	[-]
R_{i}	inner radius of flywheel rotor	[m]
R_{o}	outer radius of flywheel rotor	[m]
$R_{\text{p1}}, R_{\text{p2}}$	radius of planet gear connected to element 1 and 2 of the planetary gear set, respectively	[-]
R_{w}	dynamic wheel radius (0.307)	[m]
ρ_{air}	air density	[kg/m^3]
ρ_{f}	material density of flywheel rotor	[kg/m^3]
s	gap width between the side of the rotor and its housing	[m]
s_1, s_2	speed coverage of primary and secondary side of the variator, respectively	[-]
$s_{\text{e}}, s_{\text{f}}, s_{\text{v}}$	displacement proportional to engine, flywheel and vehicle speed, respectively	[m]
σ_{a}	maximum allowable material stress in the rotor material	[N/m^2]
t	time	[s]
T	torque	[Nm]
T_0	nominal engine torque	[Nm]
T_{brake}	brake torque	[Nm]
T_{e}	engine torque	[Nm]
T_{load}	load torque	[Nm]
T_{st}	starter torque	[Nm]
T_{w}	wheel torque	[Nm]
v_1, v_2, v_3	tangential speed of component 1, 2 and 3 of the planetary gear set, respectively	[m/s]
$v_{\text{e}}, v_{\text{v}}$	linear speed of engine and vehicle, respectively	[m/s]
$v_{\text{v,close}}$	vehicle speed at which the drive away clutch is closed	[m/s]
$v_{\text{v,max,kinetic}}$	maximum vehicle speed as far as kinetic energy can be exchanged	[m/s]
$\dot{v}_{\text{e}}, \dot{v}_{\text{v}}$	linear acceleration of engine and vehicle, respectively	[m/s]
V	volume of rotor material	[m^3]

143

V_G	peripheral velocity of the center of mass of a rotor	[m/s]
ω_0	nominal angular engine speed	[rad/s]
ω_1, ω_2	angular speed of the primary and secondary shaft of the variator, respectively	[rad/s]
ω_{cr}	first critical speed of flywheel system on elastic supports	[rad/s]
ω_f	angular speed of flywheel rotor	[rad/s]
$\omega_{f,max}$	maximum angular speed of flywheel rotor	[rad/s]
ω_i	angular speed of component i, with i=1,2	[rad/s]
ω_{max}	maximum allowable angular engine speed for proper operation	[rad/s]
ω_{max}^*	bounded maximum angular engine speed	[rad/s]
ω_{min}	minimum angular engine speed for proper operation	[rad/s]
ω_{min}^*	bounded minimum angular engine speed	[rad/s]
ω_p	angular speed of primary pulley	[rad/s]
ω_v	angular speed of vehicle wheel	[rad/s]
$\omega_{v,max}$	maximum angular speed of vehicle wheel	[rad/s]
$\Delta\omega$	harmonic part of the engine's angular speed	[rad/s]
$\Delta\omega_{trans}$	maximum possible engine speed transient	[rad/s]
Ω	angular frequency of engine torque	[1/s]
ω_I	angular speed of electric motor I 'load'	[rad/s]
ω_{II}	angular speed of electric motor II 'engine'	[rad/s]
x	distance related to drive ratio r_{drive}	[m]
x_c	elastic deformation	[m]
x_{gn}	distance related to $r_{drive,gn}$	[m]
x_{low}	distance related to $r_{drive,low}$	[m]
x_{od}	distance related to $r_{drive,od}$	[m]
$\dot{x}$	speed related to the shift speed of the variator	[m/s]
ξ	inner to outer radius ratio of flywheel rotor	[-]
Ψ	hybridization factor	[-]
Ψ_{min}	minimum hybridization factor	[-]
Ψ_{BE}	Break Even hybridization factor	[-]
z	epicyclic gear ratio of planetary gear	[-]
z'	kinematic ratio	[-]
z^*	kinematic ratio	[-]

Samenvatting

De personenauto's van vandaag staan voor een technologisch geavanceerde vorm van flexibele mobiliteit. De verbrandingsmotor, de primaire aandrijfbron van wegvoertuigen, is sterk verbeterd in de afgelopen jaren, maar zijn efficiëntie varieert nog steeds sterk met de fluctuerende vermogenvraag. Gebruikmakend van bestaande transmissies, bijvoorbeeld een getrapte of Continu Variabele Transmissie (CVT), is het moeilijk om *driveability*, d.w.z., een directe en aanhoudende beschikbaarheid van vermogen wanneer het gaspedaal wordt ingetrapt, te combineren met een zuinige afregeling van de motor. Dit probleem, veroorzaakt door de massatraagheid van de verbrandingsmotor, kan worden opgelost door een tweede vermogensbron op te nemen in de aandrijflijn. Het beperken van de kosten, het gewicht en het volume van deze toegevoegde component is belangrijk voor het bereiken van de massaproductie fase en wereldwijd gebruik. Op dit moment zijn er nog geen kosten-effectieve oplossingen gevonden.

Omdat de kosten van een systeem of produkt grotendeels worden bepaald door het toegepaste principe en concept, is er een onderzoek gedaan naar de brandstofbesparingsprincipes die gebruik maken van een tweede vermogensbron, en naar concepten die de deze vermogensbron kunnen materialiseren. Dit onderzoek heeft geleid tot een innovatief aandrijflijnconcept *de Zero Inertia (ZI) aandrijflijn*. In deze aandrijflijn wordt kinetische energie uitgewisseld tussen een vliegwiel en de massatraagheid van de verbrandingsmotor. Als alternatief is de uitwisseling van energie tussen een vliegwiel en de voertuigmassa onderzocht, maar blijkt op het moment nog niet toepasbaar. Het nieuwe transmissieconcept, bestaande uit bewezen componenten zoals een eenvoudige laagtoerige stalen vliegwielrotor en een planetaire tandwielset, is grondig geanaliseerd en zijn functionaliteit is geoptimaliseerd voor een middenklasse personenauto met 1.6 liter benzinemotor. Een ontwerpgereedschap, dat de kinematica en de dynamica van de aandrijflijn representeert en de kinematica van een planetaire set in het algemeen, bleek bruikbaar te zijn voor het onderscheiden van de functionele en constructieve parameters en het vinden van een startpunt voor de parameteroptimalisatie. Slechts twee onderling onafhankelijke parameters bleken de functionaliteit te beinvloeden. Deze functionele parameters, zijnde de maximale energieinhoud van het vliegwiel en de transmissie overbrenging waarbij de vliegwielsnelheid exact nul is, zijn geoptimaliseerd voor voertuigsnelheden van 30 tot 120 [km/h]. Om ook bij stilstand van het voertuig brandstof te besparen is het met de ZI aandrijflijn, middels toevoeging van twee extra koppelingen, mogelijk om de verbrandingsmotor te herstarten en tegelijk weg te rijden. Deze aandrijflijnconfiguratie wordt de *ZI Stop-Go* aandrijflijn genoemd. Vervolgens is een prototype transmissie, uitgaande van een conventionele CVT, geconstrueerd en zijn twee transmissies gebouwd. Hiervan heeft één de ZI functionaliteit en één de ZI Stop-Go functionaliteit. Verschillende innovatieve constructie aspecten hebben het mogelijk gemaakt om efficiënte en compacte transmissies te realiseren.

Het werk van dit proefschrift, [Vroemen, 2001] en [Serrarens, 2001] is uitgevoerd binnen

het EcoDrive project. De gemeenschappelijke doelstelling van dit project is het besparen van 25% brandstof op een specifieke rij-cyclus ten opzichte van eenzelfde auto met een 4-traps automatische transmissie, en dit zonder achteruitgang van driveability. Middels simulaties, gevalideerd met metingen in een testvoertuig, is een brandstofbesparing van 18% bereikt. Daarnaast is een aanzienlijke verbetering aangetoond op de directe beschikbaarheid van vermogen na indrukking van het gaspedaal. Dit geldt met name bij hogere voertuigsnelheden (> 50 [km/h]). Ook is het directe remgevoel bij het los laten van het gaspedaal sterk verbeterd. Dit alles dankzij het gecoördineerde samenspel tussen vliegwiel en verbrandingsmotor dat middels de CVT wordt aangestuurd. De contributie van het onderzoek beschreven in dit proefschrift heeft in grote mate bijgedragen aan het bereiken van de projectdoelstelling, d.w.z., een aanzienlijke brandstofbesparing met verbeterde driveability.

Dankwoord

Het EcoDrive project was een initiatief van Van Doorne's Transmissie BV en werd uitgevoerd in samenwerking met de Technische Universiteit Eindhoven (TU/e) en TNO Wegtransport-middelen in Delft. Het project, lopende van 1997-2001, werd gesubsidieerd door het EET programma (Economie, Ecologie en Technologie) van het Ministerie van Economische Zaken. Alle partners bedank ik hierbij voor hun ondersteuning.

Ik wil mijn persoonlijke dank uitspreken aan een aantal mensen die hebben bijgedragen aan dit proefschrift en aan het EcoDrive project als geheel. Ten eerste wil ik mijn co-promotor Nick Rosielle bedanken voor zijn constructieve bijdrage. Nick, je hebt je altijd sterk gemaakt voor mij en mijn collega's en je uitgangspunten daarbij waardeer ik ten zeerste. Ik bedank mijn promotor Jeu Schouten voor zijn stimulans. Jeu, bedankt voor het attent maken op de NWO vernieuwingsimpuls. De andere leden van mijn commissie, Bernd-Robert Höhn, Joop Pauwelussen en Nort Liebrand, bedank ik voor hun commentaar in de korte tijd die daarvoor beschikbaar was.

Vanzelfsprekend bedank ik mijn twee collega's en vrienden Alex Serrarens en Bas Vroe-men voor de zeer vruchtbare en onvergetelijke promotietijd. Alle ups en downs hebben we samen meegemaakt en ik hoop er nog veel meer mee te maken met onze nieuwe uitda-ging DTI. Erwin Meinders, onze vierde man, bleek onmisbaar voor het project. Hij voorzag iedereen van up-to-date informatie middels zijn EcoDrive up-date mailing, en hij stond altijd klaar voor ieder 'klusje', en dat waren er nogal wat. Erwin bedankt voor jouw inzet, en zoals jouw gezegde is: blijven praten! Een speciaal dankwoord gaat naar Frans Veldpaus voor zijn vrijwillige bijdrage bij het commentariëren van dit proefschrift en enkele artikelen.

In het realisatie traject hebben de werkplaatsen binnen VDT, de ateliers van Werktuig-bouwkunde en de GTD een sleutelrol vervult. Speciale dank gaat naar Toon van Gils die het testvoertuig professioneel heeft omgebouwd, Michiel van Gorp voor het nauwkeurig samen-stellen van de vliegwielunit, en Eef Reker voor zijn bijdragen aan de proefstand.

Via Janneke Zeebregts wil ik alle medewerkers van de GTD bedanken voor hun be-trokkenheid en geweldige inzet. Met veel bewondering heb ik mogen zien hoe de huisde-len en het vliegwiel uit de handen van Hans van der Westerloo en Henk van der Vleuten zijn ontstaan. Bij VDT wil ik mijn dank uitspreken aan Henk Schiricke (Bakema), Hein van Beers, Rinus van Beers en Mark van de Nieuwenhof voor de zeer plezierige samenwerking. In de groep EWG3 gaat mijn speciale dank uit naar Henk Lamers, Gert-Jan van Spijk en Stef Scholten die mij alle ins en outs op transmissie gebied konden vertellen. Marc Mussaeus be-dank ik voor zijn waardevolle bijdrage tijdens het brainstormen op de TU/e in het begin van het project.

Betreffende de EcoDrive organisatie wil ik Dick Landheer bedanken voor het voorzitten van de wekelijkse project vergaderingen en het snel versturen van de notulen. Dick, het on-verwachte 'Maxima' evenement heb je perfect opgevangen zodat wij verder konden met het

schrijven van het proefschrift, bedankt daarvoor! Hierbij wil ik zeker ook de gemeente Eindhoven, burgemeester Welschen in het bijzonder, en prins Willem-Alexander bedanken voor het verkiezen van het Zero-Inertia voertuig op 4 september dit jaar. Bram Veenhuizen wil ik bedanken voor zijn initiatief en voor het "van de grond krijgen" van het EcoDrive project.

Alle studenten die hebben geholpen om de verschillende deelprojecten binnen het EcoDrive project op te lossen wil ik hierbij ook bedanken. Mijn speciale dank gaat uit naar Peter van Tilborg die als nieuwkomer de transmissie wereld binnen stapte en vervolgens een complete transmissie op papier zette. Ik denk met plezier terug aan die tijd dat we met z'n tweeen achter de computer zaten om weer het volgende constructieprobleem uit de wereld te helpen.

Buiten het EcoDrive project om wil ik Nort Liebrand bedanken voor het opstarten van het college "voertuigaandrijvingen" waar ik met bijzonder veel plezier aan heb meegewerkt.

Als één na laatste bedank ik mijn lieve ouders Jan en José, en mijn broer Maarten voor alle ondersteuning in de afgelopen vier jaar. Jan, ik ben zeer benieuwd hoe de Panhard rijdt die je aan het restaureren bent. Veel liefs en gezondheid voor de toekomst!

Als laatste een dankwoord in het Spaans voor mijn vriendin en haar familie: Unas palabras a mi novia y a su familia: Rachele: He sido dichoso en encontrarte, gracias a tu amiga y al taxista, nos encontramos a la misma hora y en el mismo lugar, desde ese momento nuestra atraccion incrementa dia a dia, por telefono, e-mail, cartas pudimos expresar nuestros pensamientos. En julio tomaste la enorme decision de venir a Holanda para estar conmigo y desde ese entonces me encontrastes realizando la tesis, cada dia, cada hora, dificilmente pasamos tiempo juntos. Tu supistes sobrellevar la situacion y cada dia brillaron tus ojos, encontrastes la forma de adaptarte. Godi quiero agradecerte, por tu amor y apoyo un beso para ti. Estoy orgulloso de tu adorable madre Galicia, tus hermanos Ricardo y Romer que dejaron venirte de un dia para otro. Como promesa para ellos comenzare a aprender el castellano y asi podre traducir por mi mismo.

Roëll van Druten
oktober 2001

Curriculum Vitae

Roëll van Druten was born on September 19th, 1969 in Goirle, The Netherlands. He finished his Masters degree at the Technische Universiteit Eindhoven in June 1996, within the section Precision Engineering, on the design of a precision laser-drilling machine for diamond tooling. Working as a project engineer within a precision engineering company (JPE) for one and a half-year, he developed various machines for national and international companies (i.e. Philips, ASML, Diamond Tool Group, and Kinetron). During this period he finished his design project that was initiated in his Masters thesis.

In September 1997 he joined the EcoDrive project. Affiliated to Van Doorne's Transmissie he worked at the Technische Universiteit Eindhoven to study new drive train concepts using a flywheel, to coordinate the Proof of Concept (PoC) part of the EcoDrive project, and to accomplish his PhD-thesis entitled "Transmission Design of the Zero Inertia Powertrain". Together with Alex Serrarens and Bas Vroemen he developed an innovative power transmission system called Zero Inertia. All three are named as inventor on two patents held by Van Doorne's Transmissie. In November 1999 they received the prize for the most promising idea at the energy conversion day organized by the NOVEM. In June 2000 he personally received the Manuel Junoy Prize for his paper called "Design and Construction aspects of the Zero Inertia Powertrain" and for his presentation at the International Congress "Automotive Innovation for the New Millennium" in Korea.

After accomplishing the PoC part of the EcoDrive project, in August 2000, he got affiliated to the Technische Universiteit Eindhoven, Faculty of Mechanical Engineering. There he assisted the section Power Transmissions and Tribology with the preparation and teaching of a new lecture called "Vehicle Drive Trains". Recently he, Alex Serrarens and Bas Vroemen started a company called Drive Train Innovations (DTI) to support the automotive industry with innovative ideas and fundamental knowledge about Hybrid Powertrains. In December 2001 he will start with a new project, named ImpulseDrive, for which he received a premium from the NWO Technology Foundation.